Design, Dynamic Modeling, Simulation and Feedback Control of a Hydrostatic Bearing

By

Gerald S. Rothenhöfer

SUBMITTED TO THE DEPARTMENT OF MECHANICAL ENGINEERING IN PARTIAL FULFILLMENT OF THE REQUIREMENTS FOR THE DEGREE OF

MASTER OF SCIENCE IN MECHANICAL ENGINEERING
AT THE
MASSACHUSETTS INSTITUTE OF TECHNOLOGY

MAY 2007

[June 2007]

Signature of Author: _____

Department of Mechanical Engineering
May 21, 2007

Certified by: _____

Alexander H. Slocum
Professor of Mechanical Engineering
Thesis Supervisor

Accepted by: _____

Lallit Anand
Professor of Mechanical Engineering
Chairman, Department Committee on Graduate Students

Design, Dynamic Modeling, Simulation and Feedback Control of a Hydrostatic Thrust Bearing

by

Gerald Rothenhöfer

Submitted to the Department of Mechanical Engineering
on May 21st, 2007 in partial fulfillment of the
requirements for the Degree of Master of Science
in Mechanical Engineering

Abstract

A hydrostatic bearing carriage (Hydrocline) that uses an open face linear motor to drive the carriage as well as to preload the hydrostatic bearings has been developed by Professor Alexander Slocum and Gerald Rothenhöfer of the Massachusetts Institute of Technology's Mechanical Engineering Department. The Hydrocline is made to cope with the increasing requirements for accuracy in silicon wafer grinding machines. The prototype was built of aluminum oxide ceramic due to its high stiffness-to-weight ratio, low thermal expansion and corrosion resistance. In order to keep the cost of manufacturing as low as possible, a modular design that uses micron-level precision ceramic beams was chosen. Initial testing of the prototype carriage indicates that it has the following performance specifications: a vertical load capacity exceeding 5000N (theoretical limit at 12000N, max. pressure of pumps); a carriage pitch error of 0.7arc seconds; a yaw error of 0.7arc seconds; a roll error of +/- 0.6arcsec a vertical straightness at the center of the carriage of +/-0.75microns; and a vertical stiffness of the carriage of 900N per micron (load range from 0 to 1000N). A dynamic model of the hydrostatic bearing and fluid supply system has been developed and accurately predicts the performance of the Hydrocline. The model has been used to simulate a feedback control loop that adjusts the bearing supply flow such that changes in load can be compensated and theoretically infinite stiffness can be reached. In first experiments on a specially designed test setup the measured static stiffness of the single pocket test bearing could be increased by a factor 8 (load range 45 to 270N). The dynamic stiffness of the bearing could be increased by a factor of 2.5.

Thesis Supervisor: Alexander Slocum, Professor of Mechanical Engineering

Table of Contents

Index of Figures

Index of Tables

1 Introduction

As Silicon wafers are increasing in diameter, the machine tools needed to manufacture the wafers have to become more and more accurate in order to achieve the required surface finish. One major key to increased accuracy is the stiffness of the structural loop of the machine. Here, among others the stiffness of the bearings is of decisive importance. Further requirements such as cleanliness or minimal thermal expansion make hydrostatic bearings a good bearing choice. In addition, hydrostatic bearings make no mechanical contact between bearing surfaces such that motion accuracy is not limited by small surface inaccuracies.

Hydrostatic bearings and the underlying physics are well covered and rather accurate formulas can be found in different publications.[1] Common literature also describes sophisticated restrictor and valve designs that can enhance the stiffness of the bearing ("infinite stiffness devices"). However, most literature treats hydrostatic bearings as a static system and neglects the dynamics of the bearing and its interaction with the bearing fluid supply system. Making use of the above mentioned design tools a hydrostatic bearing carriage has been developed for the use in next generation silicon wafer grinding machines. The presented carriage design uses an open face permanent magnet linear motor to drive the carriage and to preload the bearings by use of the magnetic attraction between the motor forcer and the magnets. With the presented carriage design, a stiffness of 900N/micron, at a pocket pressure of 85kPa, a flow rate of 50 to 85ml/min per pocket and a nominal bearing gap of about 10 microns was achieved.

As in the case with other non-hydrostatic bearings, the limiting factor of achievable motion accuracy under the influence of changing load is the finite stiffness of the bearing. Neglecting dynamic effects, it can easily be visualized that a change in load will cause deflection of the bearing. However this deflection can be counteracted by increasing the volume flow through the bearing. Ideally

[1] Hydrostatic Lubrication, Bassani, Piccigallo, Elsevier, 1992
Hydrostatic and hybrid bearing design, W.B. Rowe, Butterworths, 1983

an "infinitely" stiff bearing should result; however, the dynamics of the bearing are more complex. Accordingly a principal focus of this work has been a dynamic model of a hydrostatic thrust bearing "system" that includes the interaction of bearing dynamics and the dynamics of the supply system. A new way is presented, to maintain a constant hydrostatic bearing gap, independent of the load and without using any mechanical "infinite stiffness devices". The model predicts that infinite static stiffness and a significant increase in dynamic stiffness of the bearing can be achieved by adequately controlling the volume flow into the bearing. In reality, due to the limited available pumping power the static stiffness of the bearing can only be maintained infinite over a limited range of bearing loads. A test setup has been built in order to double-check the predictions of the model. In the test setup an increase of static stiffness by a factor of 8 could be achieved over a load range of 45N to 270N. Based on the maximum pressure specification of the pump, the load range could be increased to 1650N, while maintaining a constant bearing gap. However, this has not been tried yet and remains as a topic for future research.

2 Functional Principle of Hydrostatic Bearings

Generally speaking a hydrostatic bearing works similarly to an air hockey table. In the case of a hydrostatic bearing the "puck" floats on an ideally incompressible bearing fluid (e.g. water) instead of on air, and the puck is a part of a machine tool. Hydrostatic bearings support loads by pressuring a bearing fluid such as oil or water into a bearing pocket. The bearing fluid is pushed out of the pocket through a narrow gap (hydrostatic gap) between the stationary table and the movable carriage that carries the load. Depending on the gap height and the volume flow rate a certain pressure will result inside the pocket. This pressure carries the carriage and the load on top of the carriage. Unless the maximum load capacity of the bearing is exceeded, the carriage floats on a thin film of fluid (1-100 microns). The maximum load capacity of the bearing mainly depends on the size (area) of the pocket and the supply system. There are two different supply systems for hydrostatic bearings: constant pressure and constant flow.

In the case of a constant pressure supply the bearing is supplied by a constant pressure pump through a restrictor such as an orifice or a capillary. If the load increases, the bearing gap decreases and less fluid flows out of the bearing. Thus the pressure drop over the restrictor decreases and a higher pressure becomes available in the bearing.

In the case of a constant flow supply, the bearing can be supplied by a positive displacement pump where the flow is proportional to the pump speed. If the load increases the gap decreases and so does the outflow resistance of the bearing. Thus the pressure in the bearing increases.

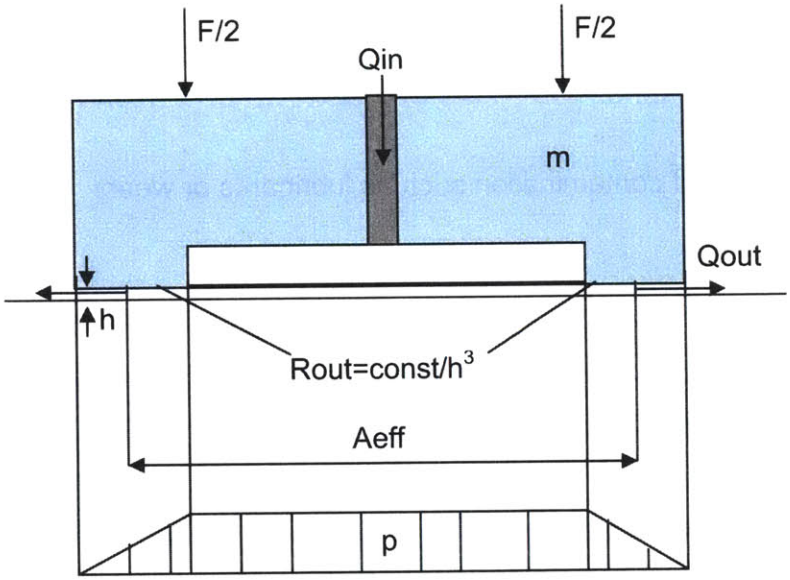

Figure 1: Single, force preloaded hydrostatic thrust bearing pad and pocket pressure profile

In order to achieve bidirectional stiffness, the bearing has to be preloaded.

The main purpose of the bearing pocket (the inner region of the bearing) is to create an area of uniform pressure to support load and to lift off the bearing from rest. The bearing lands and the bearing gap define the outflow resistance of the bearing. Furthermore the bearing lands determine the inherent "squeeze film damping" of the bearing. Squeeze film damping is the dissipation of energy through viscous flow (shear of the fluid) in the bearing gap. The bearing will only

provide significant damping if the supporting structure (table) is much stiffer than the bearing itself.

3 Designing the Hydrocline

The concept for the Hydrocline is based on previous work by Professor Alexander Slocum and Roger Cortesi of the Massachusetts Institute of Technology's Mechanical Engineering Department.[2] Its intended area of use is in next generation silicon wafer grinding tool machines. For this application it was essential to maximize:

- positioning accuracy
- repeatability
- straightness
- cleanliness (no sources of contamination such as lubricants or wear)
- stiffness

As described in the following paragraph, hydrostatic bearings were the ideal choice for this design. Because hydrostatic bearings are contact free they not only fulfill the above requirements, but also reduce the machine downtime due to reduction of the required maintenance time (no greasing necessary). In order to achieve significant stiffness, a hydrostatic bearing has to be preloaded. In the case of the Hydrocline, the preload is produced by the magnetic attraction between the linear motor coils and the permanent magnet track. In order to evenly preload the hydrostatic bearings that constrain the carriage in horizontal and vertical direction, the motor was mounted at a 30 degree angle relative to a horizontal plane. The functional principle of the preload is the same as in previous work done by Prof Slocum and Roger Cortesi:

"The attractive force between the motor coil and the magnet track preloads the bearings, which support the vertical and horizontal loads. By choosing the groove

[2] "Linear motion carriage with aerostatic bearings preloaded by inclined iron core linear electric motor", Roger Cortesi, Alexander Slocum, Murat Basaran, Anastasios John Hart, Elsevier 4 March 2003

angle (q) and motor location (ym, zm) the designer can specify the amount of preload on each bearing pair."

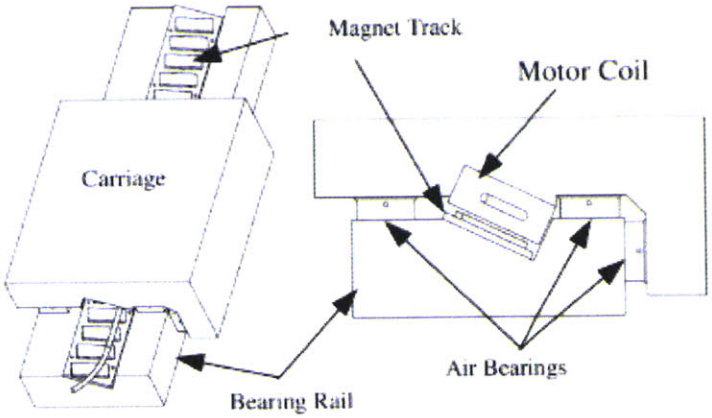

Figure 2: Motor-preloaded-bearing concept

For more detail the reader is referred to Roger Cortesi's Master thesis.[3]

3.1 Bearing Selection

The functional requirements for the bearing system have been:

- Maximize stiffness with available space
- Maintain absolute cleanliness (no contamination by lubricants or wear particles)
- Maximize straightness of motion
- Maximize repeatability
- Minimize wear

A hydrostatic bearing design has been chosen from a variety of bearing types such as rolling elements, sliding contact, aerostatic and hydrostatic bearings.

[3] "An Easy to Manufacture Non-Contact Precision Linear Motion System And Its Applications", Master Thesis of Roger Cortesi, Precision Engineering Research Group, MIT

	Max. stiffness with available space	Damping	Minimize sources of contamination	Max straightness	Max repeatability	Minimize wear
Rolling element	0	0	0	0	0	0
Sliding Contact	+	+	+	+	+	-
Aerostatic	-	+	++	++	++	++
Hydrostatic	++	++	+	++	++	++

Table 1: Bearing Selection

Rolling Element and Sliding Contact Bearings would have required a more complex design in order to keep contaminants such as the lubricant or wear particles away from the wafer grinding process. Aerostatic bearings were not an option due to the limited stiffness (about half the stiffness of a comparable size hydrostatic bearing).

3.2 Hydrocline Components

Figure 3 shows a solid model of the Hydrocline and its components:

1. The Ways: These are the base of the Hydrocline. It is the surface on which the carriage slides back and forth.

2. The Top and Side Precision Surfaces: These are the two critical surfaces of the way. The hydrostatic bearings slide over these two surfaces, hence the necessity for higher tolerances on straightness and surface finish.

3. Linear Motor Permanent Magnet Track: Together with the iron of the motor forcer he permanent magnet track provides the preload to the bearings. In addition the permanent magnet track is an essential part of the linear motor.

4. Position Encoder Scale: A magnetic scale has been chosen due to its reduced sensitivity to contamination or optical refraction compared to an optical scale. The scale is a piece of tape that allows the position encoder read head to measure the carriage's position and speed. The carriage is made up of the carriage base and the carriage fin.

5. The Carriage Base: This is the structure to which the fin and the permanent magnet linear motor forcer is attached. In addition the hydrostatic bearing pockets for the vertical direction are machined into the carriage base.

6. Carriage fin: The fin is attached to the carriage base. The hydrostatic bearing pockets that constrain the carriage in the horizontal direction are machined into the fin.

7. The Linear Motor Forcer/Coil: The magnetic attraction between the motor forcer and the permanent magnets of the magnet track provides the preload for the hydrostatic bearings and propels the carriage.

8. Position Encoder Read Head: The read-head is fixed to the side of the carriage base and moves with the carriage. It measures the position and speed of the carriage relative to the way. The read head can not be seen in Figure 3.

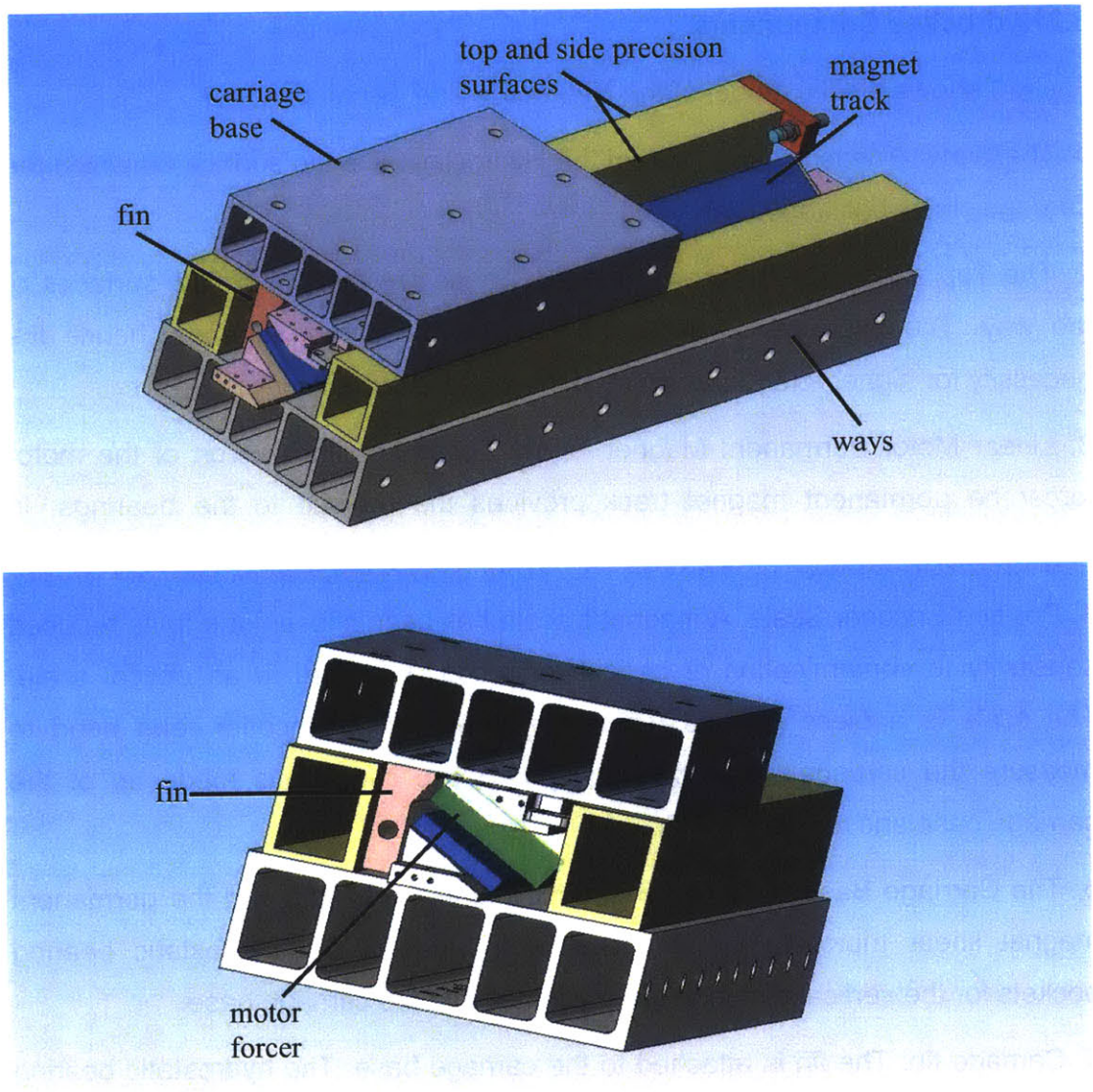

Figure 3: Hydrocline

3.3 Way Surface Selection

In order to make use of the great achievable stiffness of hydrostatic bearings and the excellent squeeze film damping properties, the material of the hydrostatic ways had to be stiffer than the bearing itself. In addition, the flatness and straightness of the ways has to be significantly less than the hydrostatic gap (about 10microns). Furthermore, the way material should not deteriorate or release any particles when flushed with the bearing fluid (here water) over an extended period of time (several years).

The functional requirements for the way material are:

- No upward divots if the way is impacted
- Required surface finish can be achieved with reasonable cost
- High stiffness to weight ratio
- No release of particles if exposed to water of extended periods of time
- No aging when exposed to water over extended period of time

As follows many materials could be ruled out:

Granite: The cost and its weight limit its use for the Hydrocline design.

Polymer Concrete: Exposure to water over an extended period of time will cause aging of the material.

Metal: Aluminum parts have to be anodized in order to prevent them from releasing particles when exposed to water over an extended period of time. Most metals will show some kind of corrosion if not coated and develop outward divots.

Ultimately it was decided to build the main structural elements of the Hydrocline out of **Aluminum Oxide**. The very high stiffness to weight ratio (three times higher than aluminum), low thermal expansion (3.7 times lower than aluminum), high achievable surface finish, low coefficient of friction (if bearing should ever run dry), no water absorption, no release of particles into the bearing fluid (water) and wear resistance make aluminum oxide the optimal material for the

Hydrocline design. The low damping of Aluminum Oxide is not an issue because of the very high damping of the hydrostatic bearing. By using standard box shaped geometries as a building element the cost of manufacturing could be reduced.

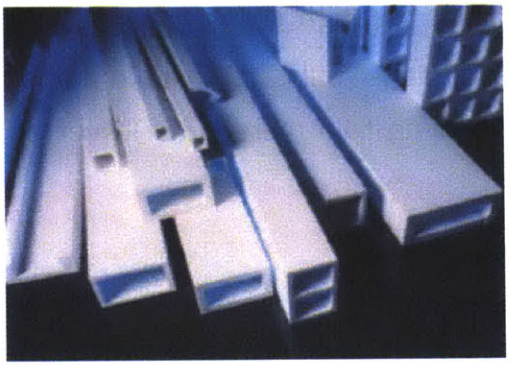

Figure 4: Standard box shaped building elements as by Coorstek Inc.

	Stiffness to weight ratio	Release of Particles	Aging	Surface Finish, Divots	Cost
Metal	0	0	0	0	0
Granite	+	++	++	++	-
Polymer concrete	-	+	-	++	0
Aluminum oxide	++	++	++	++	+

Table 2: Hydrocline material selection

3.4 Motive Power Selection

The motive power functional requirements are:

- Minimize number of components
- Resistance against humidity
- No sources of contamination (such as lubricants)
- Repeatability and accuracy of positioning
- Minimize wear
- Provides preload force for hydrostatic bearings.
- Water resistance

Given the above functional requirements a water resistant linear motor direct drive is the best choice.[4] Conveniently the attractive force between forcer and permanent magnets can be used to preload the hydrostatic bearings. In designs that use rolling element bearings or sliding bearings this attractive force is usually undesirable. For sure it would be possible to find other motive power solutions, but any other solution (e.g. air pistons, screw drive, belt drive) would also increase the amount of necessary components (e.g. to provide the preload force for the bearings or to make the design insensitive to humidity) and thus decrease the reliability of the system, bring in additional sources of errors (straightness of movement, positioning,...) and increase the cost.

3.5 Sizing the Hydrostatic Bearings (Load Capacity of the Carriage)

The load capacity of the carriage is determined by the load capacity of the hydrostatic bearings that support the carriage in the respective direction (vertical, horizontal).

- In order to maximize the stiffness of the bearing, the nominal gap has to be minimized.

[4] Anorad Corp makes a linear motor for underwater use

- The gap should be big enough such that the bearing can slide over any expected surface inaccuracy / waviness.
- The outflow resistance of the bearing is inversely proportional to the gap cubed.
- In order to carry a certain load either the bearing size (pocket area) or the volume flow through the bearing has to be increased
- The pocket area is chosen depending on the available pumping power, flow, pressure...
- The maximum load capacity of the bearings is determined by the minimum allowable gap height between the bearings and way, the pocket area and the pocket pressure.
- The working load and preload applied to each bearing must not exceed its maximum load.

A spreadsheet as well as a MATLAB based design tool has been developed in order to facilitate the design of hydrostatic bearings. The Matlab based design tool can easily be adapted to solve other design problems that can be described by a set of analytic equations. A summary of the design parameters for the Hydrocline hydrostatic bearing and the code for the Matlab based design tool can be found in the appendix. The spreadsheet as well as the Matlab code predicts a flow that is by a factor of 10 higher then the measured flow. Therefore it will be necessary to revise the spreadsheet and the Matlab based design tool.

3.6 Sizing the Carriage (Roll, Pitch Yaw and Normal Stiffness)

Measuring the angular stiffness is extremely difficult. However, ultimately the angular stiffness is determined by the normal stiffness of each pad and their spatial arrangement of the pads.

The angular stiffness is proportional to:

- The stiffness of the individual bearings
- The number of air bearings

- The bearings' distance from the center of stiffness of the carriage squared.

3.7 Fluid Supply System

The two fundamental supply system options for hydrostatic bearings are constant flow and constant pressure. The behavior of the bearing for each supply system is as follows: In the case of a constant pressure supply the supply pressure is kept constant. A restrictor in the supply line of the bearing, between the bearing and the pump automatically regulates the pressure in the bearing. If the load on the bearing increases, the bearing gap decreases and the outflow resistance of the bearing increases. Consequently the flow decreases. With decreasing flow the pressure drop over the restrictor decreases and thus if the supply pressure is kept constant the pressure in the bearing pocket must increase and the bearing finds a new stable equilibrium. A detailed model of a hydrostatic bearing is described in chapter 5.

In the case of a constant flow supply no restrictor is needed. However the flow through the bearing has to be maintained constant, independent of the load. If the bearing load increases, the gap decreases and the outflow resistance increases. Thus if the supply flow is kept constant the pressure in the bearing pocket must increase and consequently the bearing finds a new stable equilibrium.

A constant flow supply will yield a higher efficiency (i.e. higher stiffness for the same pumping power) since there are no losses over a restrictor (as in the case of a constant pressure supply). Furthermore the restrictor that has to be used in the case of a constant pressure supply can clog over time and decrease the performance of the bearing. In addition a constant flow supply has the advantage that the flow in each bearing pocket can be adjusted independently and thus it is possible to compensate for unevenly applied loads on the carriage, dynamic load changes or surface tolerances in the sliding rails. If the flow in each pocket is controlled such that it changes proportionally to a change in pressure in the corresponding pocket, theoretically infinite static stiffness can be achieved. This

is explained in more depth in chapter 5. Also it is possible to improve the dynamic response of the bearing to load changes by controlling the flow through each bearing pocket.

For the above reasons a constant flow supply has been chosen. Problems of the constant flow supply include:

- each bearing needs its own pump
- at the time when the Hydrocline was designed only one pump could be found that could deliver the required, continuous, low flow rate at pressures of about 51 to 85ml/min and 100kPa

Further requirements for the pump were:

- constant flow (independent of pressure)
- minimal pressure fluctuations

Ultimately a positive displacement (flow proportional to pump speed), external gear pump was found that could mostly fulfill above requirements.[5] The chosen pump is driven by a permanent magnet DC motor. The velocity of the pump is controlled by a closed loop proportional controller. The pump characteristics have been measured in a pressure range from 7kPa to 221kPa (Figure 4, Figure 5, Figure 6). A pressure increase of 214kPa corresponds to an increase of load on the carriage of about 8130N. It could be shown that, at a given control voltage, an increase in pressure leads to a decrease in flow. Note: the measured flow was by a factor of 10 higher than the predicted flow.

[5] Micropump Corp, GA series, x21 gear set

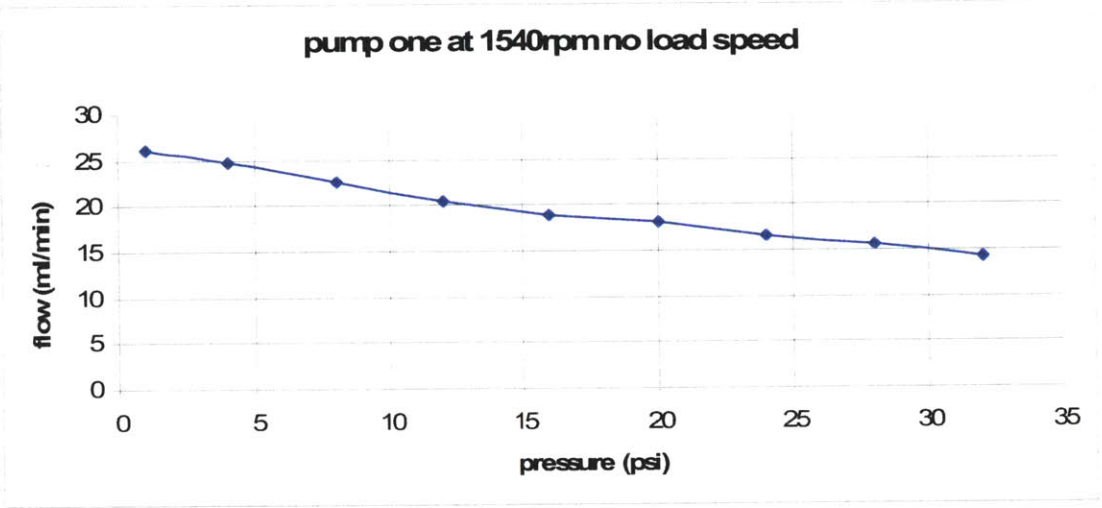

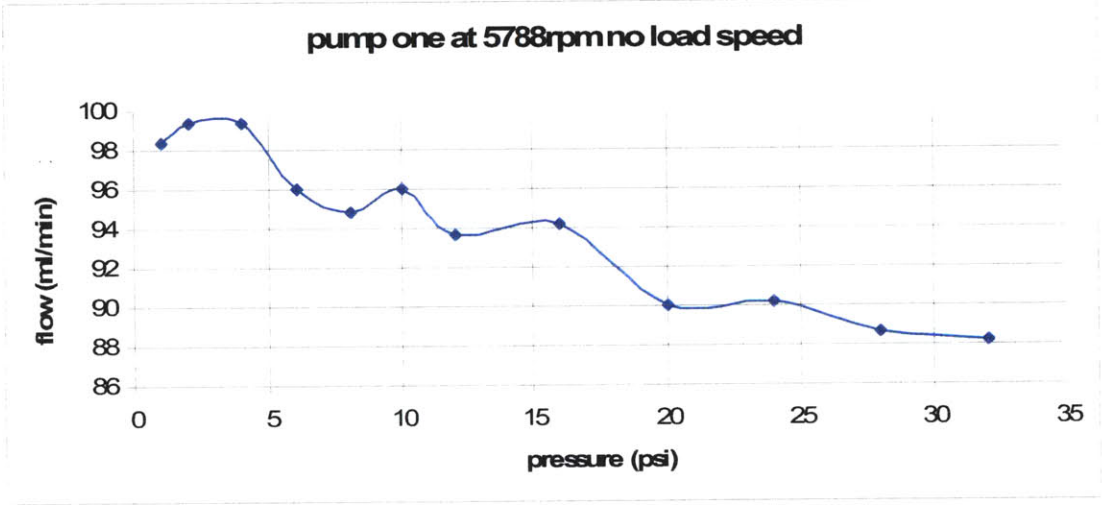

Figure 5: Measured "flow rate per minute – pressure" line of Micropump

Two effects can explain the decrease of the flow rate. As the pressure increases:

- the speed of the pumps decreases
- the flow per revolution decreases

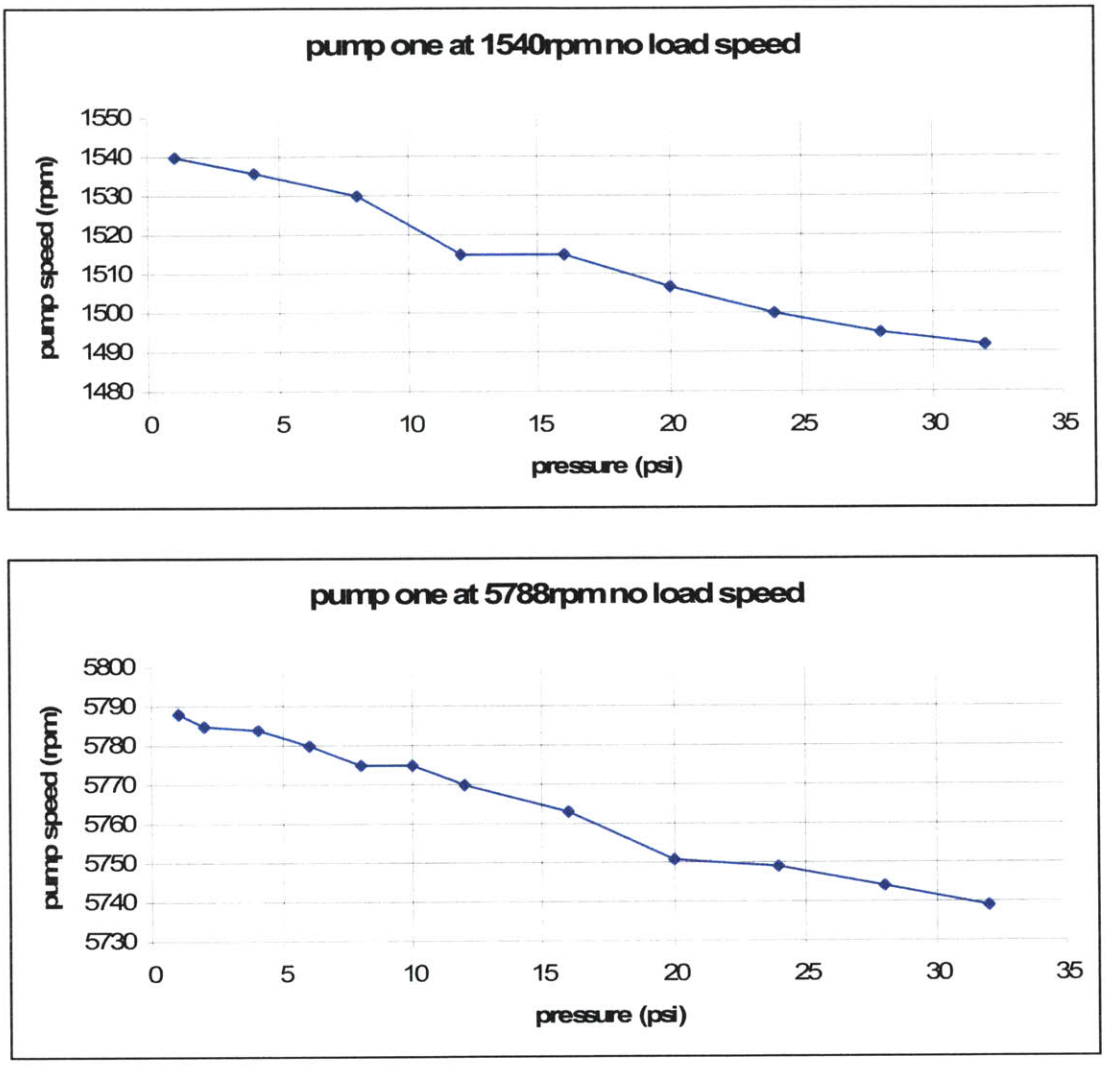

Figure 6: Measured speed-pressure line of Micropump

The decreasing speed can be explained by an increasing steady-state error of the P-controlled velocity loop. The decrease of flow per revolution can be explained by pump internal leakage.

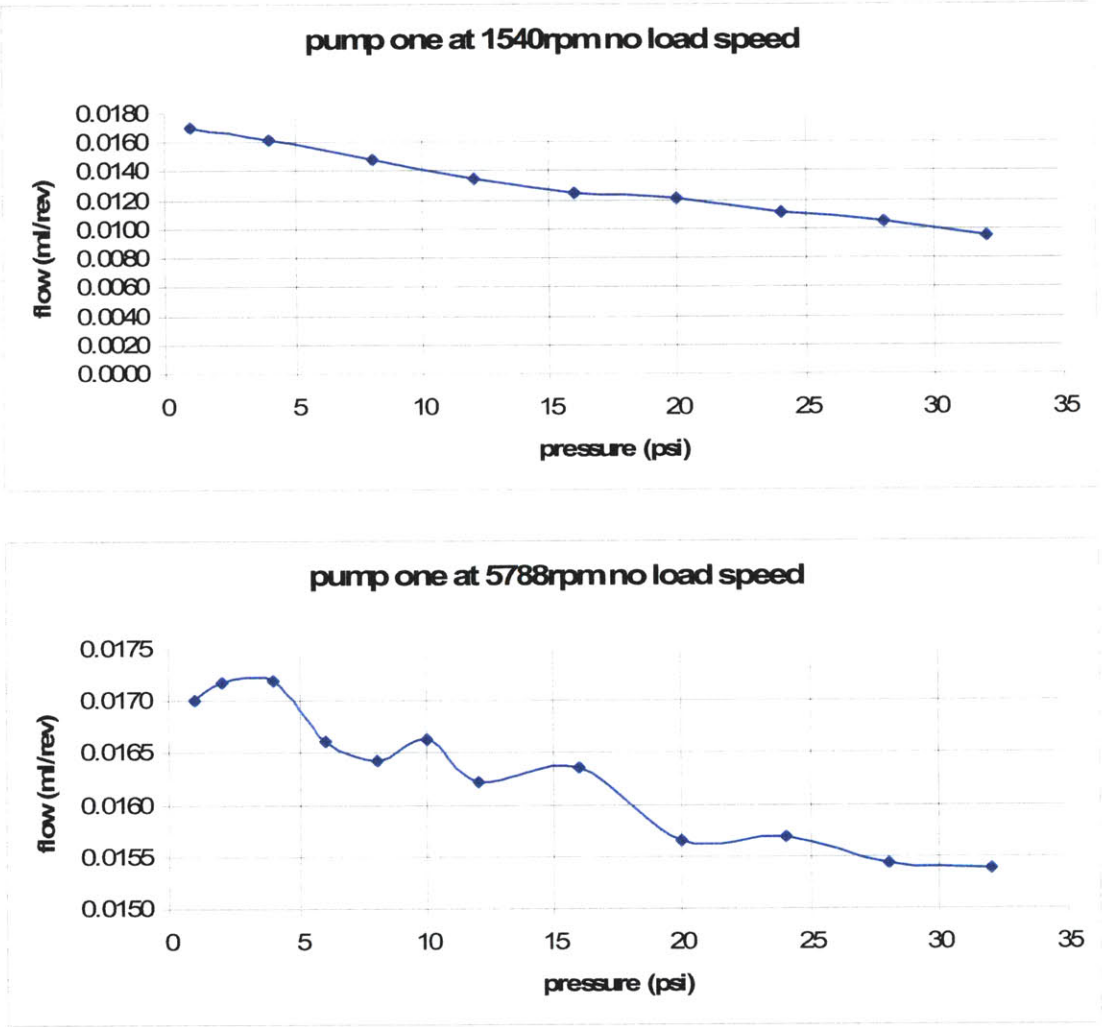

Figure 7: Measured flow per revolution - pressure line of Micropump GA X21

If the pump speed is higher than 3500rpm an increase in pressure of 214kPa causes a decrease in flow of approximately 0.9% due to the decrease in pump speed and by 8.0% to 9.6% due to internal leakage. A decrease in flow of 10% would lead to a gap that is 3.5% lower than it would be in the case of true constant flow. This can be derived by the following equations.

$$R_0 = \frac{p_0}{Q_0} \qquad (1)$$

$$R_1 = \frac{p_0}{Q_0 - \Delta Q} \qquad (2)$$

$$\Delta Q = 0.1 * Q_0 \qquad (3)$$

$$R_1 = \frac{1}{0.9} R_0 \qquad (4)$$

with

$$R_1 = const * \frac{1}{h^3} \qquad (5)$$

it follows

$$\frac{1}{h_1^3} = \frac{1}{0.9} \frac{1}{h_0^3} \qquad (6)$$

$$h_1 \approx 0.965 * h_0 \qquad (7)$$

h - *hydrostatic gap*

R_0 - *outflow resistance of bearing at* $h=h_0$

R_1 - *outflow resistance of bearing at* $h=h_1$

Q_0 - *flow at* $h=h_0$

p_0 - *pressure at* $h=h_0$

If the pumps are running at speeds lower than 3500rpm the decrease in flow in percent is significantly higher. Following an increase in pressure of 214kPa in the case of pump speeds of about 1500rpm a decrease in flow of 46% due to internal leakage has been measured. For higher speeds the change in flow becomes less and less significant. In general the bearing should be run at the lowest possible flow rate. A low flow rate means a smaller hydrostatic gap, which will give a better stiffness. However, in the case of low flow rates the percentage change of the flow in the case of a changing load is significantly higher than in the case of higher flow rates. Thus a better flow control especially for low pump speeds is necessary in order to increase the stiffness furthermore. A flow rate that decreases with pressure can explain the slight difference between the theoretically calculated stiffness and the average measured stiffness.

3.8 Assembly Lessons Learned

The assembly of the Hydrocline prototype went mostly smooth even though some painful lessons on how to handle aluminum oxide ceramics had to be learned. When the prototype first arrived at MIT the ceramics around one of the metal inserts that were glued into the carriage base and served as a connection of the fluid supply tubing to the bearing pockets had broken out. The reason is assumed to be water that had remained in gaps around the insert after the Hydrocline was first run at the manufacturer and that froze during the transport in February. The freezing water than cracked the ceramics similar to how freezing water causes potholes in Cambridge streets during the winter. The broken piece was sent back to the manufacturer who could repair it by grinding out the cracked area and gluing in a new piece of ceramic.[6]

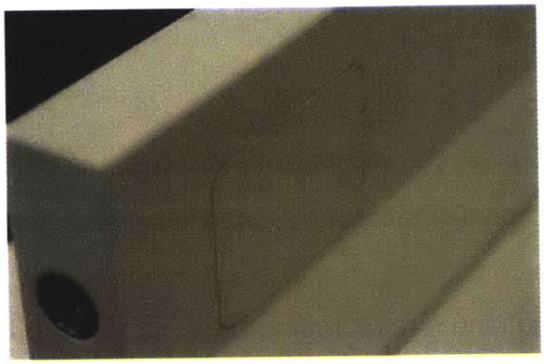

Figure 8: Repaired fin

The linear motor forcer was bolted to the carriage base. However the accessibility of the bolts was very poor, which made it unnecessarily time intense to mount the motor forcer. In addition the through holes of the bolts in the ceramic carriage base were just big enough to fit the bolt through. However, it was almost unavoidable that the bolts would touch the ceramics when mounted. After some mounting and unmounting, one of the bolts apparently chipped a miniscule piece of ceramics off the corner of one through hole. The piece fell in between the motor forcer and the ceramics and after the bolts were tightened it caused a crack in the carriage base.

[6] Unlike the city of Cambridge the manufacturer did a really good repair job.

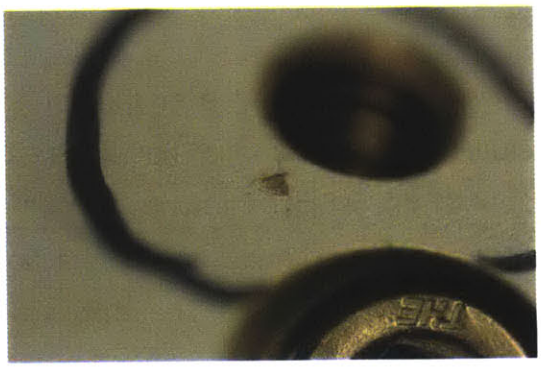

Figure 9: Indent on motor-forcer-mount caused by small particle

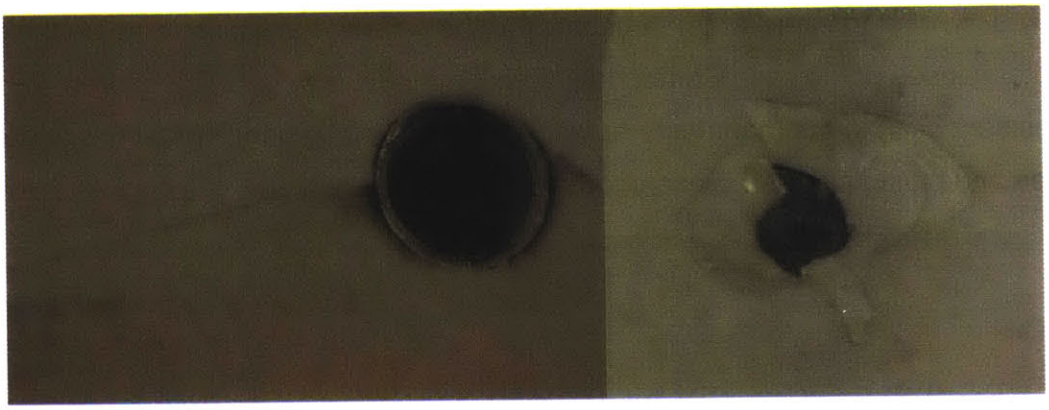

Figure 10: Crack in ceramics caused by small particle that got squeezed in between the motor forcer and the ceramics

This crack could be fixed by gluing an aluminum reinforcement over it to keep it from expanding.

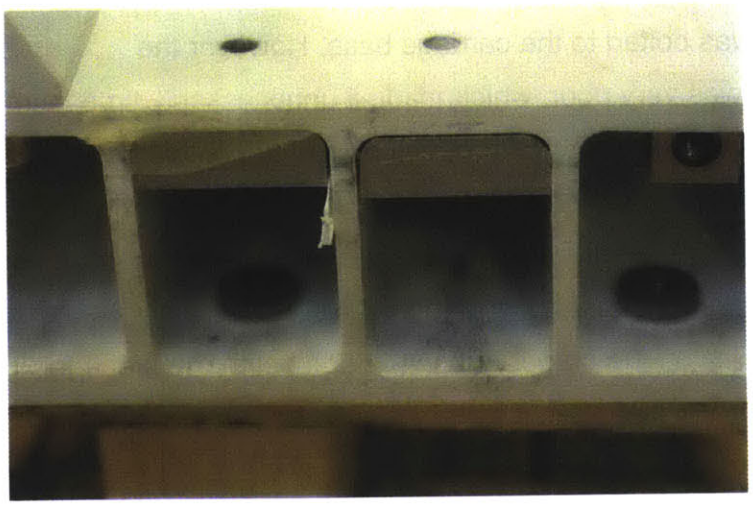

Figure 11: Aluminum reinforcement in order to stop crack from expanding

In order to avoid this problem, metal inserts should have been glued into every through hole, such that the bolt can never touch a sharp corner in the ceramics that can easily splinter off. In addition, all surfaces need to be inspected and cleaned before bolting.

3.9 Measurement System

The pressure in each pocket was measured by a pressure sensor mounted in the upstream supply line of the particular pocket.

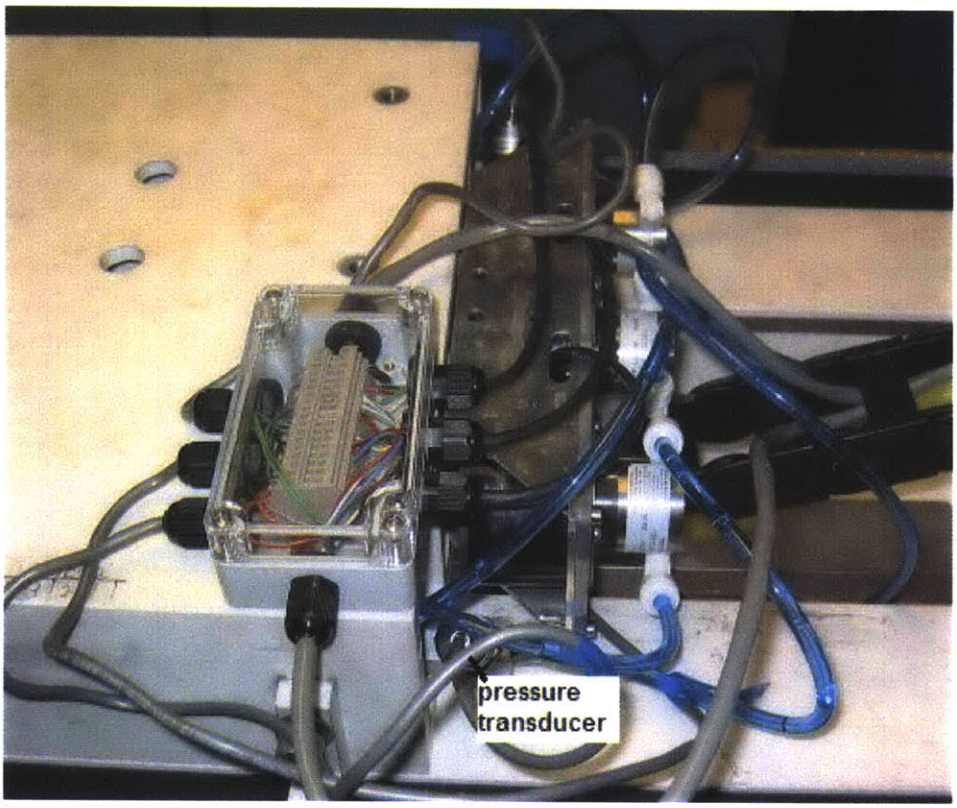

Figure 12: Pressure sensor downstream of the pump

Vertical displacement, straightness and pitch could be measured by two impedance probes on each side of the carriage base. The probes measured the distance to a straightedge that was fixed to either side of the non-moving machine base.

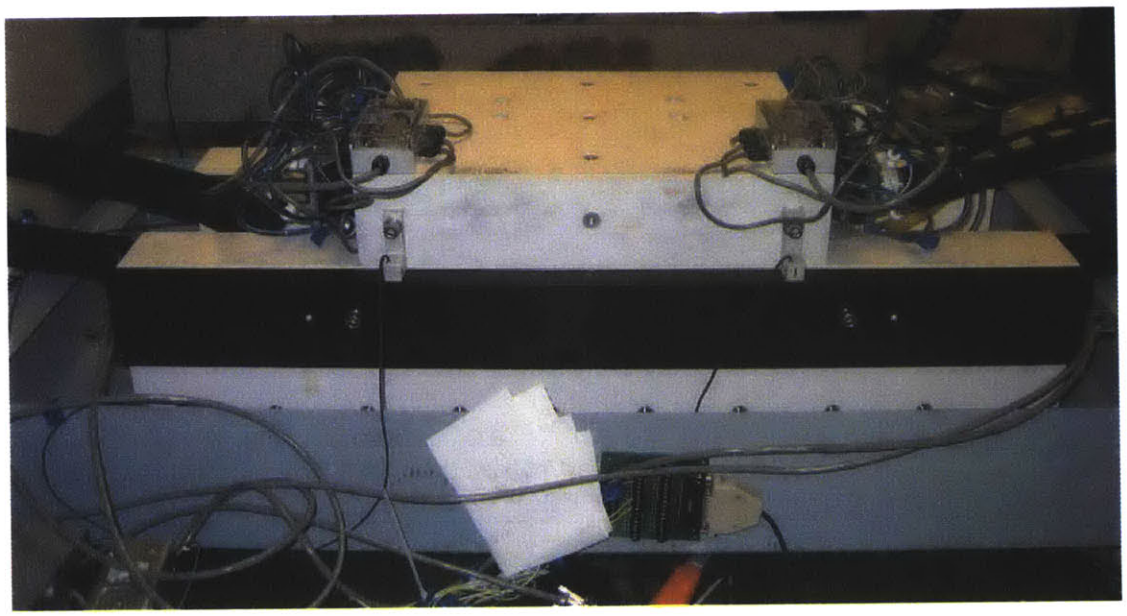

Figure 13: Hydrocline with straight edge and impedance probes

All the data (position of the carriage, pump speed of each pump, pressure in each pocket, displacement i.e. bearing gap measured by each of the four eddy current probes) was collected, evaluated and recorded in Labview.

3.10 Stiffness

The average measured stiffness in the vertical direction is about 900N/micron (225N/micron for each pad) and thus almost equal to the predicted stiffness of 957N/micron. The measured stiffness ranges from 500N/micron to 1900N/micron. Based on the measured vertical stiffness the horizontal stiffness (only two pads) was calculated as 450N/micron and the resulting angular stiffness was calculated as 140Nm/arcsec in pitch and yaw direction and 92Nm/arcsec in roll direction.

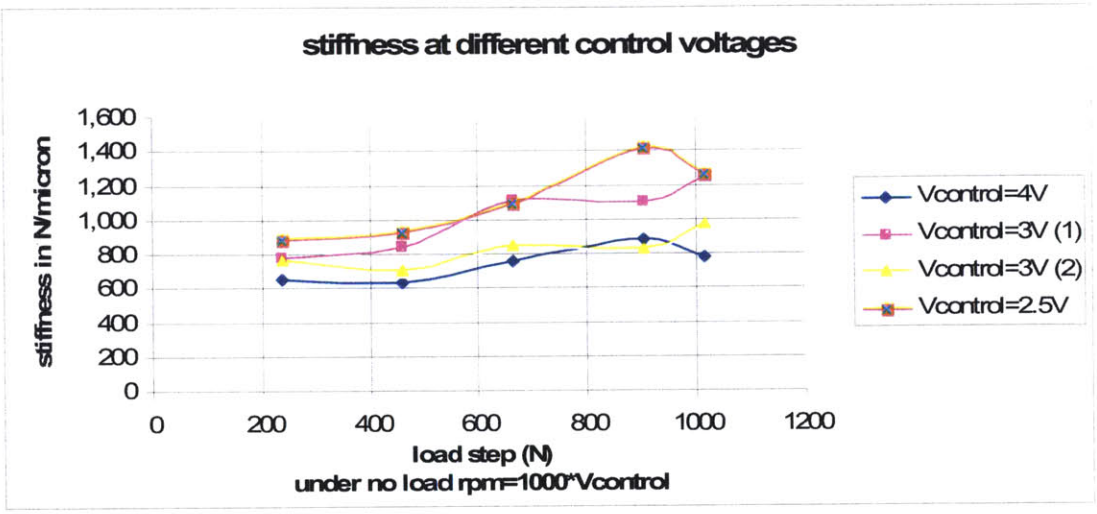

Figure 14: Stiffness averaged over all four pads at different pump speeds

The low stiffness values ($V_{control}$=4V, corresponds to 4000rpm no load pump speed) have been measured at the beginning of the measurements when the bearing (i.e. the pumps) had just been switched on. Remaining air in the bearing pocket lowered the stiffness during the first measurements at a higher flow rate. Over time the air got pushed out of the bearing and thus the stiffness increased. Generally, in the case of constant flow the stiffness at low flow rate and thus small bearing gaps must be higher than at high flow rates. However the difference between the lowest stiffness values that were measured right after switching on the bearing and the highest stiffness values can not only be explained by the different bearing gap at different flows, but must also be explained by air leaving the bearing pockets over time. Besides the variation in the measured stiffness values it is important to note that the measured pocket pressures are not the same in all the pockets and that the pocket pressures change slightly depending on the position of the carriage. This can only be explained by the orientation of the bearing pockets relative to the sliding rails (see following measurements). Given that the bearing is supplied by a flow that decreases with increasing pressure higher stiffness can be achieved by establishing truly constant flow. At least equally important in regards to optimizing the stiffness is to design the bearing such that no air gets entrapped in downstream of the pump.

3.11 Straightness

Figure 15 shows the location of the impedance probes that have been used to measure the straightness.

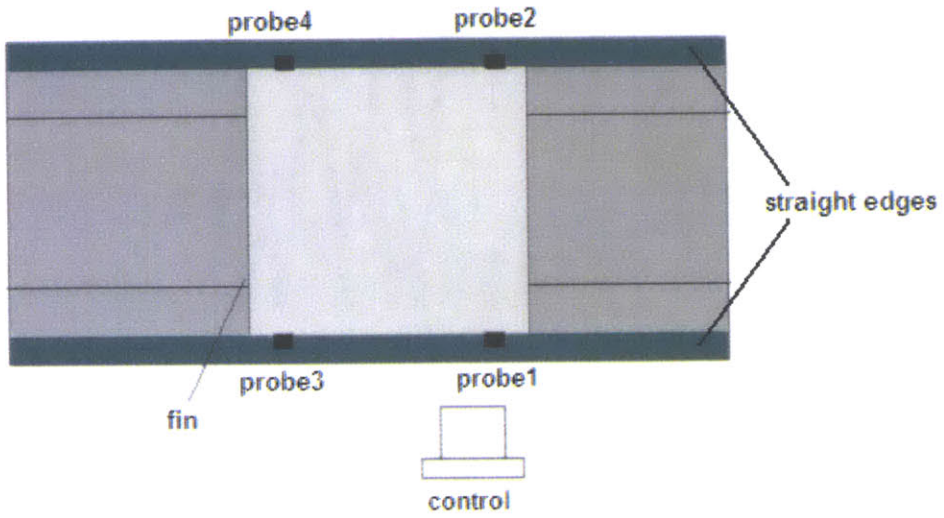

Figure 15: Location of the impedance probes

The raw data (distance to the straightedge) as measured by the probes is shown in the following two figures. The measured straightness is +/- 3microns. However, this includes surface tolerances of the straightedge.

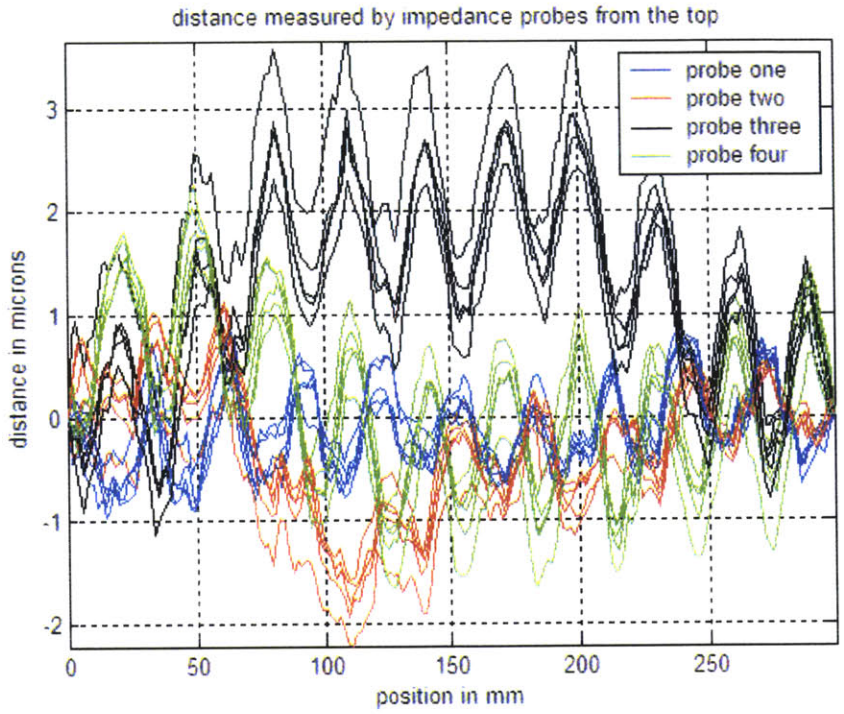

Figure 16: Distance measured by probes from the top

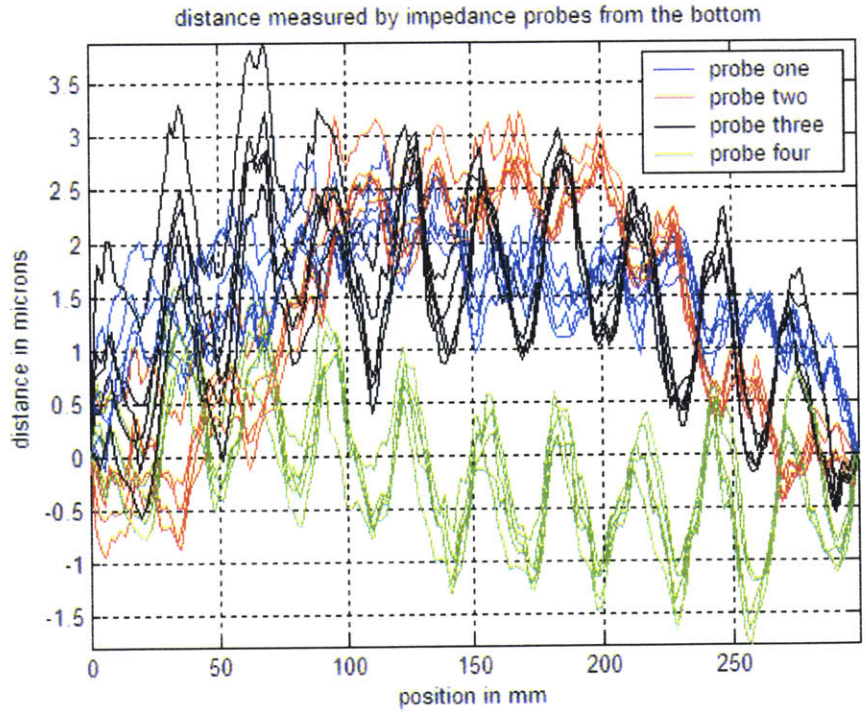

Figure 17: Distance measured from below the straightedge

In order to compensate for surface tolerances of the straight edge such as waviness reversal has been used. The distance between the straightedge and the probes has been measured with the probes above the straightedge. Then the straightedge has been flipped and the probes have been mounted below, measuring relative to the same face of the straightedge. By using reversal, the vertical straightness of the carriage independent of the straightness of the straightedge itself can be calculated as follows.

$$\Delta = 0.5*(d_1 - d_2) \qquad (8)$$

d_i *distance as measured by impedance probe i*

Δ *straightness of the carriage*

The resulting straightness including the effects of pitch of the carriage after reversal is +/- 1.5microns.

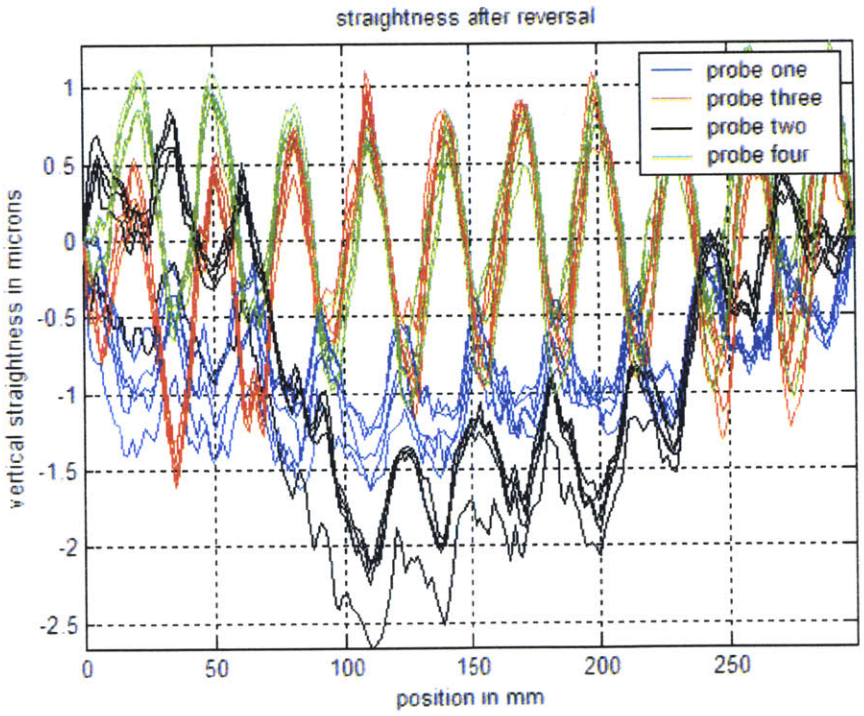

Figure 18: Measured straightness using reversal technique

When subtracting out the effects of pitch of the carriage, the straightness is about +/-0.75microns over a range of motion of 300mm. The measured straightness is mostly independent of flow. Only for very low flows is the measured straightness

slightly worse (only in the case of probe four). This can be explained by the thinner hydrostatic gap at low flows. The thinner the gap the more the surface quality of the sliding rails will influence the straightness. Figure 18 shows the impact of the sinusoidal pitch of the carriage on the straightness measured by probe one and two is less than the impact of the pitch on the straightness measured by probes three and four. This can be explained as follows: If the "magnetic center" of the motor forcer is not equal to its geometrical center (see Figure 19) the motor will pitch around an axis that is not in its geometrical center plane. However, the motor forcer and the impedance probes are mounted symmetrical to the center plane of the carriage. As vertical distance is equal to the horizontal distance from the "magnetic center" of the forcer multiplied by the pitch angle, probes on different sides of the geometrical center of the carriage will be more or less impacted by the pitching.

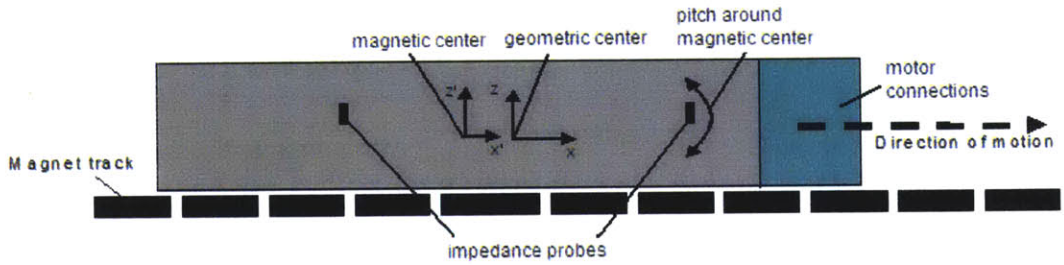

Figure 19: Geometric center and magnetic center of motor forcer

3.12 Pitch, Yaw and Roll

A sinusoidal pitch of 0.6 to 0.7 arcsec magnitude could be measured with the motor moving the carriage at almost zero load as well as with the motor switched off and the carriage being moved by hand.

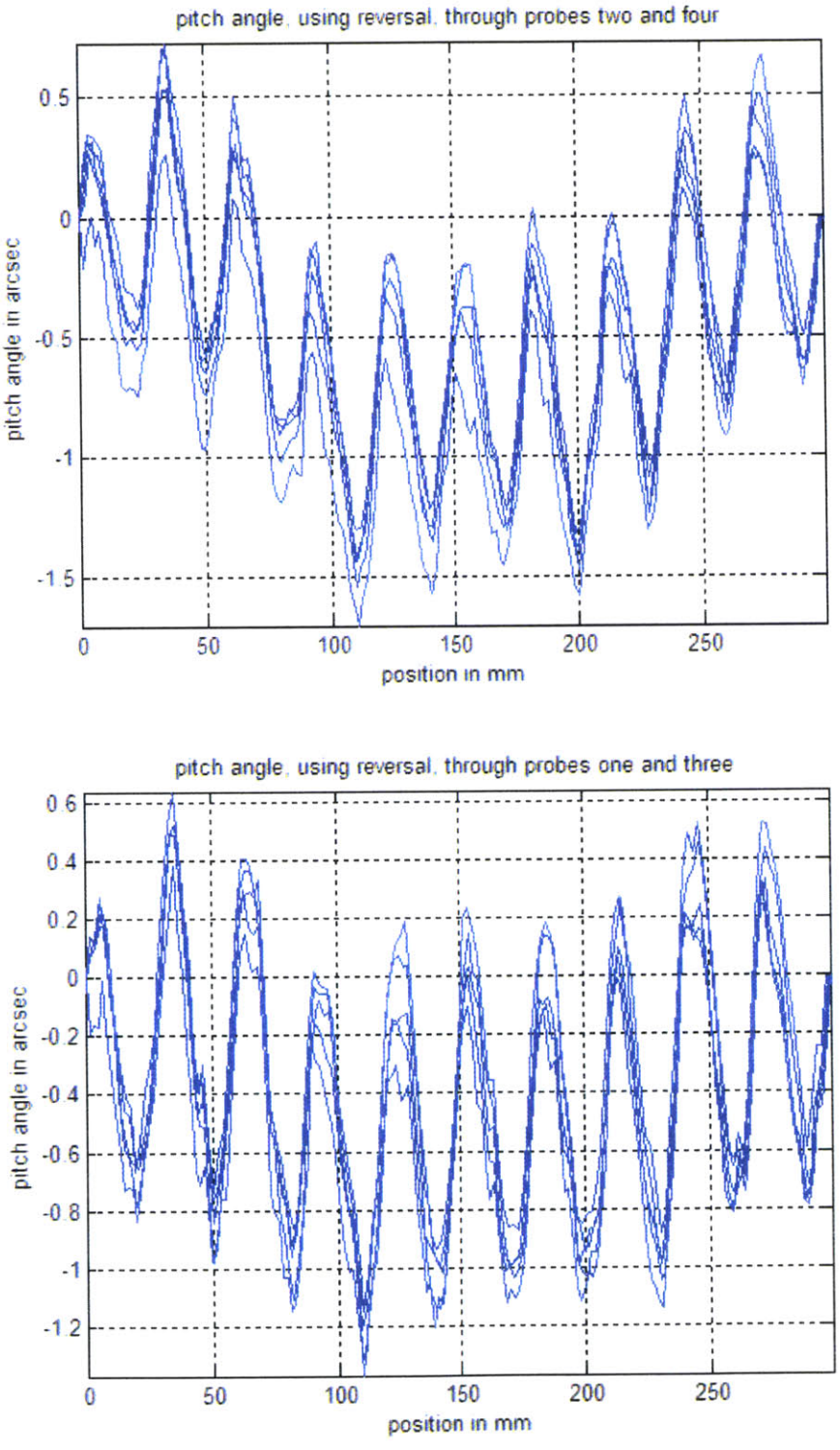

Figure 20: Pitch of the carriage

The sinusoidal pitch of the carriage is caused by the attraction between the magnet track and the motor forcer. It shows a periodicity of 29.5mm, which is equal to the magnet pitch of the magnet track.

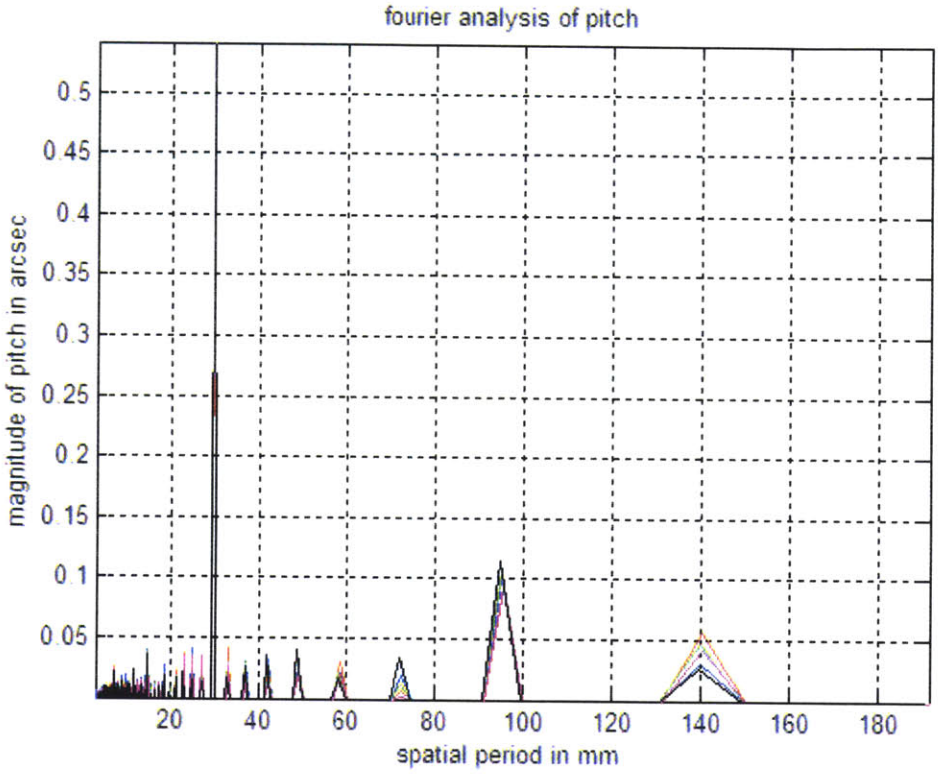

Figure 21: Fourier analysis of pitch of the carriage

Depending on the motor forcer's sheet metal geometry (the structure around which the windings are formed) and the magnetic field of the magnet track as well as on the relative position of the motor forcer over the magnet track, the attracting forces on the two halves of the motor forcer will differ. Given a periodic magnetic field of the magnet track the motor forcer will periodically pitch back and forth as it is moved along the magnet track. The more the magnet track's field resembles a sine curve the better it will be possible to compensate for the pitching, that is induced by the attracting forces between forcer and magnet track, by using external "pitch nullers".[7] However the influence of the motor

[7] "Nulling the Pitch Error of Permanent Magnet Open Face Linear Motion Components", Gerald Rothenhöfer, Alexander Slocum, 6th Euspen International Conference, Baden/Wien, May 2006

currents on the pitch of the carriage remains to be examined before compensation can be considered.

Since the motor is mounted at an angle there are force components in the horizontal y-direction that result from the magnetic attraction between the motor forcer and the magnet track. The hydrostatic bearing carriage has been designed such that the bearing preload caused by the magnetic attraction is almost evenly spread over all six bearing pockets. Thus the carriage will also show a sinusoidal yawing, that will be of the same order of magnitude as the pitching. The measured roll is +/- 0.6 arcsec.

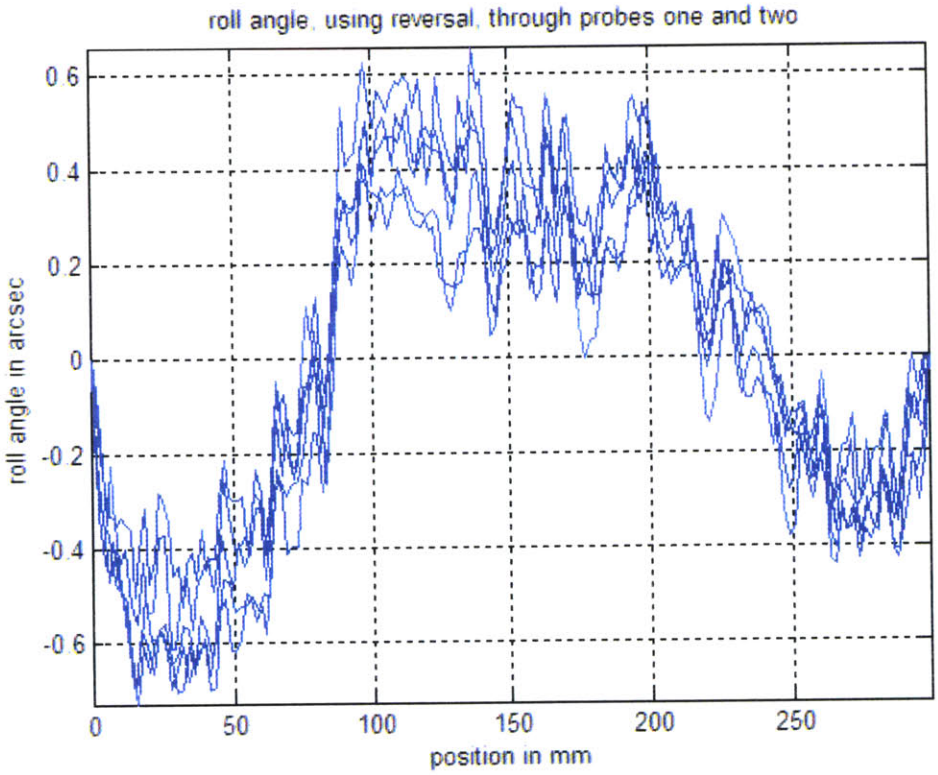

Figure 22: roll of the carriage, as measured by probes one and two

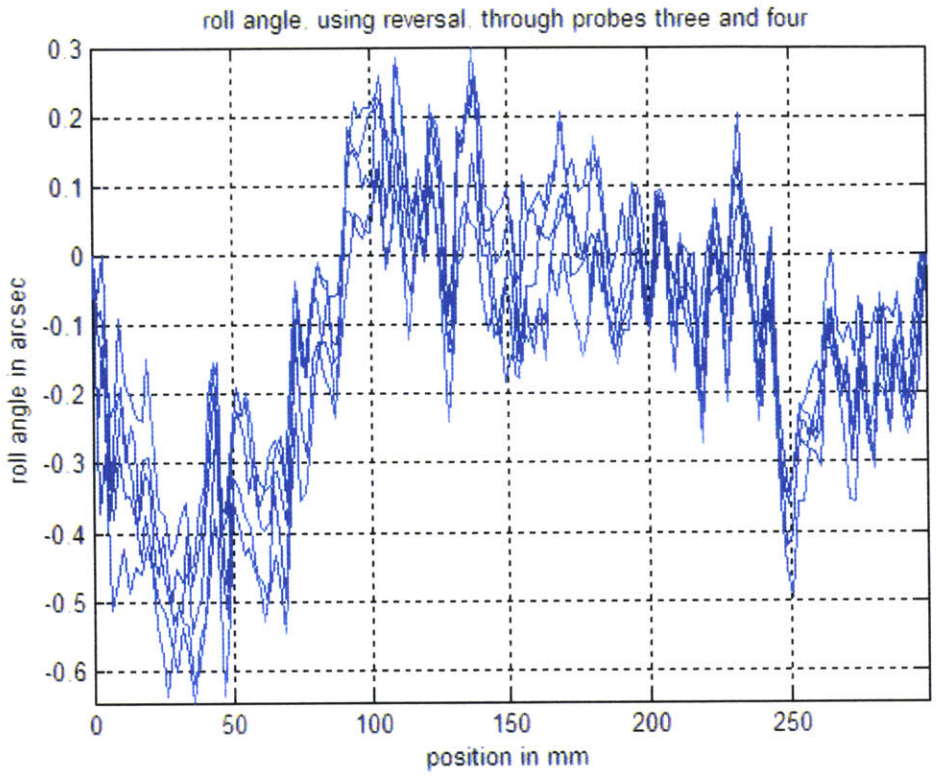

Figure 23: Roll of the carriage, as measured by probes three and four

3.13 Possible Design Changes for a Next Generation Hydrocline

Based on the presented measurement results following design changes are proposed for an improved version of the Hydrocline.

3.13.1 Pump Mount

Vibrations caused by the pumps may cause straightness noise on the order of less than 0.5microns. In order to take out this noise the pump mount should be changed such that vibrations caused by the pumps are dampened out before they reach the carriage or the bearing. This can be done by putting damping material in between the pump mount and the ceramics of the carriage.

3.13.2 Symmetric Pitching

As shown in previous chapters, the carriage does not pitch around an axis that is in the geometrical center plane of the carriage. In order to yield a "symmetrical pitching" the motor mount should be changed such that the "magnetic center" of

the motor, i.e. the center of pitch of the carriage, is coincident with the center plane of the carriage.

3.13.3 Pitch of the Carriage

Pitch nullers should be used in order to decrease the pitch of the carriage. Alternatively, standard open face linear motors as offered by Siemens, Anorad and others could be analyzed with respect to pitching and the best standard motor could be chosen.[8]

3.13.4 Inertia effects

In the case of very high accelerations (depending on the weight that is put onto the carriage and the stiffness of the bearing) the carriage will pitch. This effect can be overcome by mounting the motor such that the carriage is driven through its center of gravity.

3.13.5 Mounting

The mounting of the carriage has to be simplified in regards to accessibility of the mounting and assembly bolts, ease of centering the motor over the magnets, lifting off of the ceramic carriage and cable routing.

3.13.6 How to Further Improve the Bearing Stiffness

In order to further increase the stiffness of the bearing the pump control should be changed such that true constant flow is achieved. In a next step the flow control should be modified such that an increase in load i.e. pocket pressure leads to a proportional increase in flow. In this case theoretically infinite stiffness can be achieved. In reality the maximum possible stiffness will be limited by the torque speed (i.e. pressure-flow) curve of the pumps.

3.13.7 Achieving True Constant Flow

Currently the flow produced by the pumps is not constant because of pump internal leakage (flow per revolution decreases with pressure) and decreasing

---

[8] "Nulling the Pitch Error of Permanent Magnet Open Face Linear Motion Components", Gerald Rothenhöfer, Alexander Slocum, 6th Euspen International Conference, Baden/Wien, May 2006

speed of the pumps with increasing pressure. Both effects can be overcome as follows:

- By using a PI velocity controller a constant velocity can be maintained - within the limits given by the torque-speed curve of the DC motor. However the low resolution (two pulses per revolution) of the pumps' encoder signal will possibly cause problems when implementing a PI velocity control.

- A mathematical model of the internal leakage or a look-up table can be used to change the speed of the pumps with increasing pressure in order to compensate for the decreasing flow per revolution. In chapter 5 a model of is presented that also takes into account internal leakage of the pump.

3.13.8 Feedback Controlled Flow

In the ideal case, the bearing gap is constant independent of the load and transient, dynamic load changes. A constant bearing gap would mean a constant hydraulic outflow resistance of the bearing. However the outflow resistance of the bearing can only be kept constant if the flow out of the bearing is changed proportionally to changes in pressure i.e. load changes. In the static case this is easy to do since the flow out of the bearing is equal to the flow into the bearing. The flow into the bearing can be calculated based on the pump speed. If in addition the pocket pressure is measured, the outflow resistance of each bearing pocket can be calculated. A simple static control has already been implemented in a very first attempt. The results are shown in Figure 24 and Figure 25. The limitations of the static control that has been implemented are that the flow has been assumed as constant i.e independent of pressure. Furthermore the control has been implemented on a Microsoft Windows system and thus is inherently slow due to the limited cycle time of Windows. The under-damped response can be explained by the low encoder resolution of only 2 pulses per revolution and the proportional control of the pump speed.

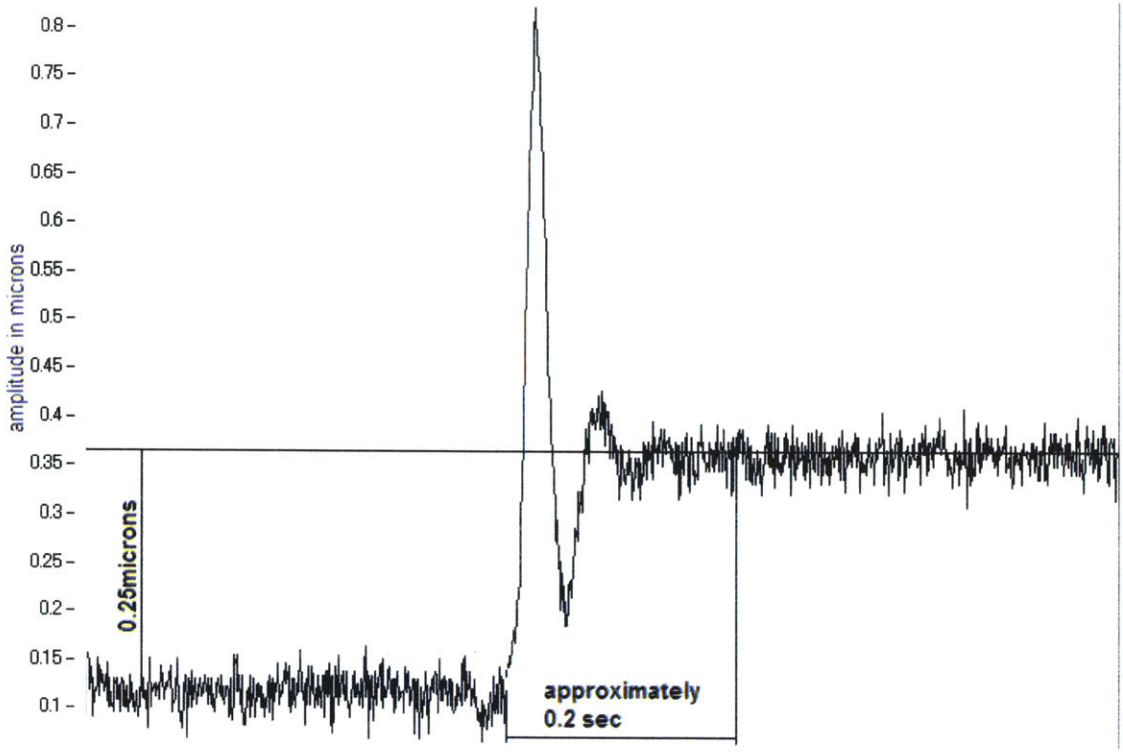

Figure 24: Changing bearing gap after -230N load step without control

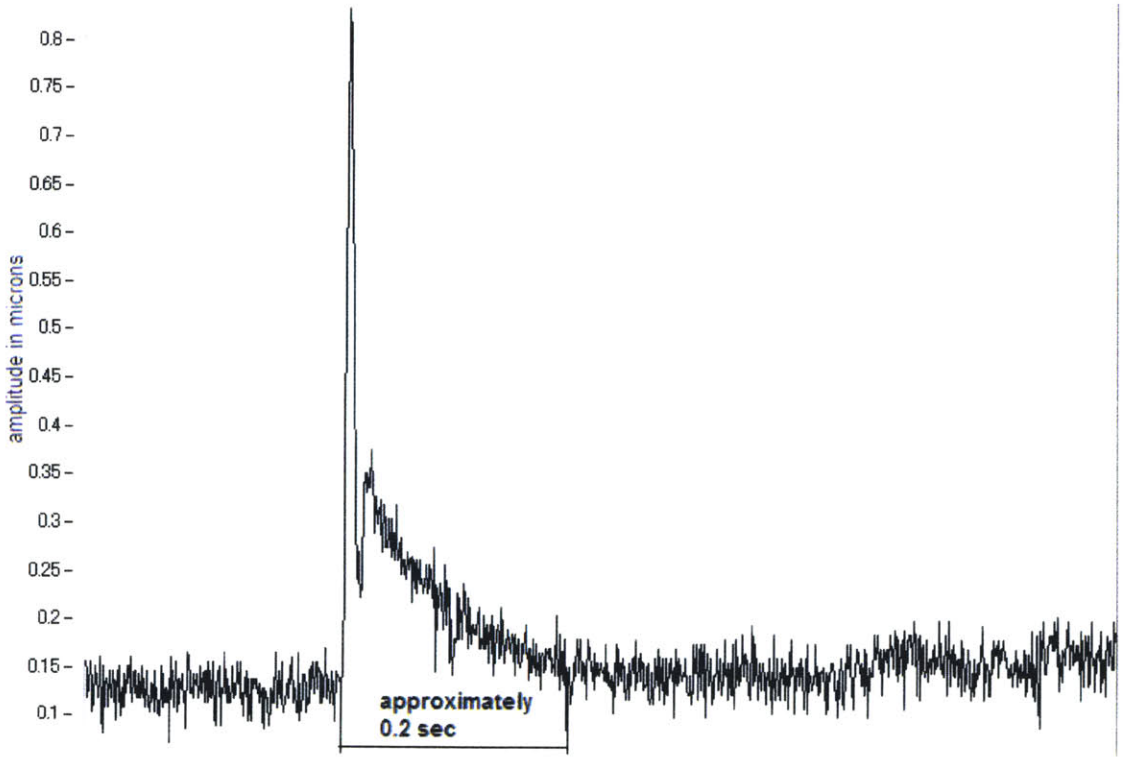

Figure 25: Changing bearing gap after -230N load step with static control

In the dynamic case some flow gets stored in the bearing system e.g. in the expansion of the plastic tubes that connect the bearing pockets to the pumps. Thus a model of the bearing will be necessary in order to calculate the flow out of the bearing. If the flow out of the bearing is known also in the dynamic case, dynamic load changes can be controlled in a similar way as static load changes. It remains to examine how fast such a control can react to a load change.

3.13.9 Method to Improve Straightness

In a first step the magnetically induced pitch of the carriage should be minimized by using external pitch nullers. If it should result that a compensation of the pitch is not possible by reasonable means due to the influence of the motor currents on the pitch of the carriage, the choice of another linear motor could be considered. Another option is to change the flow such that surface tolerances in the sliding rails are compensated by changing the hydrostatic gap. [9]

4 Designing a Single Pocket Test System

In order to double-check the results of the below presented dynamic model of a hydrostatic thrust bearing a test setup with a single hydrostatic bearing pocket has been built. The functional requirements for the test setup have been:

- Support the hydrostatic bearing pocket in tilt direction. Hydrostatic bearings have very low tilt stiffness and tilt of the bearing decreases the stiffness.
- The tilt support should not significantly change the dynamics of the system.
- In order to achieve significant bidirectional stiffness the bearing has to be preloaded.
- It should be possible to run the test setup on a force tester.

[9] Precision Engineering, July 2006, "Compensation for five DOF motion errors of hydrostatic feed table by utilizing actively controlled capillaries", C.H. Park, Y.J. Oh, E.Shamoto and D.W. Lee

- The bearing pocket has to be dimensioned such that it does not deform under pressure.
- The bearing pocket should be designed such that it behaves similar to the bearing pockets of the Hydrocline (same outflow resistance, same effective area, same squeeze film damping).
- Pocket pressure, bearing gap and pump velocity have to be measured when the test setup is being run.
- The same gear pump head as in the Hydrocline prototype should be used
- A PI velocity control of the pump should be implemented in order to make the pump speed independent of load (within a limited load range).

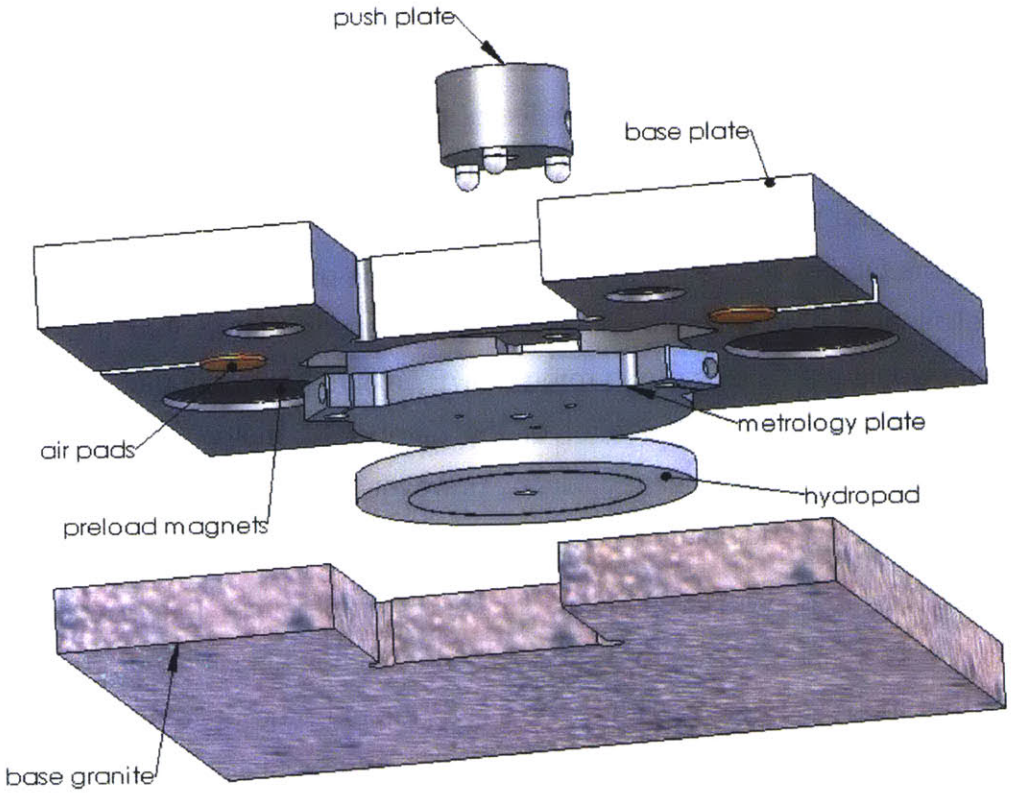

Figure 26: Single pocket test setup

4.1 Pump Selection

As discussed in earlier chapters the pumps that were used for the Hydrocline had the following problems:

- speed decreases with increasing pressure
- flow per revolution decreases with increasing pressure
- under-damped step response due to only two encoder pulses per revolution

All the problems could be solved by using a higher resolution encoder in combination with a PI velocity control and corresponding reference signal in order to compensate for the pressure dependent flow per revolution. After some searching a company was found that offers a DC motor driven pump with the same external gear pump head as the Hydrocline pumps. The motor shaft of the used DC motor sticks out to both sides of the motor such that the pump head could be attached to one side of the motor and the encoder disc could be mounted on the motor shaft on the other side of the motor. A magnet coupling couples the DC motor shaft to the driven gear of the pump head and at the same time eliminates any leakage path. The specifications stated that the magnet coupling would start slipping at a torque of 78.5mNm. The manufacturer claimed to have implemented a PI control of the pump (DC motor) speed using an encoder with 120 pulses per revolution. However, after receiving the pump the following problems and solutions were found:

- The pump had a strong eccentricity and thus produced lots of noise while it was jumping around on the lab table. Unmounting the pump revealed that the noise was caused by the attachment of the drive side magnet to the motor shaft. The magnet was molded into a plastic cup that was then fixed to the motor shaft by a steel set screw. Shortening the steel set screw could already decrease the eccentricity significantly. However, ultimately the drive side magnet had to be cut out of the plastic cup on a lathe and glued into a tight fit aluminum cup. Before

gluing in the magnet the aluminum cup was heated up with a hot air gun and shrink-fitted to the motor shaft.

- The PI control was only working for accelerating speeds whereas the pump speed was slowly stopped by friction if the reference signal was decreased. The pump controller was exchanged with a standard "Faulhaber" DC motor drive, as describe in chapter 5.8.
- The encoder disc was pushed on a flange and was held in position by a tooth lock washer. The flange was fixed on the motor shaft by a set screw. The mounting of the encoder disc on the flange was executed very poorly. The encoder disc was deformed like a potato chip which resulted in a sinusoidal noise superimposed on the actual velocity signal. Ultimately the encoder was replaced by a quadrature encoder with 500pulses per revolution.

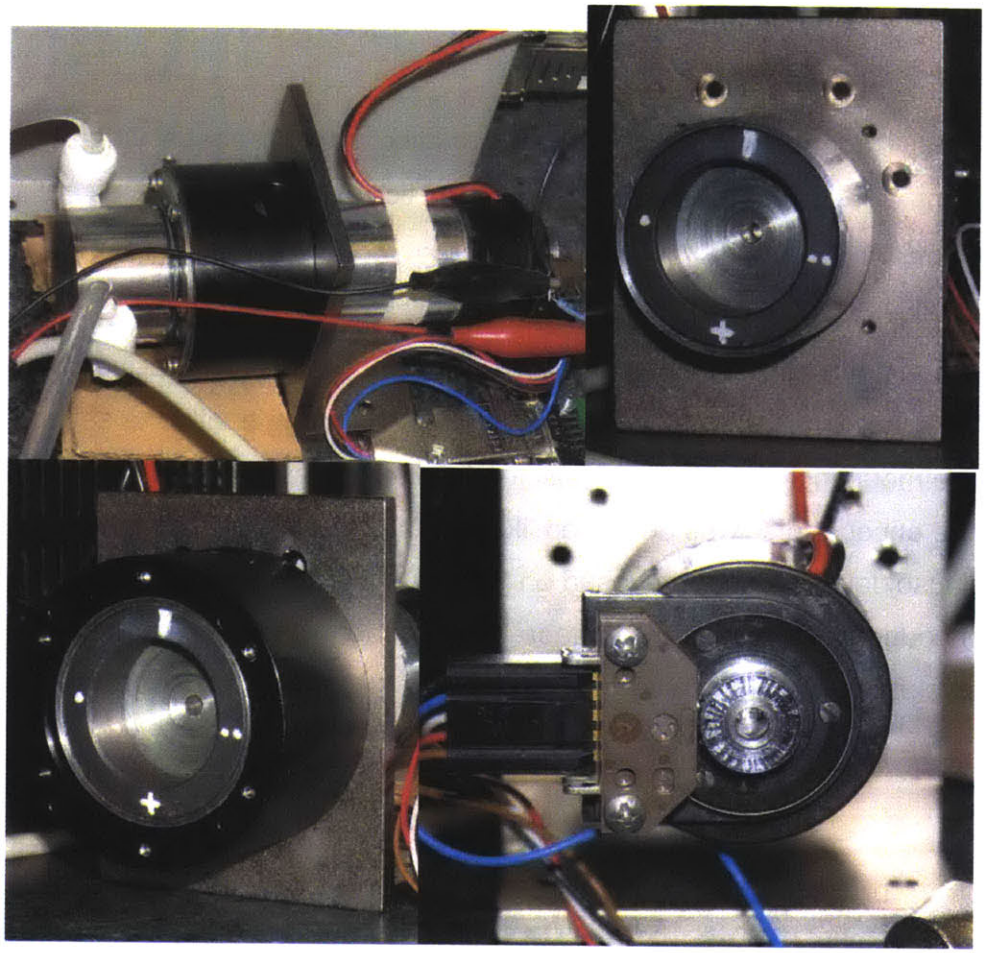

Figure 27: Pump motor (upper left) with encoder (lower right) and magnet coupling

4.2 Tilt Support and Magnetic Preload of the Hydrostatic Bearing Pad

The following options were considered:

- **Air bushings:** In order to achieve sufficient tilt stiffness the air bushings would have had to be spaced far apart. In addition it would have been necessary to pot the bushings in place.[10]

[10] "The bushing mounts inside a bore on o-rings to be compliant enough to allow the bushing to self-align. In applications where higher stiffness is required, the bearing may be set in-place by a precision potting procedure", www.Newwayairbearings.com

neglecting the tilt stiffness of each bushing			
maximum load	N	1000	
maximum load angle	degree, radians	5	0.087266
length of shaft and hydro pad	mm	700	
tilt moment	Nm	30.50	
Bearing pad diameter	Mm	50	
acceptable tilt of bearing center	Microns	0.1	
acceptable tilt angle	radians, degree	4E-06	0.000229
Bushing length	Mm	76.2	
Bushing inner diameter	Mm	40	
Bushing radial stiffness	N/micron	33	
Bushing pitch stiffness	Nm/microrad	11	
maximum acceptable tilt moment	Nm	3.1	
maximum acceptable radial load	N	347	
Is load acceptable?		0	0
min. required spacing of bushings	Mm	679.85	

Table 3: Tilt support by air bushing

- **Flexure:** A flexure that could give sufficient tilt support would have significantly changed the dynamics of the bearing and therefore was ruled out.
- **Aerostatic thrust bearings:** In the final design three small, cylindrical air bearing pads with low stiffness (as compared to the stiffness of the hydropad) were placed in the corners of an equilateral triangle with the hydropad in its center of stiffness. The triangle was sized such that the the air bearing pads would give sufficient tilt support to the hydropad.
  By equilibrium of moments around the center of stiffness of an equilateral triangle it can be shown that:

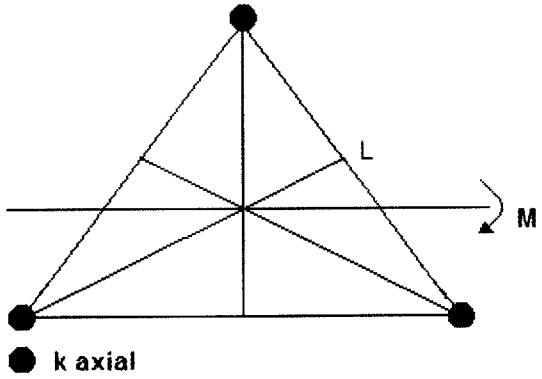

Figure 28: Tilt stiffness of triangle supported by three points (springs)

The angular stiffness of the triangle shown in Figure 28 is:

$$k_{angular} \geq 0.5 * k_{axial} * l^2 \qquad (9)$$

Viscosity of bearing fluid	Mu	Nsec/m^2	0.001	
hydro pad geometry				
Diameter of bearing pocket	Dp	Mm	130.84	
land width	Wl	Mm	19.67	
effective area	Aeff	mm^2,m^2	9706.99	9.71E-03
land area	Aland	mm^2,m^2	6869.01	6.87E-03
Nominal hydro gap	hhydro	microns, m	9	9.00E-06
Hydrostatics				
weight of carriage	M	Kg	15	
Magnetic preload		N	600	
Nominal preload of hydro pad	Whydro	N	747.15	
Nominal pressure	Pr	N/m^2	76970.30	
Pocket resistance	R	Nsec/m^5	9.37E+11	
Nominal flow	Q	m^3/sec, lpm	8.22E-08	4.93E-03
Nominal stiffness	khydro	N/micron	249.05	
Aerostatics				
Hhydro-hair spacer	T	microns, m	5.00	
stiffness of air pad	kair	N/micron	13	
additional preload for air pads	Wair	N	250.71	
Resulting air gap	hair	microns, m	4.00	
Double check preload:				
displacement of hydro pad under air pad preload	delta	microns, m	1.01	
load taken by each air pad		N	83.57	
Double check value			1.00	
total required preload **System tilt stiffness**	Wtotal	N	850.71	
Tolerable tilt	deltah	microns	2.7	
Tolerable tilt angle	phi	mrad, rad	0.04	4.13E-05
stiffness ratio air/hydro			0.15	
side length of equilateral triangle	L	M	0.1	
Resulting angular stiffness	ktilt	Nm/rad	64285.71	
max acceptable tilt moment	Ttilt	Nm	2.65	

Table 4: Tilt support by three air pads

The magnetic preload of the bearing has been designed for a 9micron hydrostatic bearing gap. As granite is not really magnetic [11], pieces of 440C stainless steel[12] have been glued to the surface of the granite plate.

[11] even though slightly

[12] only ferritic stainless steels such as 440C are magnetic. Addition of Nickel and/or Chromium will make the steel martensitic or austenitic and thus motor only slightly magnetic.

	Cost	Changing dynamics	Tilt support
Additional hydrostatic pads	0	0	0
Air Bushings	++	++	-
Flexure	++	-	-
Aerostatic thrust bearing pads	++	+	++

Table 5: Selection of Tilt Support

4.3 Design of the Metrology Frame

- In order to accurately measure the hydrostatic gap a tight metrology loop was desirable. For this purpose three capacitance probes [13] were placed close to the outer diameter of the hydropad. All three probes were mounted into the same aluminum "metrology plate". The hydropad was glued to the metrology plate. The metrology plate was then screwed to the base plate by three screws. In order to leave room for deformation of the metrology plate/hydropad assembly three spacer washers were put in between the metrology plate and the base plate. The bolt radius was determined such that the deformation of the metrology plate in the area of the capacitance probe holders was minimized (airy points [14]).

[13] Lion Precision

[14] If a beam of length l is supported at n points, the supporting points should be spaced apart by l/sqrt(n^2-1) . No error in parallelism of the ends of the beam results.

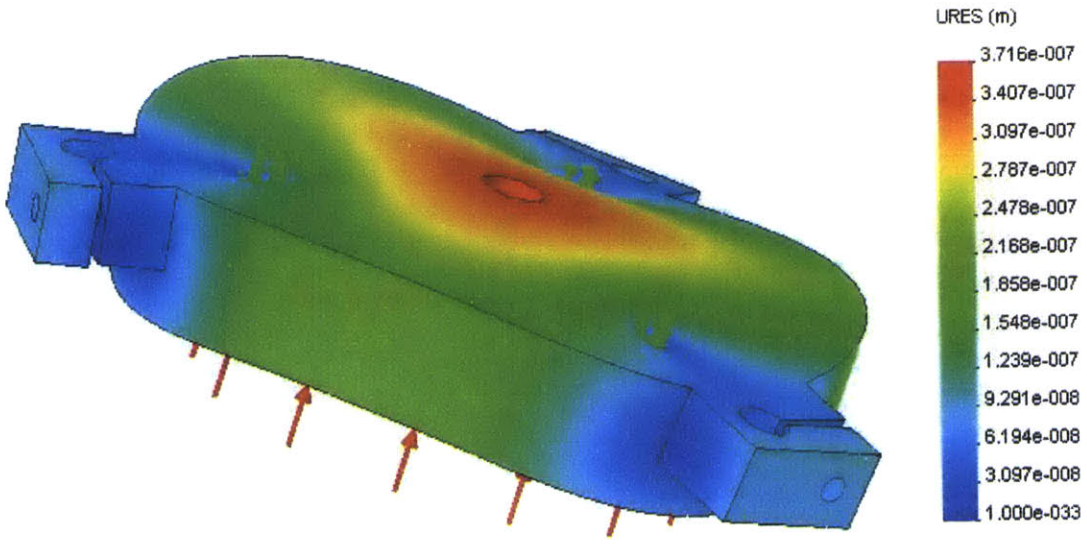

Figure 29: FEA of metrology plate

4.4 Design of the Push Plate

The functional requirements for the push plate have been:

- has to include the fluid supply connection for the hydropad
- has to include a mount for the pressure transducer
- it has to be possible to transmit pushing force exerted by a wobble pin
- the outer diameter of the push plate should not exceed 25mm (bench press weights have a 25mm hole, it should be possible to load those easily available weights on the bearing)
- the position of the push plate on the base plate should be highly repeatable

The push plate has been designed such that pressure transducer and fluid supply can optionally be mounted either to the side (diameter) of the push plate or to the top of the push plate. If the push plate is loaded by pushing through a wobble pin the pressure transducer and the fluid supply have to be mounted to the side of the push plate (not enough space at top). If the bearing is loaded by

weights the pressure transducer and the fluid supply are mounted to the top of the push plate (25mm diameter should not be exceeded).

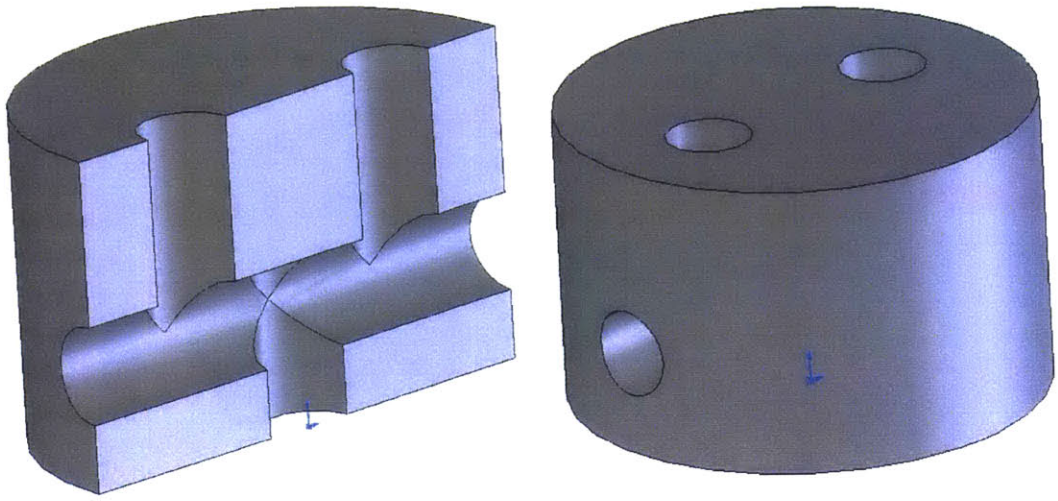

Figure 30: Push plate

A kinematic coupling has been used in order to position the push plate on the base plate as repeatably as possible. A threaded PTFE tube has been used in order to connect the fluid supply through the push plate to the hydropad.

4.5 Improving the Test Setup

Due to the pieces of stainless steel that have been glued to the granite surface and that stick into the base plate, the bearing can only be moved by +/- 1mm. In order to be able to quickly double-check whether the bearing is floating or not, without having to measure the bearing gap, the cut outs in the base plate should be made such that the bearing can be rotated around its center axis. Ideally one big magnet ring should be used in order to preload the bearing. In this case the bearing would still be constrained in x and y-direction, but it would be possible to quickly double-check whether the bearing is floating or not. Currently the capacitance probes are mounted to the metrology plate. This has the disadvantage that the probes are very close to the bearing fluid (here water). If wetting of one of the probes should occur, the probe will shorten out. In order to avoid this it would be better to attach the probes to the top of the back plate and let the target stick out through the back plate. This would have the further

advantage of easier mounting of the probes (100micron range). Alternatively impedance probes, that are not sensitive to water exposure, could be used.

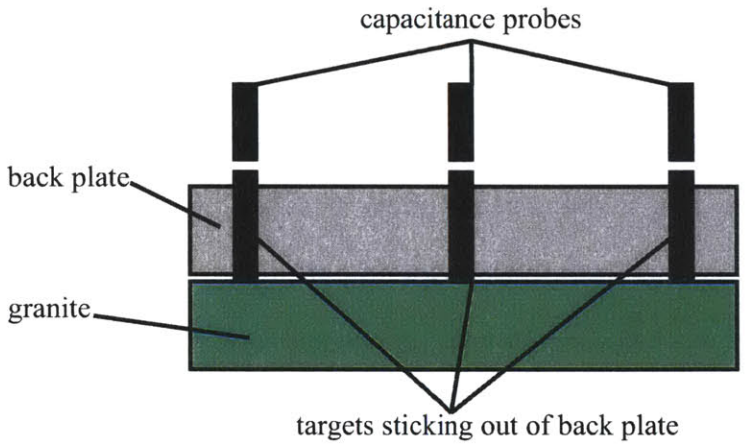

Figure 31: Improved probe mount

5 Dynamic Model of a Hydrostatic Thrust bearing

The simplest way to model the reaction of a hydrostatic bearing to a load change is to consider it as a spring with a finite stiffness in parallel to a damper and preloaded by a mass. It can be seen that the bearings' reaction to a load change is a displacement. If the bearing is supplied with fluid from a positive displacement pump where the pump flow is proportional to the pump speed it should be possible to increase the stiffness of the bearing by changing the pump speed depending on the pocket pressure or the bearing gap. As it is possible to change the bearing gap by changing the flow an increase in load (decrease of the gap) can be compensated by an increase in flow (increase of the gap). Theoretically it should be possible to reach infinite stiffness by increasing the flow proportionally to the increase in pressure (as described above). However the pressure-flow characteristics of the pump, in the case of very slow load changes and the dynamics of the entire system in the case of dynamic load changes, limit the achievable stiffness. In order to control the hydrostatic bearing gap it does not seem to be necessary to directly measure the bearing gap. Rather it should be possible to control the bearing gap based on a model of the bearing, the flow (speed of a positive displacement pump) and the pressure in the bearing gap.

Both, pump speed and pressure are easy to measure. Combined with a stiff machine frame (structure) such a feed-back controlled hydrostatic bearing could significantly contribute to increase the accuracy of present wafer manufacturing tool machines. A model of a hydrostatic thrust bearing that is supplied by a PI-velocity controlled DC motor, which drives an external gear pump, has been developed. The model can predict the measured static performance, such as flow rates, load capacity and stiffness of the above described Hydrocline.

5.1 Model Assumptions and Component Specifications

In the presented model the following simplifying assumptions have been taken:

- Fluid is incompressible
- No mechanical deformation of supporting structure
- Laminar flow in bearing
- Density of fluid is zero (weightless fluid)
- Constant flow supply (under static load)
- No limitation on pump speed or pressure. Therefore the simulation results have to be double-checked in regards to speed limits and pressure limits of the pump. The speed limit of the pump is at 5000rpm. The magnet coupling starts slipping at 78mNm. The recommended pressure range for the pump head reaches up to 275kPa.
- Effective bearing area: A_{eff}=.00951m^2
- γ=5.25e-4Nsec/m^2 (pocket resistance proportionality factor, $R=\gamma/h^3$)
- Squeeze film damping has been approximated as: [15]

$$b = K_s \frac{\mu w^3 l}{h_0^3} \qquad (10)$$

where μ is the viscosity of the bearing fluid, w is the width of the bearing lands (area that contributes to the squeeze film damping), l is the total length of the bearing lands and Ks is a geometric factor related to the

[15] http://pergatory.mit.edu/2.75/2_75%20Lectures/PMD%20Topic%2018a%20Hydrostatics%201.pdf

bearing. For a rectangular bearing:

$$Ks = 0.7925 - \frac{1.1005}{e^{\frac{w}{l}}} + \frac{0.0216}{e^{\frac{w}{l}}} + 0.0153\frac{w}{l} \qquad (11)$$

- The moment of inertia of the magnet cup + drive side magnet has been calculated as $58*10^{-5}kgm^2$. Comparison of the measured frequency response of the motor (magnet cup + drive side magnet mounted to the motor shaft) with the predicted frequency response lead to a corrected moment of inertia of $37*10^{-5}kgm^2$
- The moment of inertia of the load side magnet and gears has been calculated as $1.5*10^{-5}kgm^2$
- Based on the motor current and change in rotor position under load the stiffness of the magnet coupling has been measured as 0.266Nm/rad
- Based on the pump specs the relation of pressure and motor torque has been linearized. The proportionality constant is $k_{T/p}=1.04*10^{-8}m^3$.
- Based on the pump specs the no-pressure torque has been calculated as $T_{(p=0)}=4mNm$
- The pump is driven by a Faulhaber "3557012CS" DC-motor (R=1.34Ω, L=220 µH, k_T=20.9mN/A, T_{stall}=185mNm, =5400rpm, V_{supply}=12V).[16]

5.2 Constant Flow Behavior of the Bearing

Under the assumption of constant flow the behavior of the bearing is dominated by its outflow resistance that is inversely proportional to the third power of the gap. The simplest model can be built by linearizing this resistance as follows

[16] www.faulhaber.com

5.3 Linearized Model of the Modulated Outflow Resistance

$$R_{out} \approx R_0 + \left[\frac{\partial}{\partial h}\left(\frac{\gamma}{h^3}\right)\right]_{h=h_0} = R_0 - 3\frac{\gamma}{h_0^4}h \qquad (12)$$

$$\Delta p = Q_{out}\Delta R_{out} = Q_{out}(-3)\frac{\gamma}{h_0^3}\frac{1}{h_0}h = -3\frac{p_0}{h_0}\Delta h \qquad (13)$$

$$\Rightarrow k = -3\frac{F_0}{h_0} \qquad (14)$$

$$Q_{in} = Q_{out} + Q_{stored} \qquad (15)$$

$$Q_{stored} = \frac{\partial h}{\partial t}A_{eff} \qquad (16)$$

F_0 – *nominal load*

h_0 - *nominal gap*

γ – *proportionality factor, depends on geometry of bearing pad*

p – *pressure*

Q – *flow*

A_{eff} – *effective bearing area, depends on geometry of the bearing pad*

According to the above equations the linearized outflow resistance acts like a spring. This coincides with the general observation that a hydrostatic bearing shows spring like behavior. The calculated stiffness is as found in diverse literature. However, this simplified model can not be right since a modulated resistance (i.e. the outflow resistance) is an energy dissipator and thus should not be modeled as energy storage as in Figure 32. In this model R describes the previously mentioned squeeze film damping.

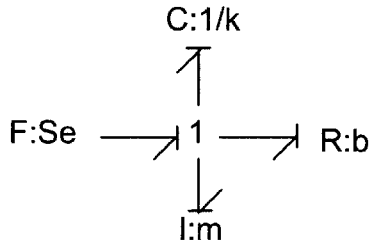

Figure 32: Bond graph model, linearized outflow resistance

5.4 Nonlinear Model of the Modulated Outflow Resistance

$$p = Q_{out} R_{out} = Q_{out} \frac{\gamma}{h_0^3} \quad (17)$$

$$\frac{\partial p}{\partial h} = -3 Q_{out} \frac{\gamma}{h^4} \quad (18)$$

$$\frac{\partial p}{\partial t} = \frac{\partial p}{\partial h} \frac{\partial h}{\partial t} = -3 Q_{out} \frac{\gamma}{h^4} \frac{\partial h}{\partial t} \quad (19)$$

$$\frac{1}{p} \frac{\partial p}{\partial t} = -3 \frac{1}{h} \frac{\partial h}{\partial t} \quad (20)$$

$$\Rightarrow p = p_0 (\frac{h_0}{h})^3 \quad (21)$$

Again the modulated resistance seems to behave like a spring (in this case a nonlinear spring) and again it is not possible to describe changes in flow, and thus the lift-off of the bearing. Even though the above models apparently are not good models of the bearing they still can give insight to the functioning of the bearing.

5.5 Model the Outflow Resistance as Modulated Resistance

A better model of the bearing is shown in Figure 33.

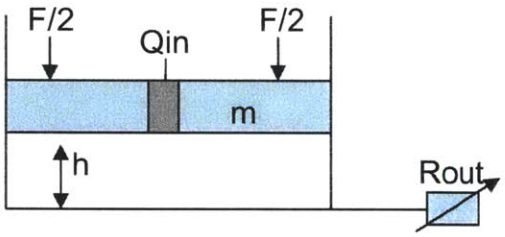

Figure 33: Model of a hydrostatic bearing pad

Here the weight of the column of bearing fluid within the bearing is neglected.

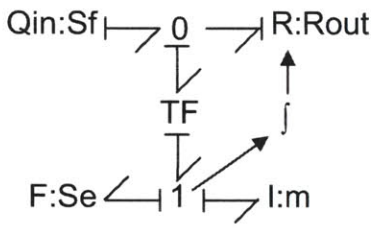

Figure 34: Bond graph model of modulated resistance and inertia

This model may seem right. However, the reader should wonder why the inertia is in differential causality, since according to the bond graph it could as well be in integral causality.[17] In theory integral causality is preferable due to more accurate computation. However, in this case it is not possible to run a simulation with the inertia in integral causality. This can be visualized as follows: If the bearing is at rest and the gap is zero the outflow resistance is infinite. Consequently a step in flow will cause infinite pressure in the bearing and infinite acceleration of the bearing. In order to fix this problem the simulation can only be run starting from a nonzero bearing gap. Apparently this can not be a good model either, since it only works in differential causality or for nonzero initial gaps. Furthermore, when having a second look at the above bond graph model the reader will realize that this model can not be accurate since there is no elasticity. However, it is not

[17] "System Dynamics: Modeling and Simulation of Mechatronic Systems", by Dean C. Karnopp, Donald L. Margolis, and Ronald C. Rosenberg (Hardcover - Jan 3, 2006)

realistic to have a fluid supply system without elasticity in the tubing or the fluid itself (bulk elasticity). Also the pump will exhibit a pressure dependent leakage flow where fluid flows back from the high pressure side to the low pressure side. This can be confirmed by measuring the flow per revolution of the bearing for different pressures (as shown in previous chapters).

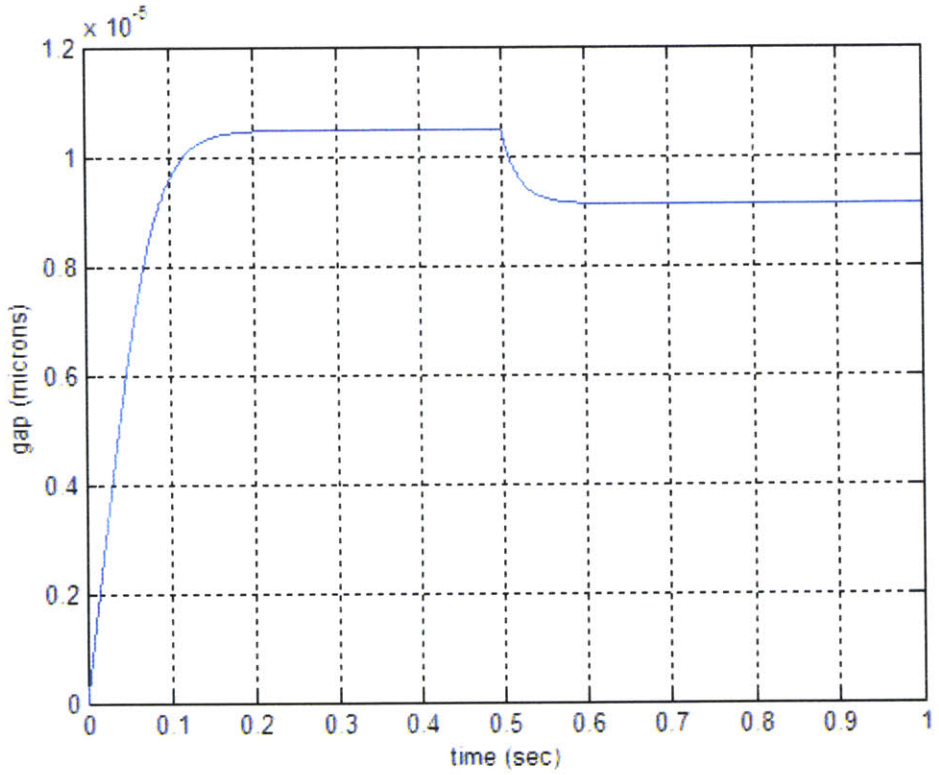

Figure 35: Modulated resistance and inertia model, step input flow (Q_{in}=1.05e^{-7}m^3/sec) at t=0sec, step input load (+900N) at t=0.5sec

5.6 Improved Model with Elasticity of Tubing and Leakage Flow

If the elasticity of the tubing is being included in the model a simulation of the model can be run in all integral causality. The elasticity of the tubing has been calculated as follows:

$$0 = 2\sigma t + pD \Rightarrow \sigma = \frac{p}{2t} D \tag{22}$$

$$\varepsilon = \frac{\sigma}{E} = \frac{pD}{2tE} \tag{23}$$

$$\Delta D = \varepsilon D = \frac{pD^2}{2tE} \tag{24}$$

$$\Delta V = L\pi\left(\frac{(D+\Delta D)^2}{4} - \frac{D^2}{4}\right) = \frac{L\pi}{4}\left(2D + \frac{D^2}{2tE} p\right)\frac{D^2}{2tE} p \tag{25}$$

$$p = \frac{2tE}{D^2}\left(-D + /- \sqrt{D^2 + \frac{4\Delta V}{L\pi}}\right) \tag{26}$$

after linearization at $\Delta V = 0$

$$p = \frac{2tE}{D^3}\Delta V \tag{27}$$

$$k_t = \frac{2tE}{D^3} \tag{28}$$

D – *inner diameter of tubing*

p – *pocket pressure*

t – *thickness of tubing*

ΔV – *volume change*

σ – *normal stress in tubing*

With the elasticity of the tubing included the behavior of the bearing can be described by:

$$\frac{\partial^2 h}{\partial t^2} = \frac{p * Aeff - F - F_b}{m} \tag{29}$$

$$Q_{in} = Q_t + Q_{out} + \frac{\partial h}{\partial t} * Aeff + Q_{leak} \tag{30}$$

$$Q_{out} = \frac{p}{R_{out}} \tag{31}$$

$$Q_{leak} = \frac{p}{R_{leak}} \tag{32}$$

$$p = k_t * \int Q_t * dt + p_0 \tag{33}$$

F_b – *damping force due to squeeze film damping*

Q_t – *flow that gets stored in the tubing*

In order to achieve a model that can simulate the lift-off of the bearing the support has to be included in the model. This can be done by an activated junction structure.

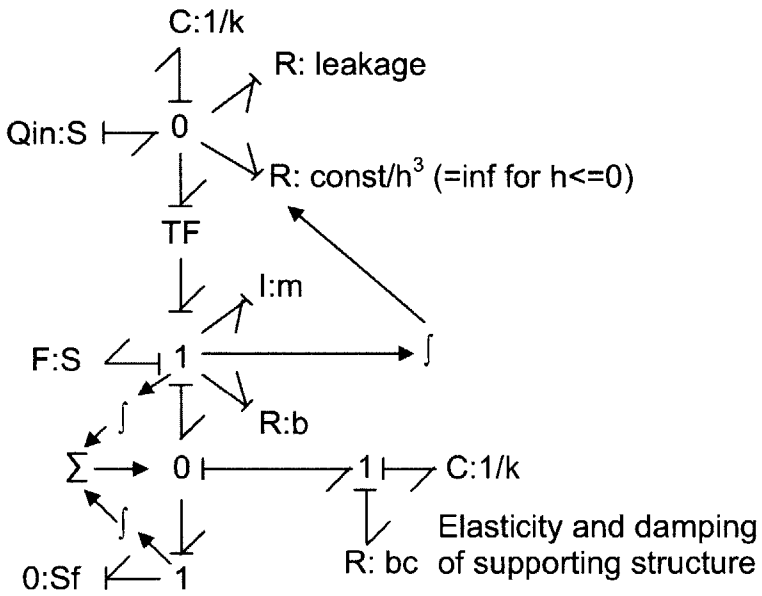

Figure 36: Complete model of hydrostatic bearing

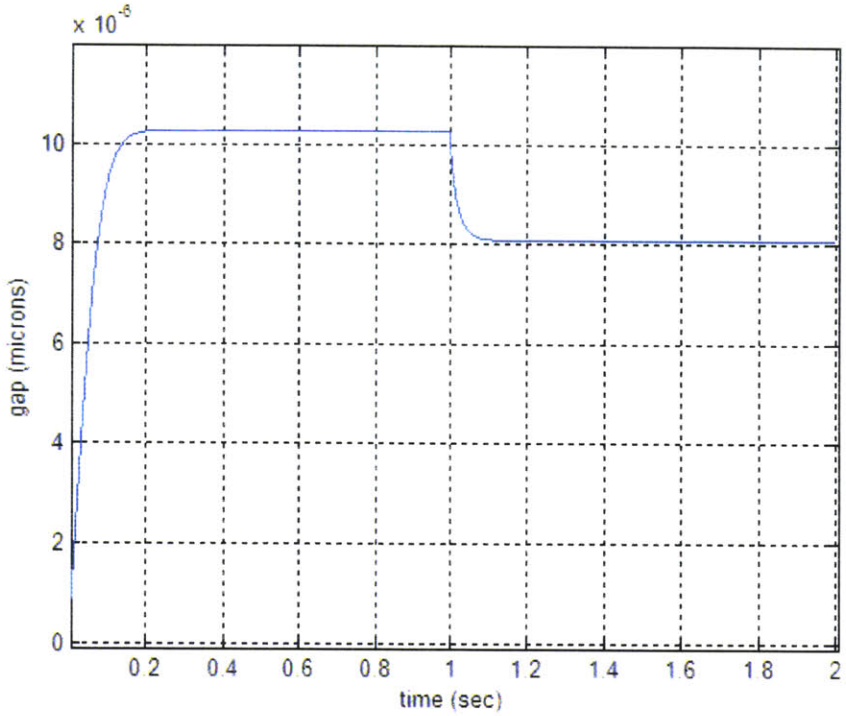

Figure 37: Complete model, step in flow at t=0sec, step in load (+90kg) at t=1sec

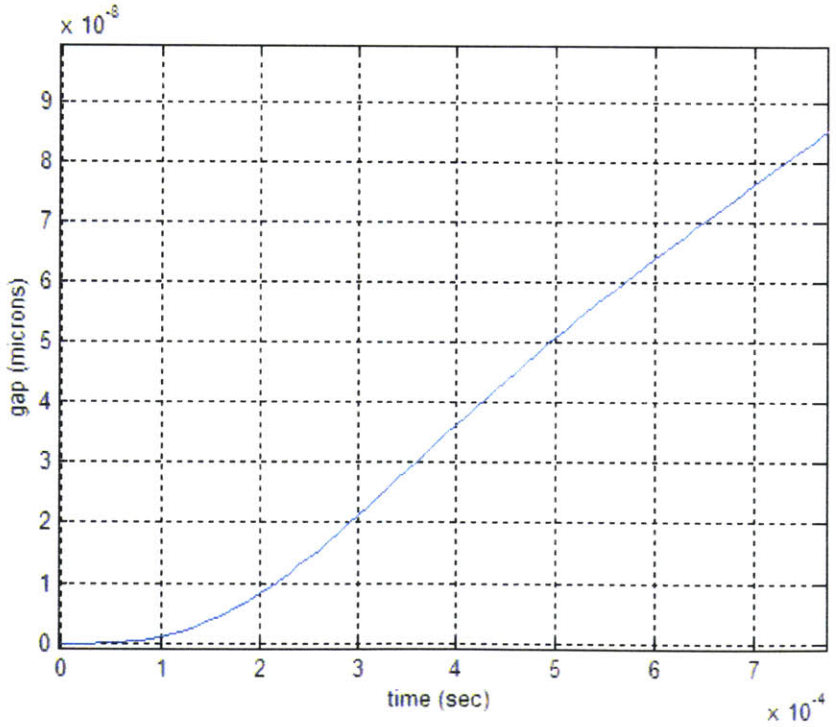

Figure 38: Lift off of the bearing after step input flow

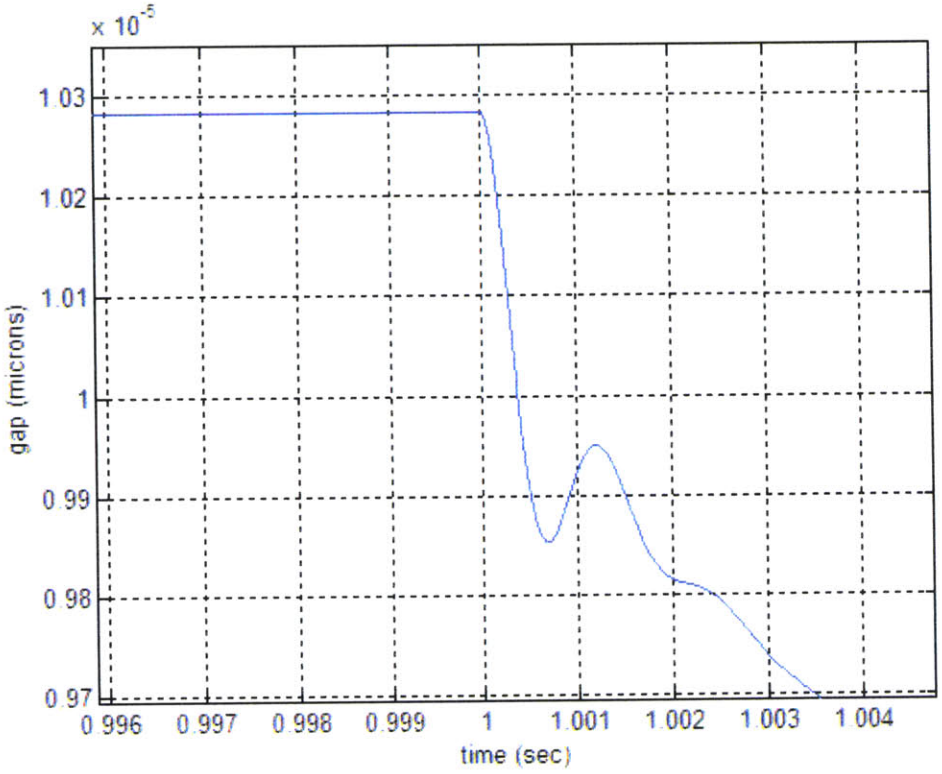

Figure 39: Slight over-swing after load step due to elasticity of the tubing

5.7 Comparison between Measured and Modeled Step Response

In order to compare the two step responses it has to be taken into account that the Hydrocline carriage is supported in the vertical direction by four bearing pockets. Therefore its stiffness is expected to be four times higher than the predicted stiffness for only one bearing pocket. Consequently the model is reasonably accurate in predicting the static performance of the bearing such as the bearing gap and the stiffness. However the model can not explain the overshoot in the step response of the Hydrocline carriage. It is believed that the overshoot is caused by the motor dynamics of the pump (proportional control with only two pulses per revolution encoder resolution).

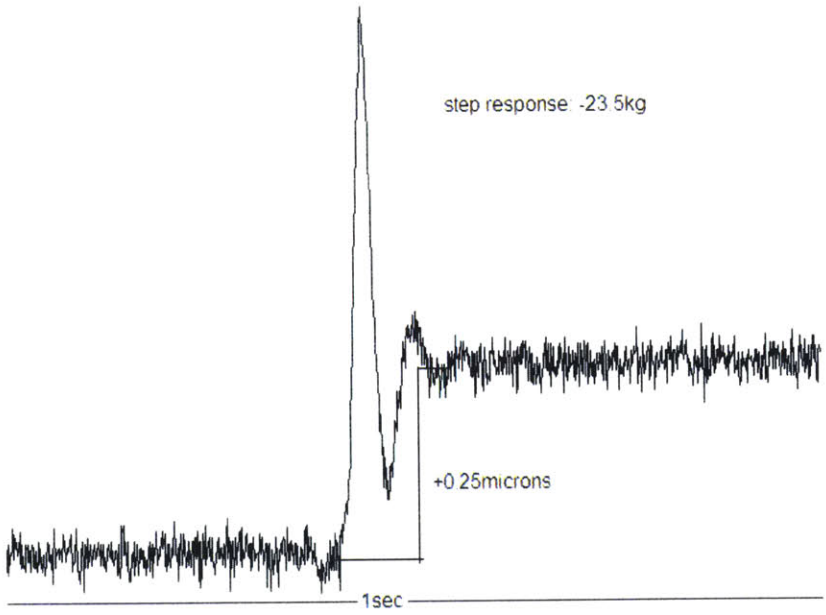

Figure 40: Measured response of Hydrocline (four pads in vertical directon), 2500rpm

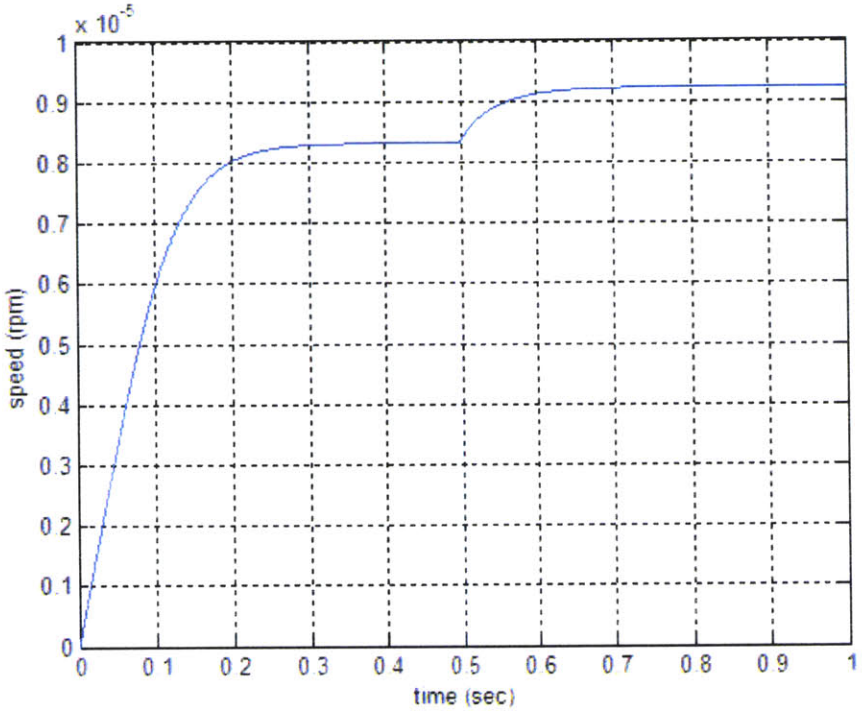

Figure 41: Step response of single pad model, 2500 rpm

5.8 Including the Motor Dynamics in the Model

The following model exclusively describes the dynamic behavior of the single pocket test system. The Hydrocline bearing has different pump dynamics and therefore the following model will not describe the dynamic response of the Hydrocline carriage. However the model can be used in order to proof the feasibility of an infinite stiffness control. Furthermore the model can be used in the dynamics design and dimensioning of hydrostatic bearings. So far the dynamics of the pump have been neglected. In the case of the single pocket test setup, as described in chapter 0, the dynamics of the pump include the DC motor (see appendix) as well as the dynamics of the magnetic coupling.

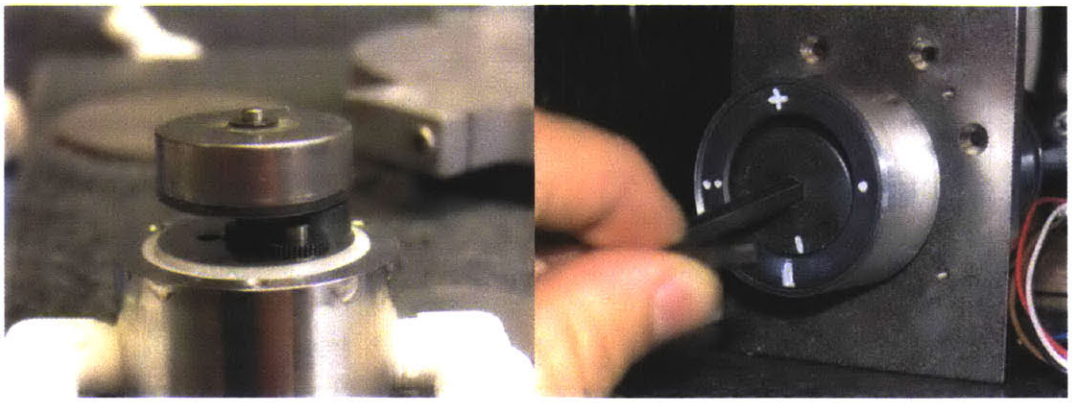

Figure 42: Pump head side of magnet coupling (left), motor side of magnet coupling and stiffness test (right)

The dynamics of the magnet coupling have been approximated by a spring mass dashpot. The stiffness of the magnet coupling has been measured based on the motor current (see appendix). The damping has been estimated such that an over-damped response resulted. Based on first measurements this estimate seemed to be reasonable.

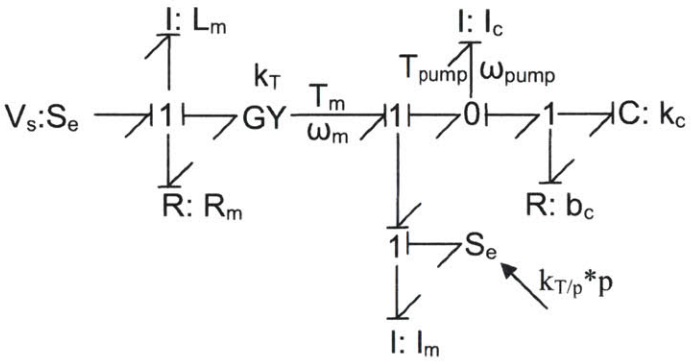

Figure 43: Bond graph model of the motor including the magnetic coupling and the back effect of the bearing

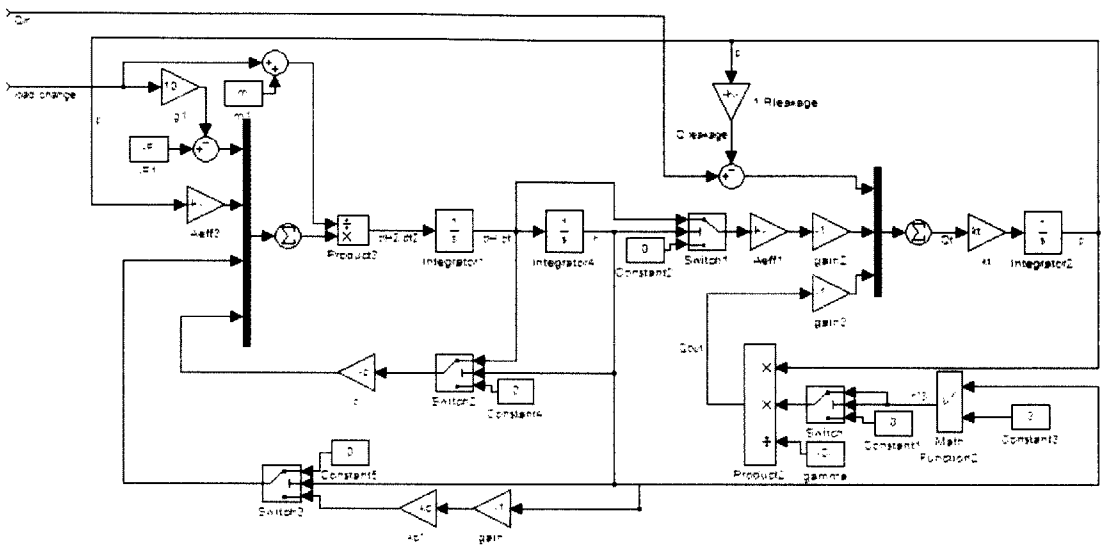

Figure 44: Model of the hydrostatic thrust bearing

The above model correctly models the dynamics of the bearing and the pump, but it does not yet include the velocity feedback loop that controls the pump speed. The velocity was controlled by a standard DC motor drive.[18] Unfortunately the dynamics of the drive were unknown. Since it was not possible to simply measure the open loop frequency response, the dynamics of the drive had to be identified as follows:

The model of the DC motor (see appendix), with the magnet coupling not engaged, predicts the open loop frequency response shown in Figure 45 and closed loop step response shown in Figure 46. Figure 46 compares the step response of the model with the measured step response of the motor and thereby confirms the model.

[18] Faulhaber MCDC2805

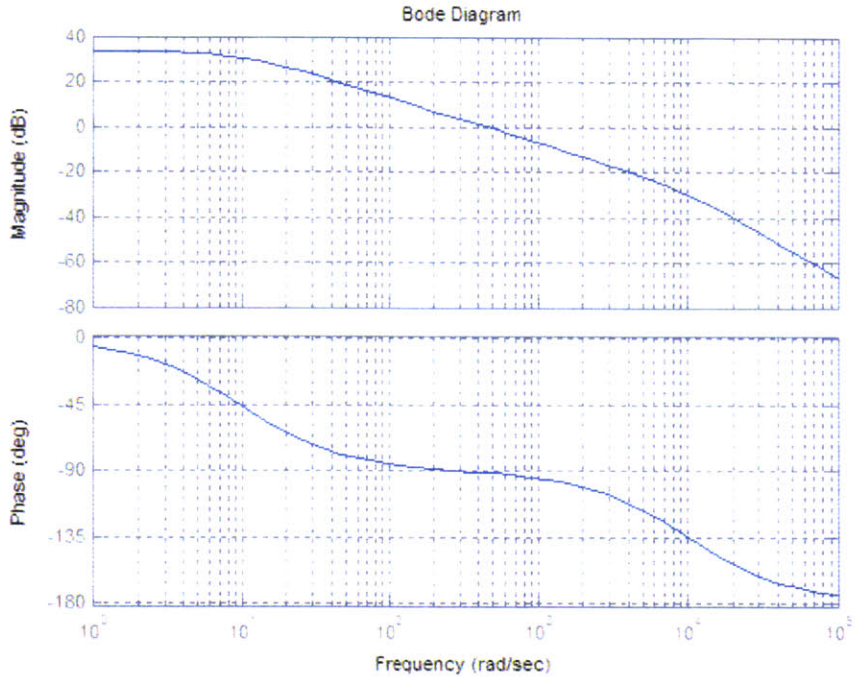

Figure 45: Predicted DC motor frequency response, magnet coupling not engaged

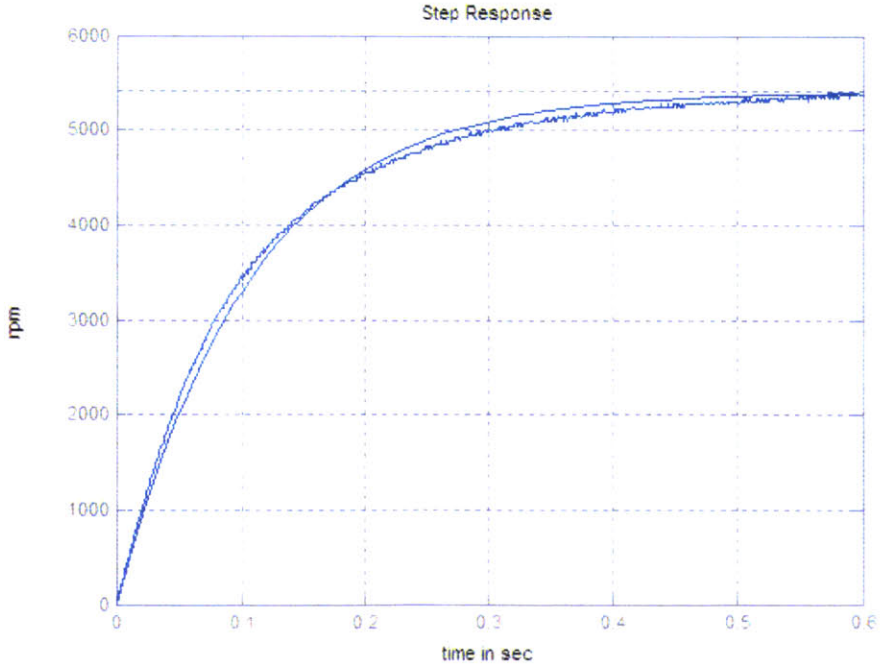

Figure 46: Measured and predicted DC motor step response (11.84V)

It was assumed that the drive (blackbox that had to be identified) implemented at least a PI-controller. The PI controller parameters have been determined as follows:

- k_p=0.00255 (maximum possible proportional gain)
- k_I=1.5

This corresponds to a controller zero at k_I/k_p=588rad/sec and a controller pole at 0 rad/sec. The resulting frequency response of the open loop and step response of the closed loop are shown in Figure 47 and Figure 48.

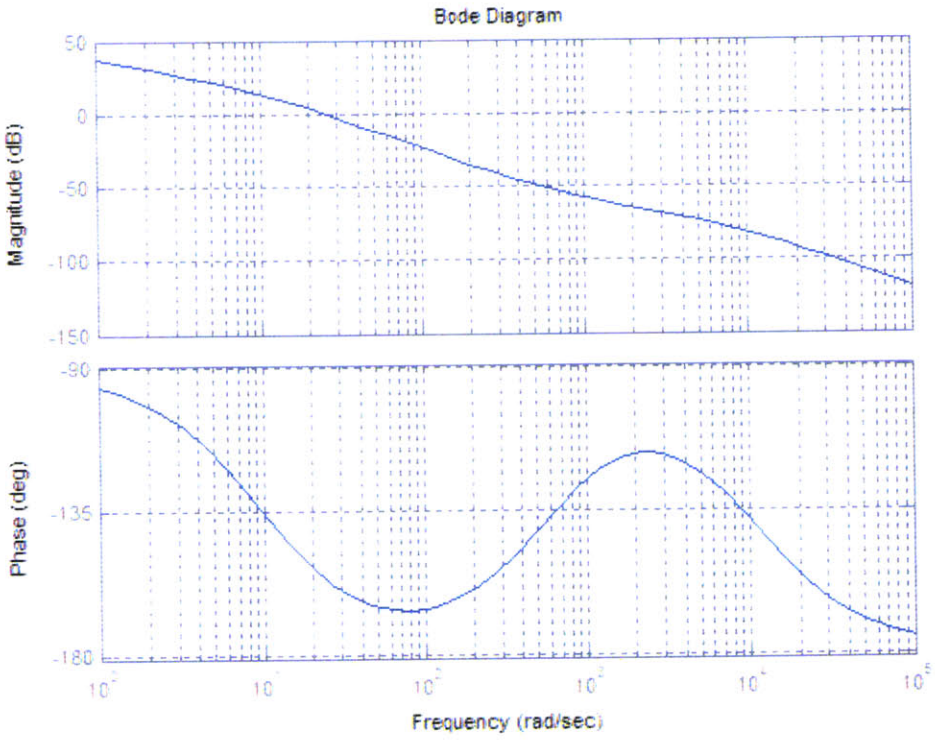

Figure 47: Predicted frequency response of open loop k_p=0.00255, k_I=1.5, DC motor and drive

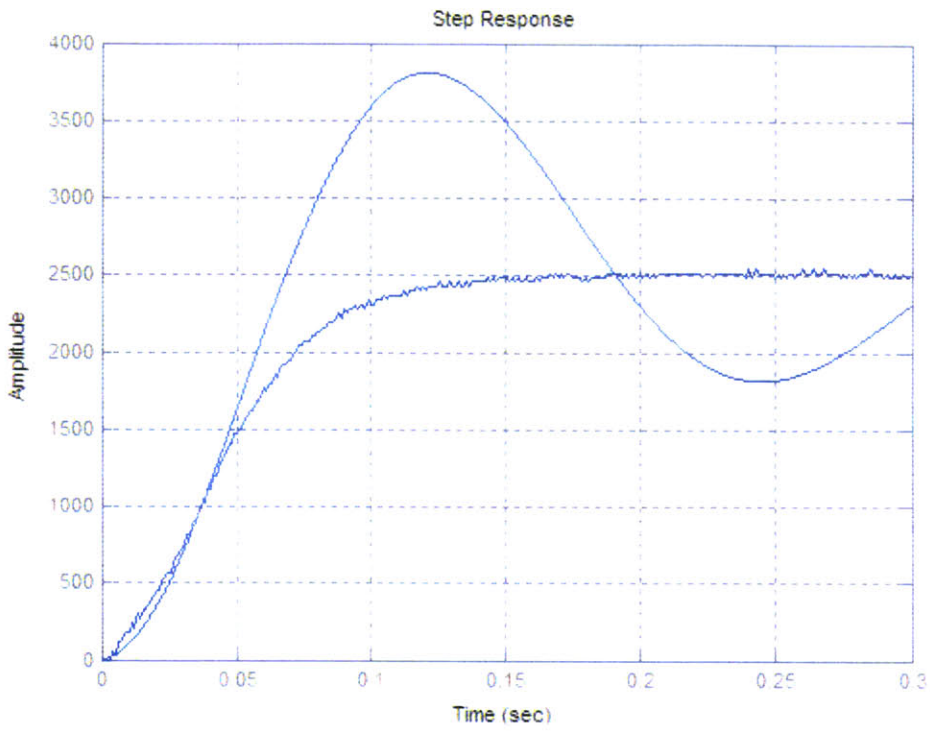

Figure 48: Measured and predicted closed loop step response k_p=0.00255, k_I=1.5, DC motor and drive

Apparently the real closed loop (DC motor and drive) is over-damped whereas the PI controlled model is under-damped. In order to increase the damping of the closed loop and thus further approximate the model to the response of the drive a lead controller has been included. The resulting controller yields a close fit of the model step response to the real closed loop step response, Figure 50.

$$lead = \alpha * \frac{\alpha Ts+1}{Ts+1} \qquad (34)$$

$$\alpha = 4.5$$

$$T = 0.0255$$

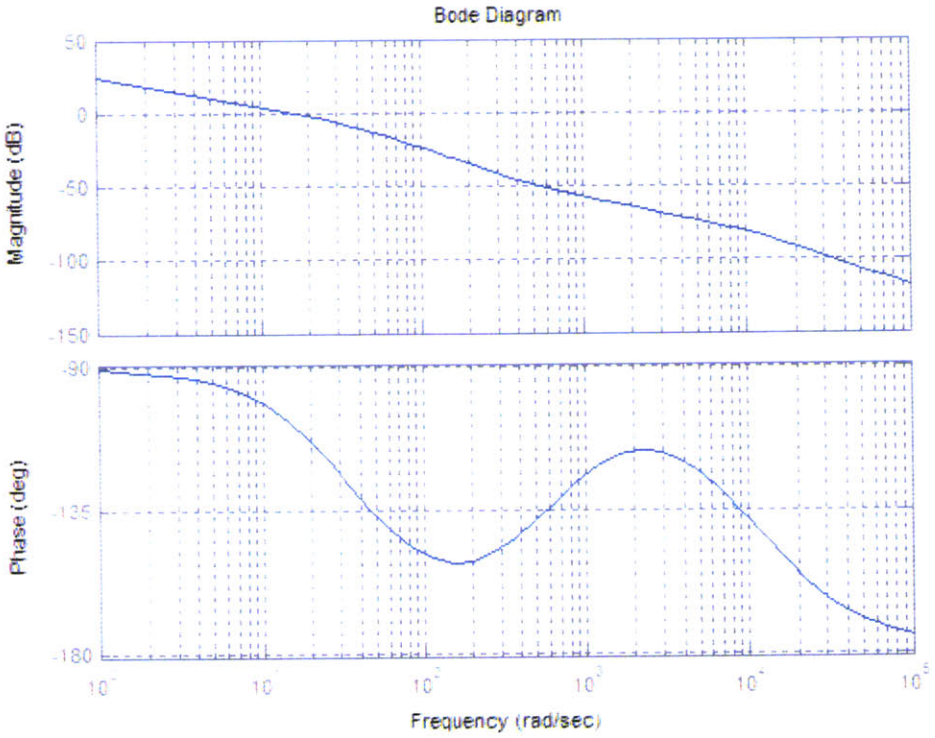

Figure 49: Predicted open loop frequency response k_p=0.00255, k_I=1.5, alpha=4.5, T=0.0255, DC motor and drive

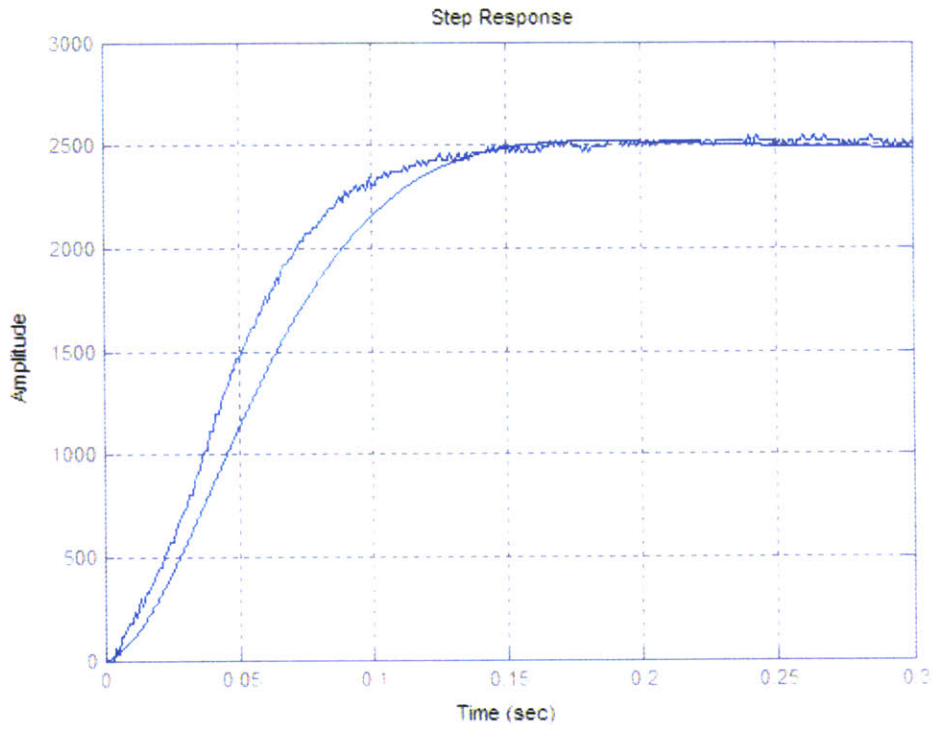

Figure 50: Measured and predicted closed step response k_p=0.00255, k_I=1.5, alpha=4.5, T=0.0255, DC motor and drive

Finally non-linearities of the drive, such as anti-windup and current limits have been included in the model.

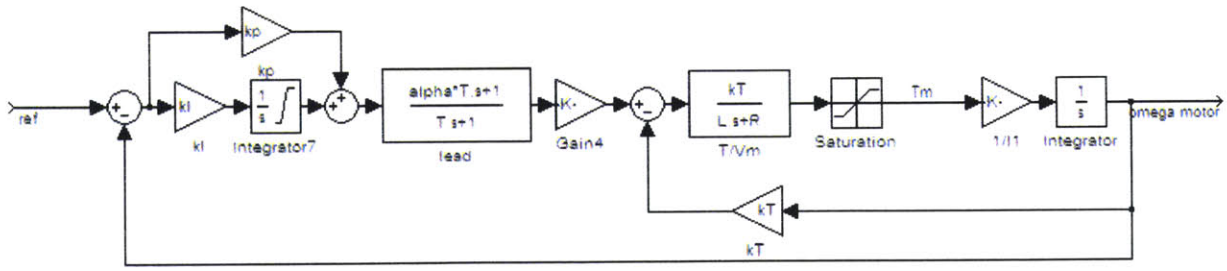

Figure 51: Velocity feedback loop including anti-wind and current limit of the motor drive

Now that a reasonably accurate model of the motor dynamics and a model of the hydrostatic bearing itself has been developed it remains to connect the two models, as shown in Figure 45.

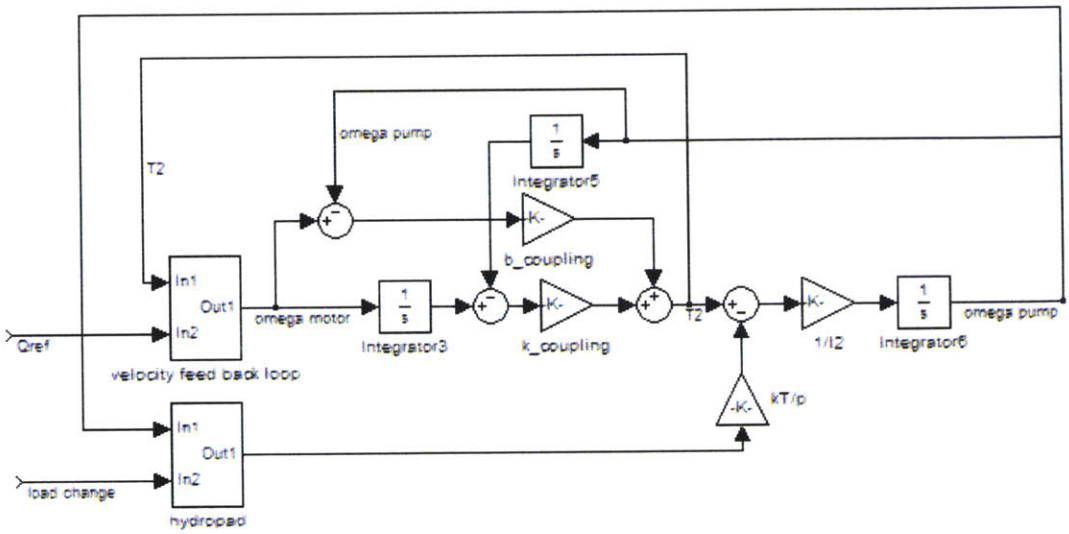

Figure 52: Complete model of the supply system and the hydrostatic bearing

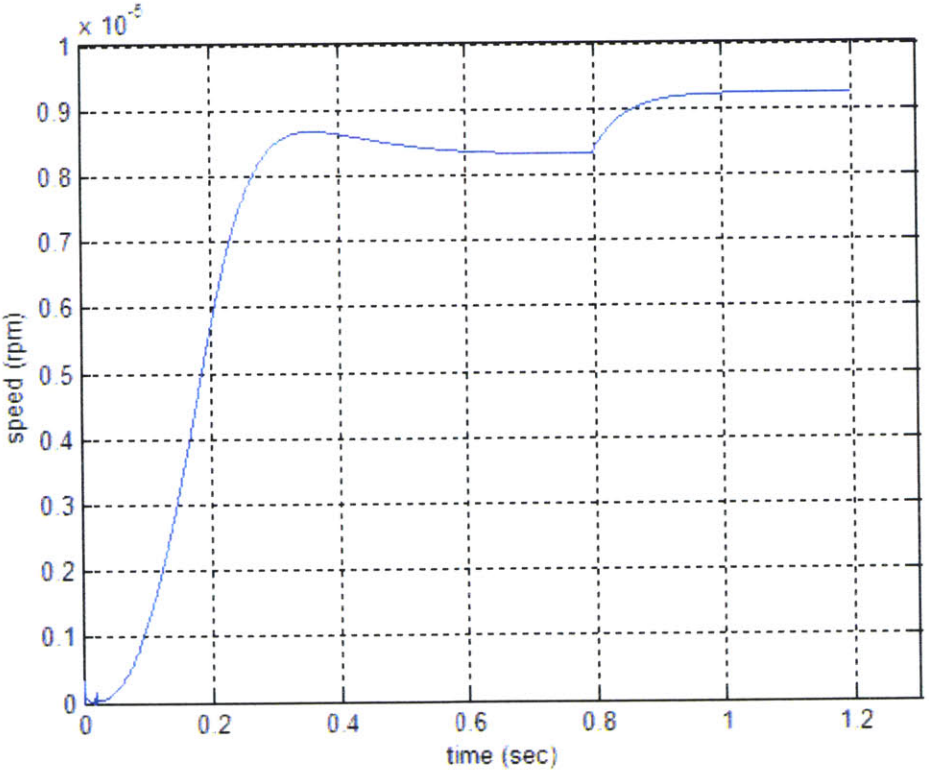

Figure 53: Simulated step in reference velocity of pump (+2500rpm) at t=0sec, load step (-235N) at t=0.5sec

5.9 Infinite Stiffness Control

The basic thought of infinite stiffness control is to make the flow out of the bearing proportional to the pressure in the bearing pocket and thus maintain a constant outflow resistance. As the resistance is inversely proportional to the gap cubed a constant outflow resistance of the pocket is equivalent to a constant gap. In order to determine the outflow resistance both flow and pressure have to be measured. In the static case, where the gap is not changing, this can easily be done based on the pump speed and a pressure sensor downstream of the pump. If the dynamics of the bearing are neglected, a constant gap can be maintained by simply increasing the flow (pump rpm) proportional to the pressure change. The proportionality constant in this case is the desired outflow resistance.

$$Q * \frac{\gamma}{h^3} = p \tag{35}$$

$$\frac{\partial Q}{\partial t} * \frac{\gamma}{h^3} - 3 * Q * \frac{\gamma}{h^4} * \frac{\partial h}{\partial t} = \frac{\partial p}{\partial t} \tag{36}$$

$$if \frac{\partial h}{\partial t} = 0, h = h_0, R_0 = \frac{\gamma}{h_0^3} \tag{37}$$

$$\frac{\partial Q}{\partial t} * R_0 = \frac{\partial p}{\partial t} \tag{38}$$

and thus

$$\Delta Q = \frac{\Delta p}{R_0} \tag{39}$$

In the case of dynamic load changes the flow produced by the pump is not anymore equal to the flow out of the bearing. Some flow gets stored in the expansion of the tubing or in the bearing itself, as it moves to another height i.e. bearing gap. Even though the control law presented above will still work, it will be far from ideal to control dynamic load changes. The bearing gap can be controlled better by using a model based observer where R_0 is the desired resistance.

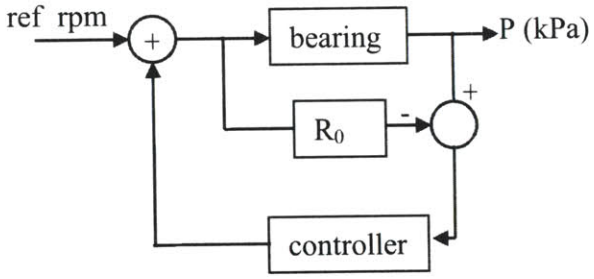

Figure 54: Model based observer for control of bearing gap

Within the scope of this work there was no time to systematically design the ideal observer. The controller was chosen based on the following thinking: Due to the relatively noisy signal of the pressure transducer, a pure proportional controller would cause a very noisy velocity reference input to the pump drive. Even in the case of an ideal (or low pass filtered) pressure signal a pure proportional controller would always show a steady state error. Therefore a PI controller was chosen. The controller gains were gradually increased until the velocity signal of the motor became noisy (k_p=0.01, k_I=0.15). The following plots show the bearing gap in response to five load steps of each 45N for the uncontrolled bearing and for the controlled bearing.

Figure 55: Test setup loaded with 90N

The nominal gap (no load) of the bearing was about 10microns in the uncontrolled case and about 6microns in the controlled case. The signals of the three capacitance probes differ due to tilting of the bearing. As can be seen in the appendix the measurements were highly repeatable.

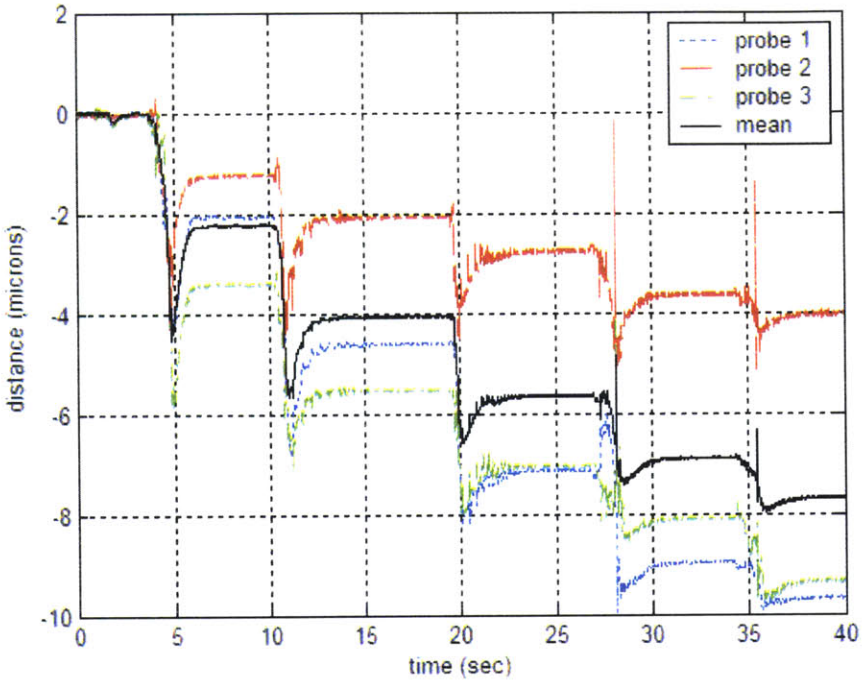

Figure 56: Response of uncontrolled bearing to +45N load steps

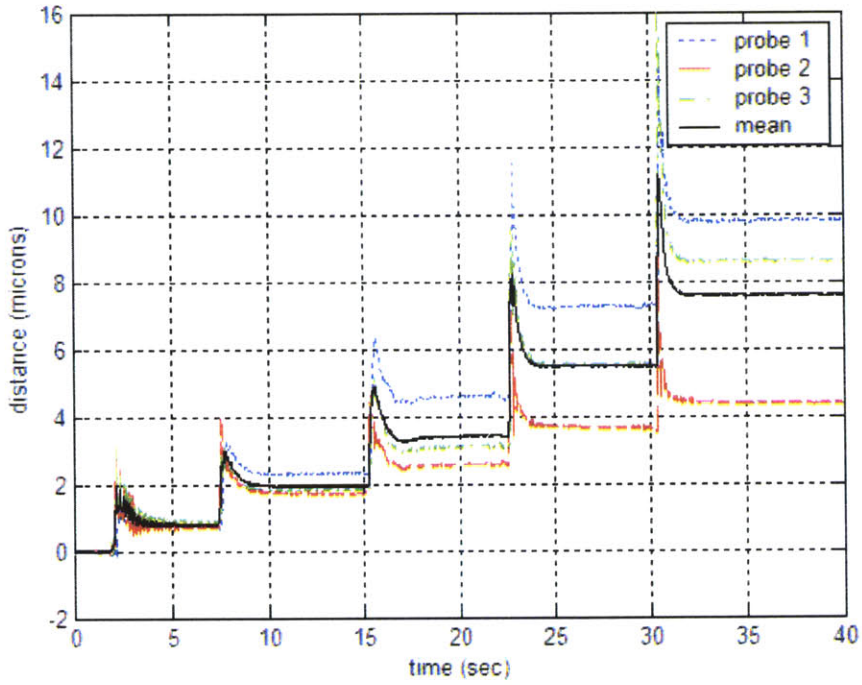

Figure 57: Response of uncontrolled bearing to -45N load steps

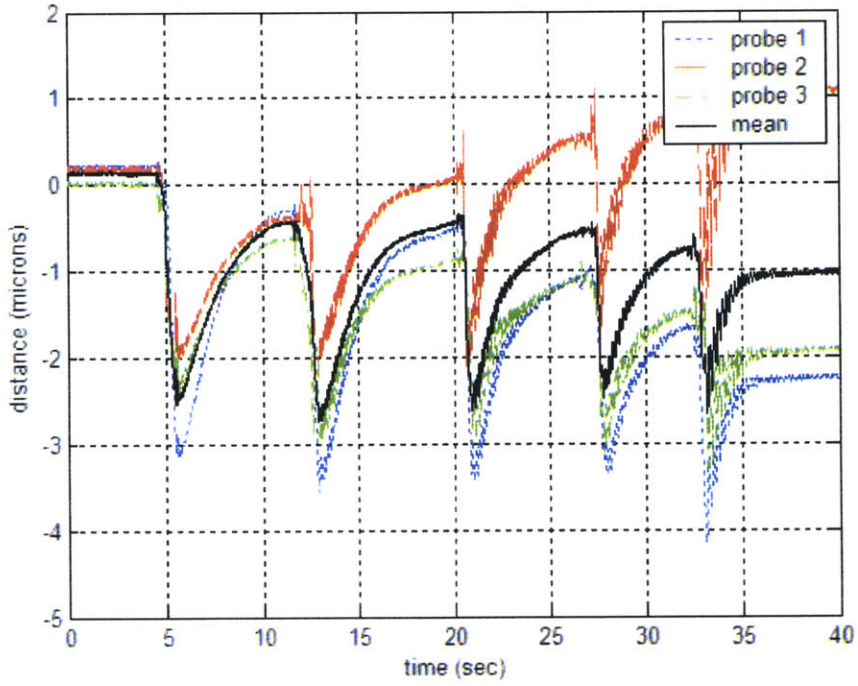

Figure 58: Response of controlled bearing to +45N load steps

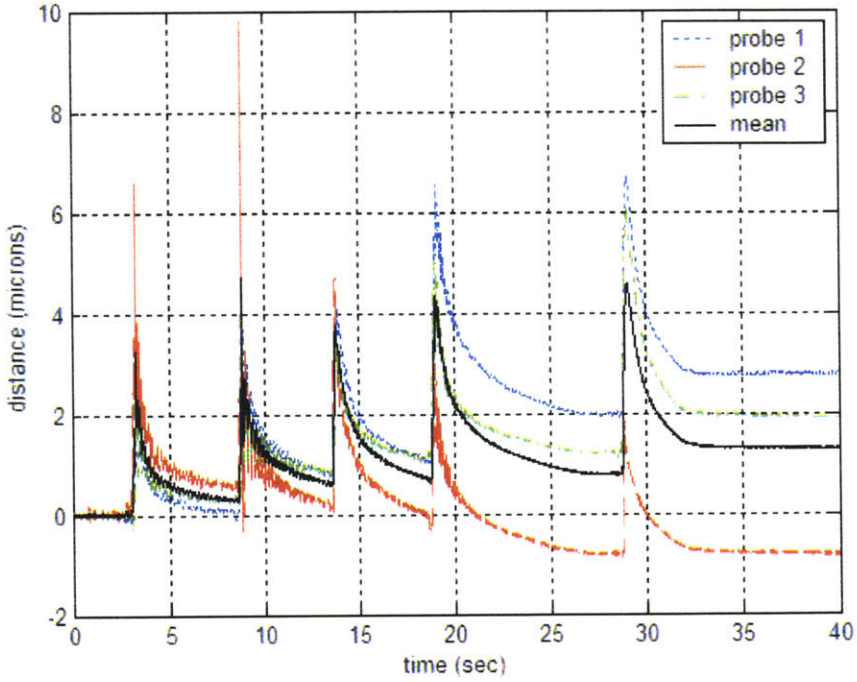

Figure 59: Response of controlled bearing to -45N load steps

In order to assess the influence of the stiffness of the tubing the same measurements have been repeated using stiffer tubing (copper tubing instead of common polypropylene tubing). But as predicted by the model stiffer tubing did not make a whole lot of a difference in the behavior of the bearing.

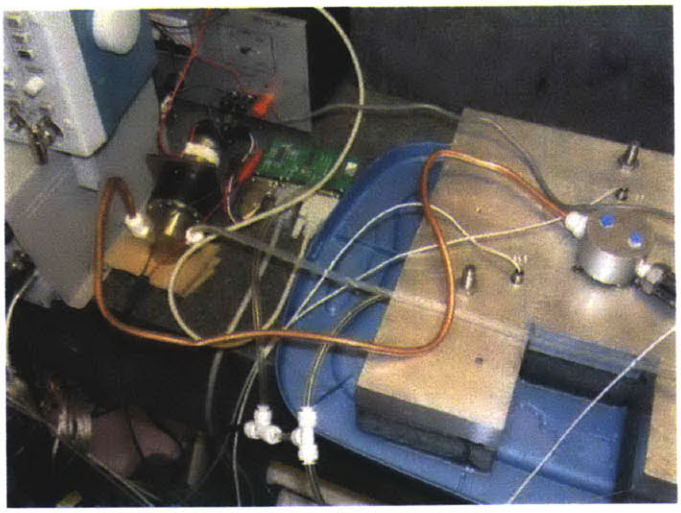

Figure 60: Fluid supply through copper tubing

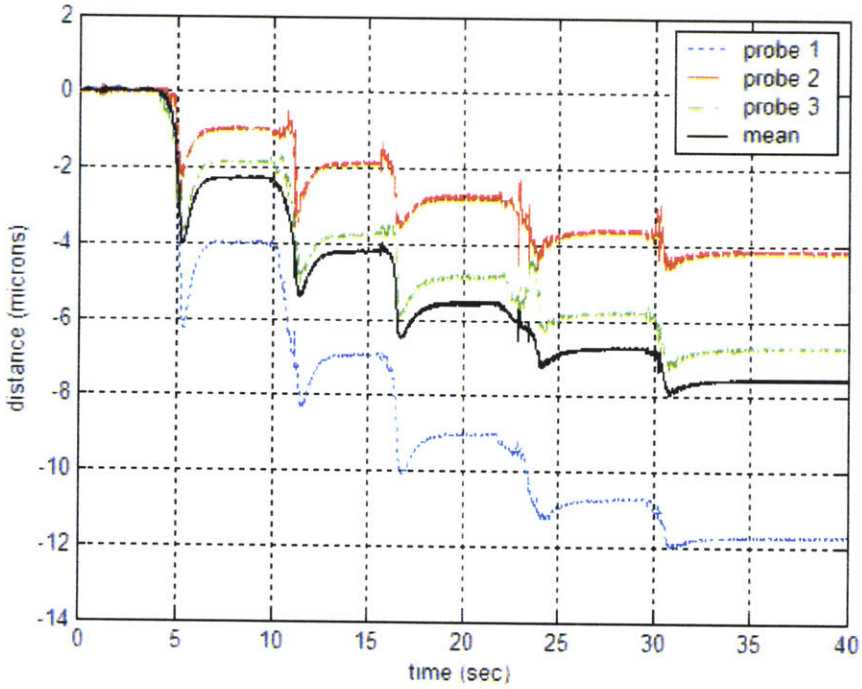

Figure 61: Response of uncontrolled bearing to +45N load changes, copper tubing

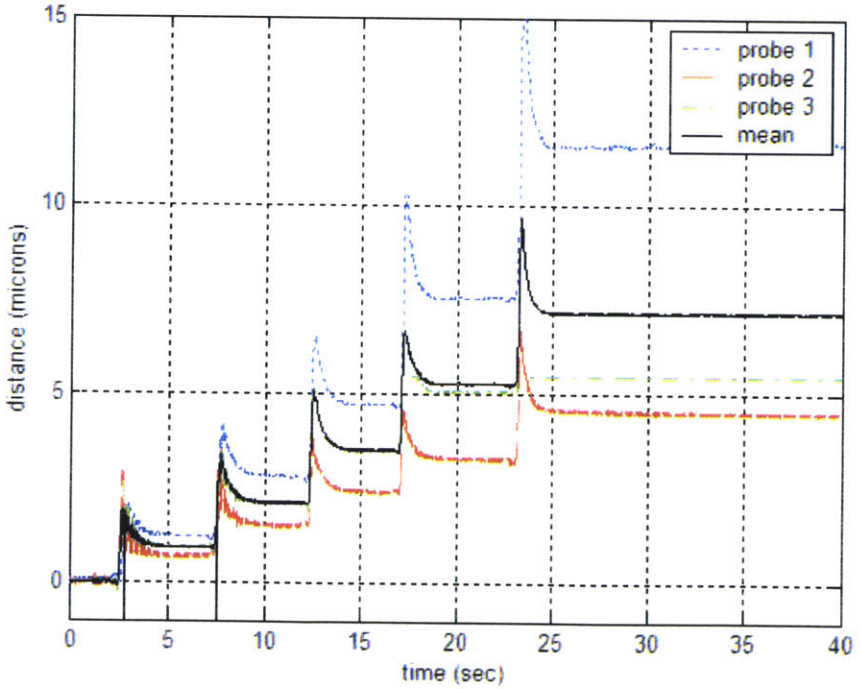

Figure 62: Response of uncontrolled bearing to -45N load changes, copper tubing

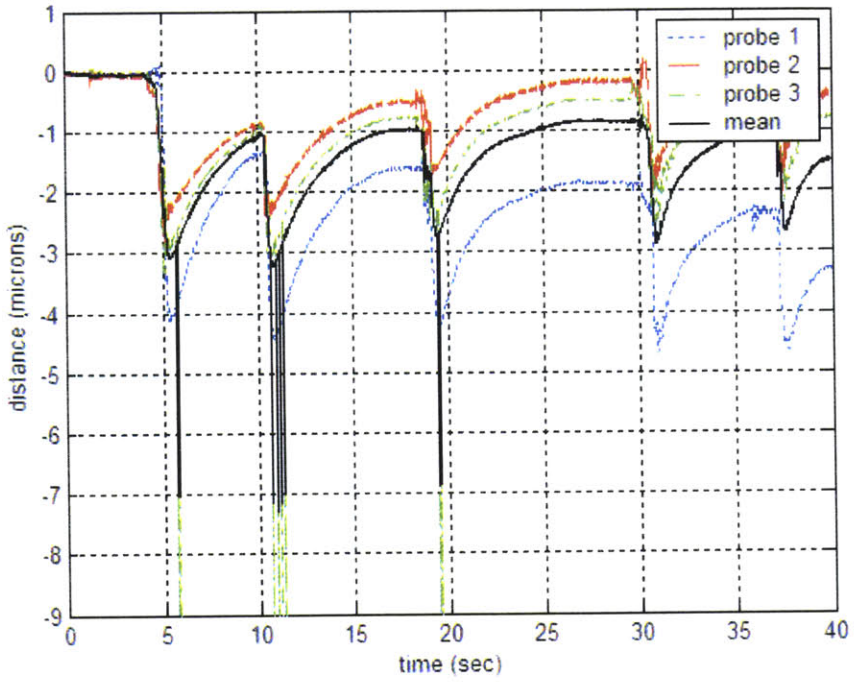

Figure 63: Response of controlled bearing to +45N load changes, copper tubing

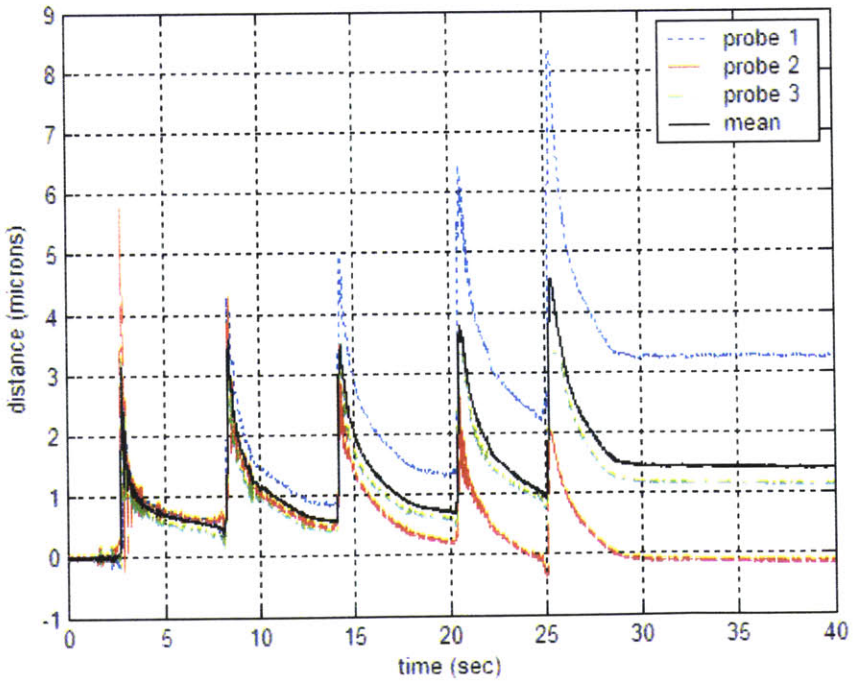

Figure 64: Response of controlled bearing to -45N load changes, copper tubing

5.10 Discussion of Measurements

Before the discussion of the above data, a look at the predicted response of the model will be taken.

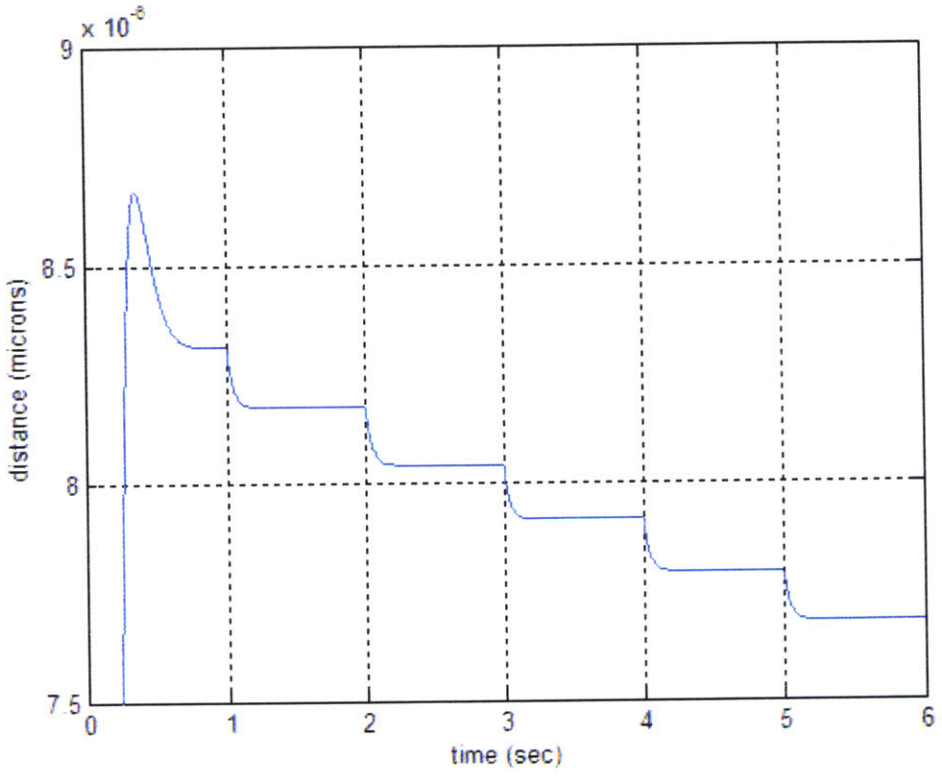

Figure 65: Predicted response of the bearing to +45N load steps

Apparently the model does not predict the over-swing of the bearing following each load step. The over-swing can only be reproduced by the model if the stiffness of the tubing is lowered by several orders of magnitude. This does not seem very likely - given that the use of stiffer copper tubing barely reduced the over-swing, as compared to the default polypropylene tubing, Figure 61. It seems more plausible that the over-swing can be explained by air that is enclosed in the bearing pad or in the supply line. Air in the bearing pocket would gradually be pushed out of the pocket and thus the over-swing would decrease over operating time of the bearing. Therefore the only remaining explanation is air in the supply line of the bearing. Taking into account the T-shaped channels (cross-section) of the push plate and the low flow rates it seems to be very plausible that air can

get caught within the push plate. This would decrease the dynamic stiffness of the bearing and explain the observed over-swing. The predicted stiffness of the uncontrolled bearing at a pump speed of 2500rpm and a nominal gap of 8micron is 355N/micron (Figure 65). The measured stiffness of the bearing at 2500rpm and a nominal gap of 8microns is only 37.5N/micron (Figure 56, Figure 57, Figure 61, Figure 62). Thus the measured stiffness seemed to be 10 times lower than the predicted stiffness, Figure 66. The controlled bearing shows a six to seven times higher static stiffness (Figure 58, Figure 59, Figure 63, Figure 64). However, the load step response of the controlled bearing shows an over-swing that is significantly higher than the prediction of the model. The slight ringing of less than .03microns in the predicted response (Figure 66) would be too small to even be detected by the capacitance probes (general noise level). By choosing another controller with derivative term or with a smaller integral gain the ringing could be eliminated completely.

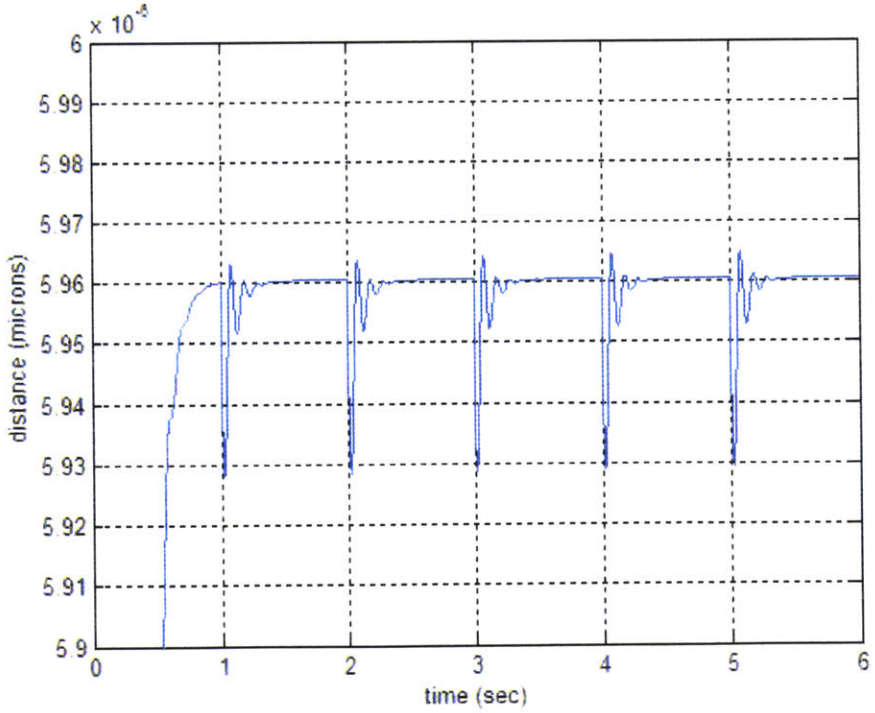

Figure 66: Predicted response of the controlled bearing to +45N load steps

The lower measured stiffness of the test bearing does seem even more surprising, given that the model could accurately predict the stiffness of the Hydrocline carriage. Possible reasons that could explain the lower measured stiffness are:

- Malfunctioning of the pump: In order to test the pump the downstream supply line of the bearing has been blocked. As expected the current consumption of the motor rose significantly. However, when the pump was connected to the bearing and the bearing load was changed (5x45N) the current consumption did not rise significantly. Apparently the load change did not represent a significant load to the pump motor.
- Tilt of the pocket: Tilt of the pocket could explain the lower stiffness of the bearing as well as the fact that the current consumption of the DC motor did not rise significantly with increasing load (5x45N). However, in the case of excessive tilt of the bearing (12micron change in measured distance at one of the three capacitance probes at a nominal gap of 10microns, Figure 61) the bearing would partially touch the granite. This was not the case. The bearing has been unmounted and the bearing pocket has been loaded with 270N + manually induced pushing force. However the bearing could still be moved smoothly and was obviously not sitting down on the granite.

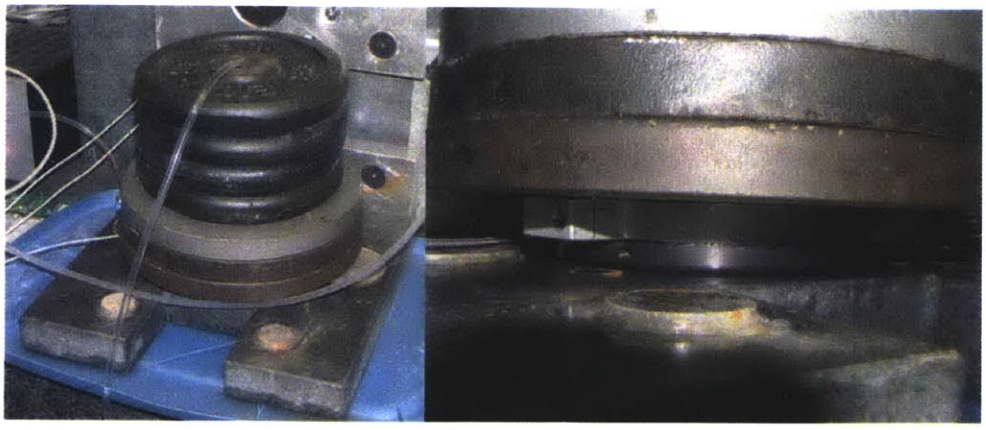

Figure 67: Hydrostatic pocket loaded with weights, no tilt support by air pads

- Measurement errors: It is very likely that the distance changes as measured by the capacitance probes are too big. The probe targets were elevated and therefore no shorting of the probes due to water in between the probe and the target could occur. However, there was plenty of water surrounding the probe targets and even though the probes were not shortened out, it is still possible that the capacitance was significantly reduced by humidity. It remains as a topic for future research to test this hypothesis.

The measured but most likely erroneous stiffness was by a factor of 10 lower than the prediction of the model and the measured stiffness per pocket of the Hydrocline carriage. Nevertheless it could be proven that the control of the hydrostatic gap as proposed in chapter 5.9 is working. As can be seen in Figure 56 to Figure 64 the control could increase the measured apparent stiffness by a factor bigger than 5. It remains to examine how much of the remaining deflection was due to tilting of the pad and how much was actual deflection in the vertical direction.

6 Conclusion and Outlook

A model has been developed that can accurately describe the static and dynamics performance of a hydrostatic thrust bearing. Based on the model a controller has been implemented and tested on a single pocket hydrostatic bearing test setup. In first experiments the bearing seemed to have a much lower static stiffness than predicted. However, it could be proven that this lower static stiffness must be due to measurement errors. Also the dynamic stiffness of the bearing seemed to be lower than predicted. The lower dynamic stiffness could be explained by air in the supply line of the bearing. Aside from the lower than expected stiffness it could be proven that it is possible to control the hydrostatic bearing gap using a model based observer control strategy. The benefit of this control strategy is that the gap does not have to be measured directly. It is sufficient to measure the pressure in the bearing pocket. Since pressure transducers are relatively cheap and easy to include in the supply line of the bearing, this control approach significantly reduces the cost of a future industrial application. The controller that has been chosen for the above presented first experiments is extremely simple and improvements seem to be very feasible. For instance the observer could be based on a more accurate model of the bearing (in the presented experiments a pure resistance has been used). In addition, in future work the controller parameters should be chosen more systematically (pole placement). The advantages of the described control are:

- As the gap is controlled the bearing can be run at a relatively lower nominal gap which results in a higher stiffness independent of the control
- The gap control can significantly increase the stiffness of the bearing and infinite stiffness over a limited pressure range seems to be feasible
- The gap control can be used in order to adjust the bearing gap
- In the case of a machine tool where a translational carriage is being supported by several hydrostatic bearing pads, the gap control can be used in order to compensate for waviness in the two surfaces moving relative to one another.

- In a first prototype of a hydrostatic bearing linear motion carriage, a bearing stiffness of 900N/micron was achieved. However, besides error motion due to surface tolerances it could be shown that the magnetic attraction between the linear motor forcer and the magnets causes a sinusoidal pitch error motion of the carriage of +/- 1.5arcsec as the carriage moves along the magnet track (http://web.mit.edu/~geraldr/www/CV/minimizing%20pitch.pdf and http://web.mit.edu/~geraldr/www/CV/Nulling%20Pitch.pdf). Furthermore, in the case of high accelerations and if the driving force is not aligned with the center of stiffness of the carriage inertial forces cause pitch of the carriage. In the case of a constant flow supplied bearing deflection in the bearings due to load changes can in theory be compensated by a change in flow.

7 Appendix

A. Hydrocline Design Spreadsheet Summary

Originally the measured flow was by a factor of 10 higher than the predicted flow. Therefore a correction factor has been introduced in the outflow resistance. It remains to find the error in spreadsheet and correct it.

HydroCline_Axtrusion.xls
For designing Water HydroStatic Axtrusion™ axes with Contsant Flow Supply
Alex Slocum&Gerald Rothenhofer, last modified May 2006
The axtrusion design is covered by US Patent 6,150,740. Contact slocum@mit.edu

Inputs (N, mm) in BOLD, Outpus in RED			
Bearing pads			
bearing width	au (mm)	**84**	
bearing length	bu (mm)	**162**	
land width	lu (mm)	**17**	
pocket radius	rpu (mm)	**3**	
effective bearing area	Aeffu (mm^2, m^2)	**9510**	**0.009510**
Nominal gap	h (microns, m)	**9**	**0.000009**
Gap at maximum load	(microns)	**4.5**	
Overall carriage dimensions			
Side plate thickness	(mm)	**30**	
Carriage width (not including side plate)	wc (mm)	**350**	
Total carriage length	Lc (mm)	**486**	
Bearing rail edge chamfer	(mm)	**1**	
Motor			
Axial force (H20 cooled) (N)		**600**	
Attractive force (N)	(N)	**3314**	
Pitch nullers' total attraction force (N)	(N)	**0**	
Total preload force	Fmm(N)	**3314**	
Mounting angle	(degrees)	**30**	
Preload ratio (top to side bearing pads)		**1.03**	
Motor total height (Fanuuc)	(mm)	**36**	
Motor total width	(mm)	**130**	
Total projected width	(mm)	**130.6**	
Total projected height	(mm)	**96.2**	
Distance to center of force (typically B28/2+15)	(mm)	**60**	
Fluid			
Viscosity mu	(Nsec/m^2)	**0.001**	
Density rho	(kg/m^3)	**997**	
specific heat	(joule/kgram °C)	**4186**	
apparent bulk modulus of lubricant (here water, approximately)	Kla (N/m^2)	**2000000**	

System performance summary				
Stiffness				
Vertical	(N/micron)	957		
Horizontal	(N/micron)	478		
Pitch	(N-m/microrad)	16.7		
Yaw	(N-m/microrad)	8.3		
Load capacity				
Minimum gap, h	(microns)	4.5		
Vertical	(N)	229601		
Vertical load capacity/pumping power	(N/W)	726668		
Horizontal	(N)	114800		
Pitch	(N-m)	15154		
Fluid Supply				
Total (6 pads) Q	(lpm, m^3/s)	0.377	6.28E-06	
Minimum pressure	(atm, kPa, psi)	0.75	75	11
Minimum pump power (6 pads)	(W)	0.47		
Max pressure	(atm, kPa, psi)	60.36	6,036	875
Maximum pump power	(W)	37.92		
Maximum velocity (with no pre-feed)				
Avg. flow velocity out of pocket	(m/s)	0.24		
Max. velocity (p at leading edge becomes atmospheric)	(m/s)	39.52		

Table 6: Hydrocline Performance Summary

B. Step Responses of Single Pad Test Setup

a. Polypropylene tubing, no feedback control, each step +45N

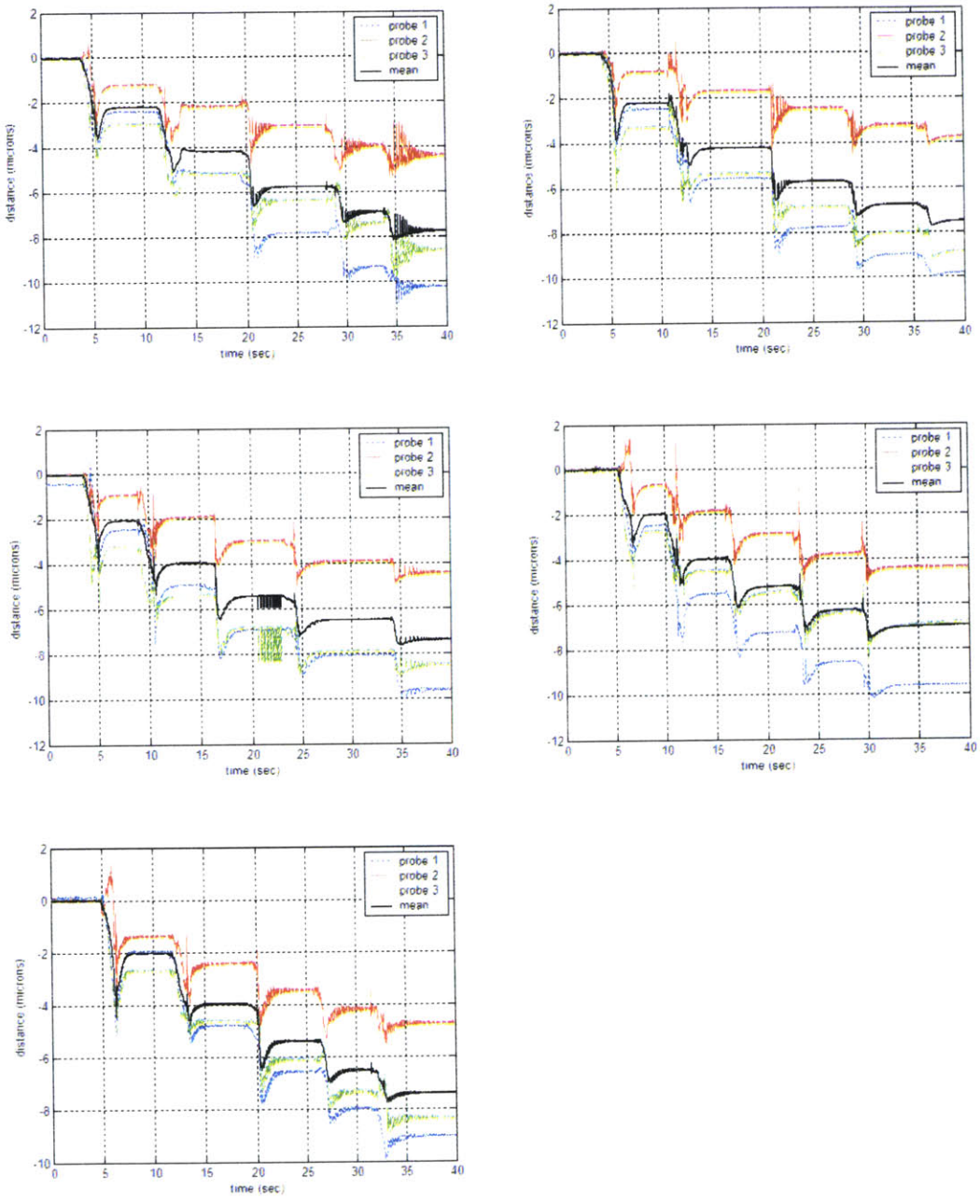

Figure 68: PP tubing, no control, +45N per step

b. Polypropylene tubing, no feedback control, each step -45N

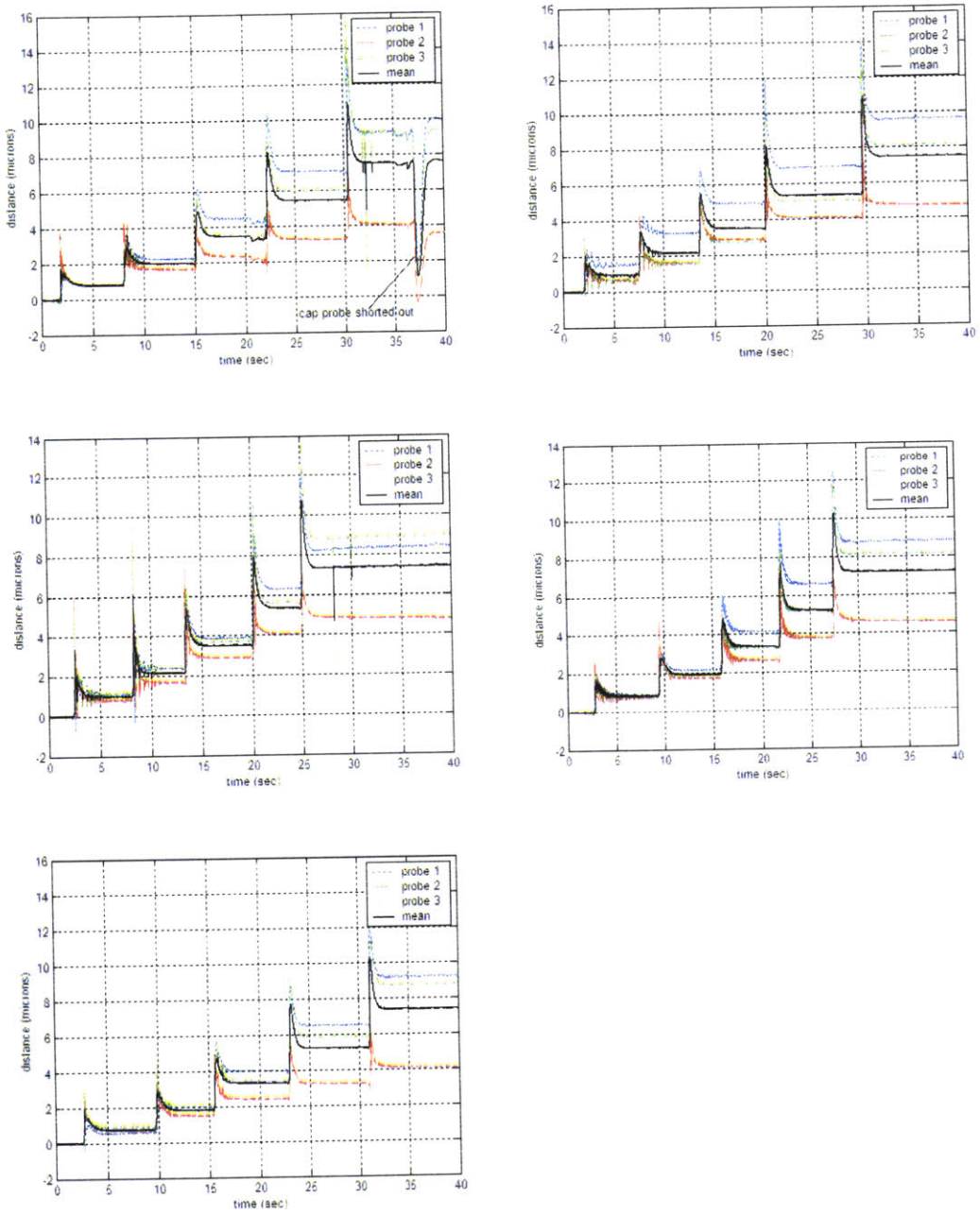

Figure 69: PP tubing, no control, -45N per step

c. Polypropylene tubing, feedback control on, each step +45N

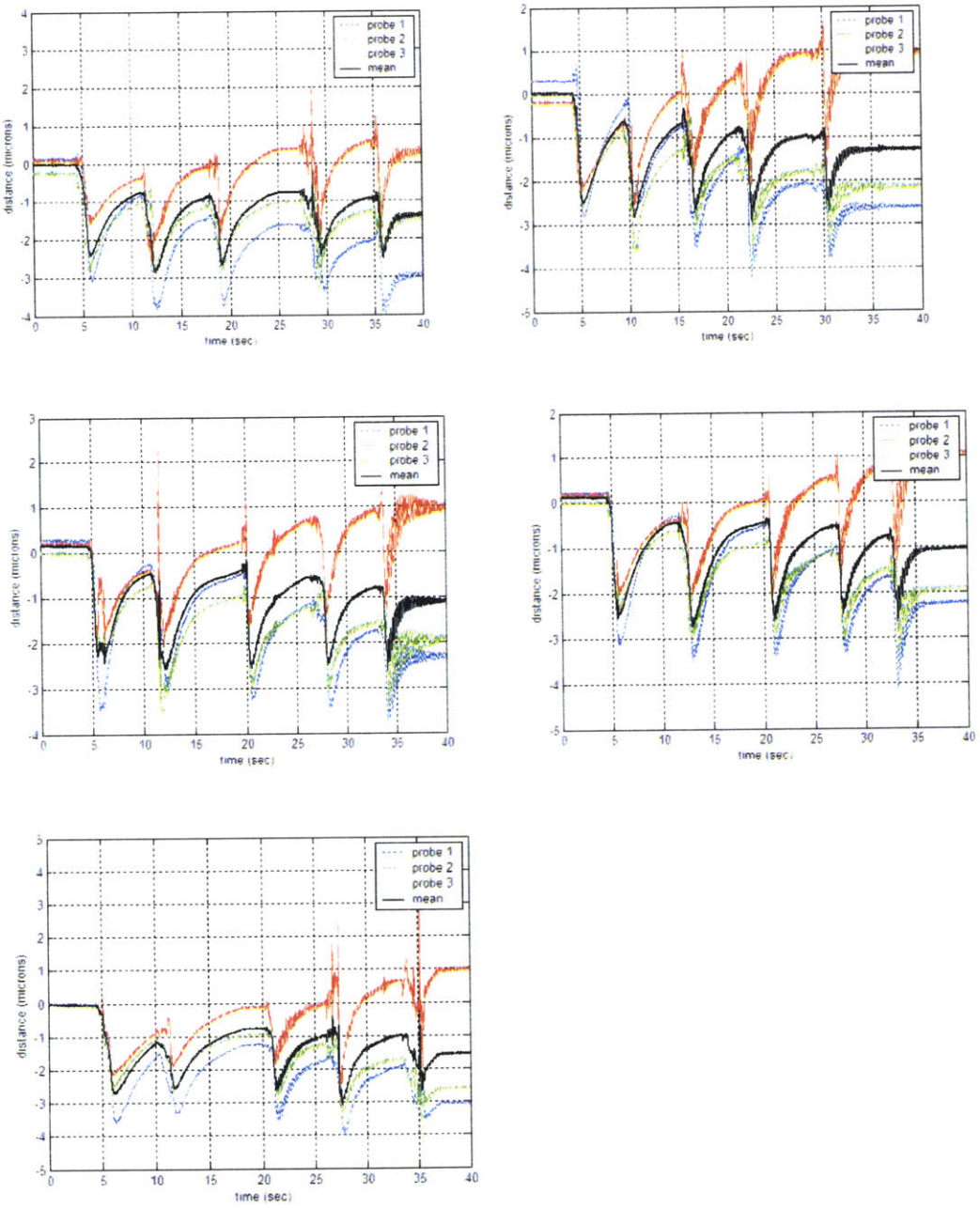

Figure 70: PP tubing, feed back control on, +45N per step

d. Polypropylene tubing, feedback control on, each step -45N

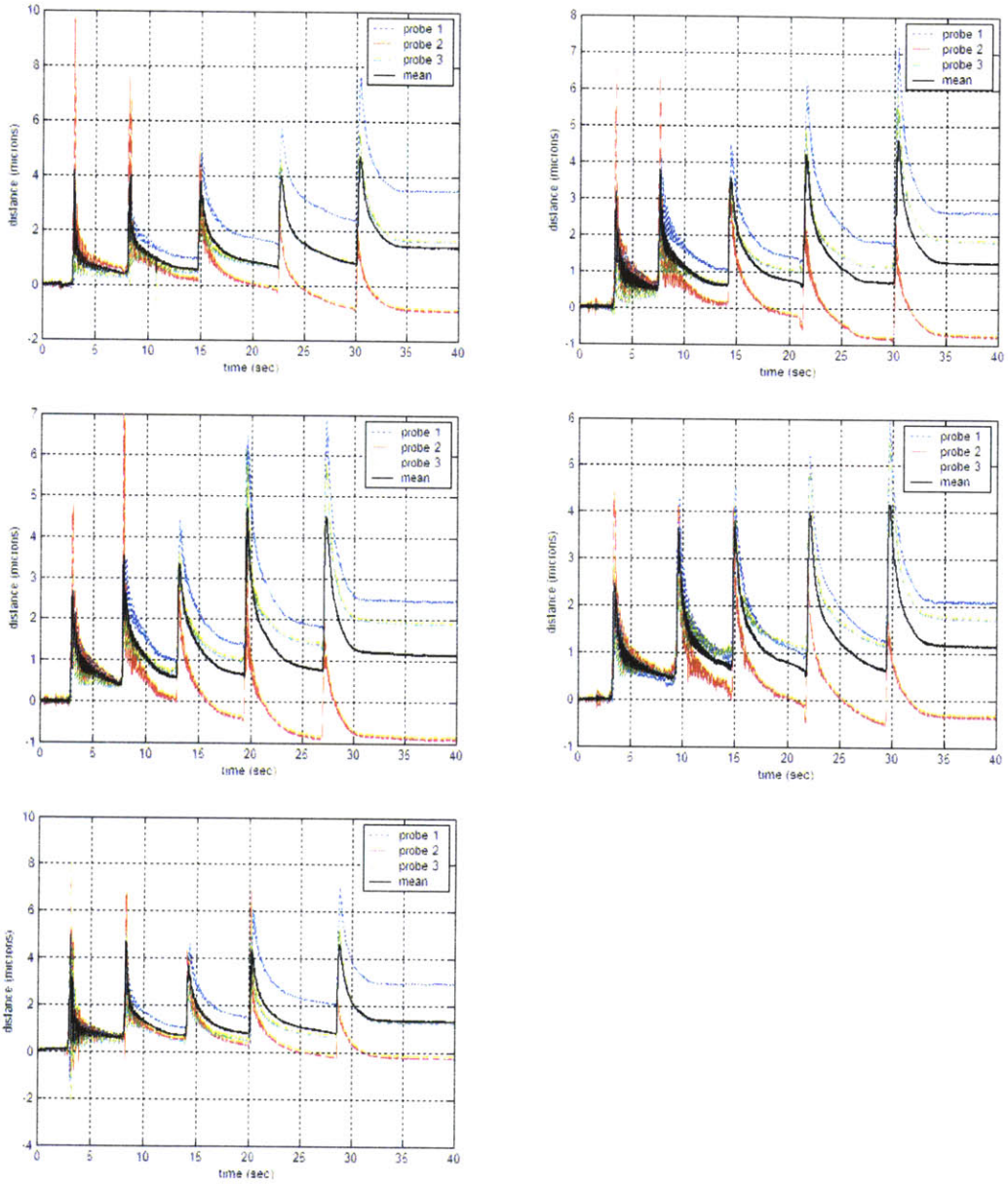

Figure 71: PP tubing, feed back control on, -45N per step

e. Copper tubing, no feedback control, each step +45N

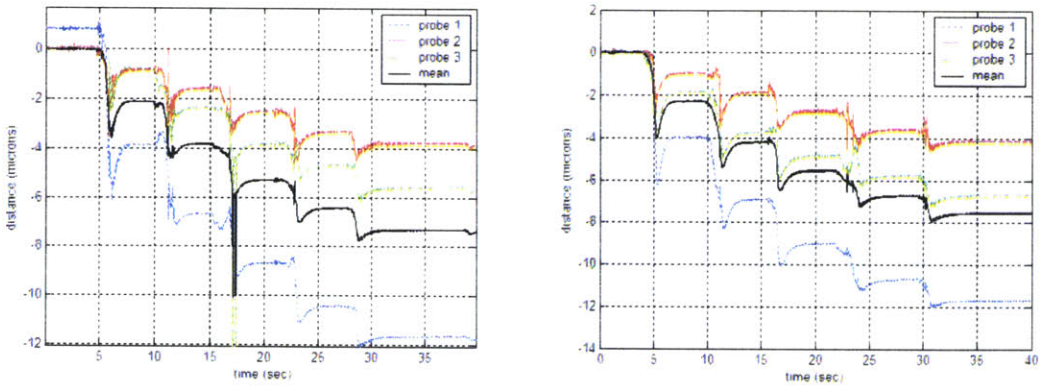

Figure 72: Copper tubing, no feed back control, +45N per step

f. Copper tubing, no feedback control, each step -45N

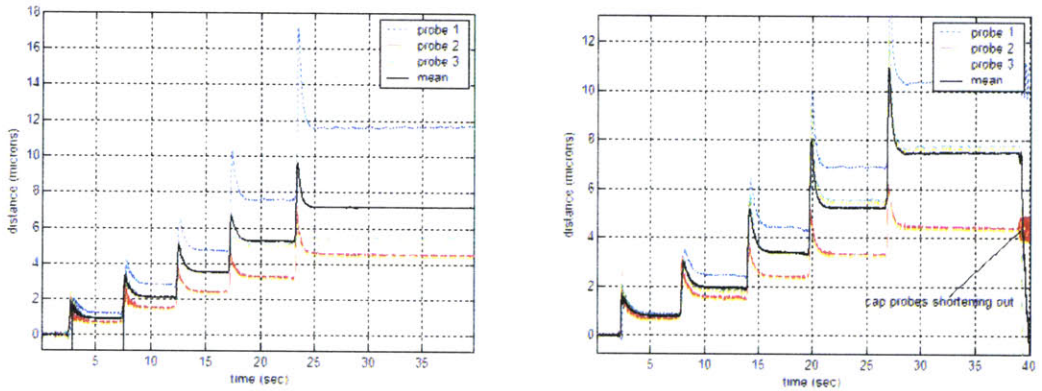

Figure 73: Copper tubing, no feed back control, -45N per step

g. Copper tubing, feedback control on, each step +45N

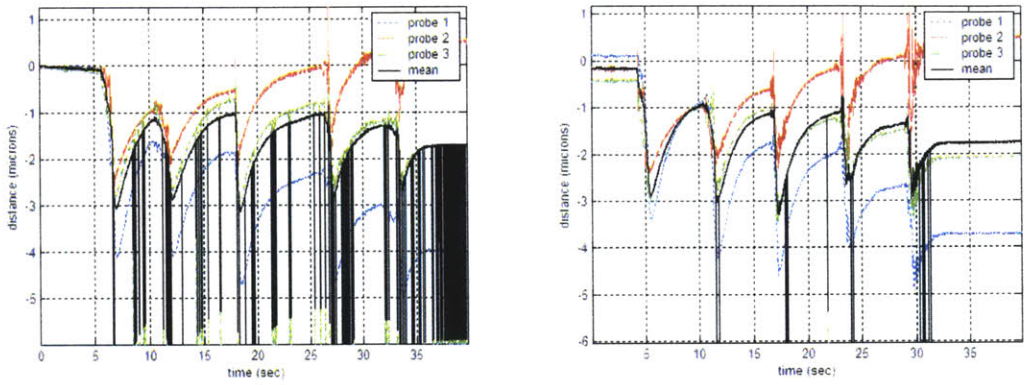

Figure 74: Copper tubing, feed back control on, +45N per step

h. Copper tubing, feedback control on, each step -45N

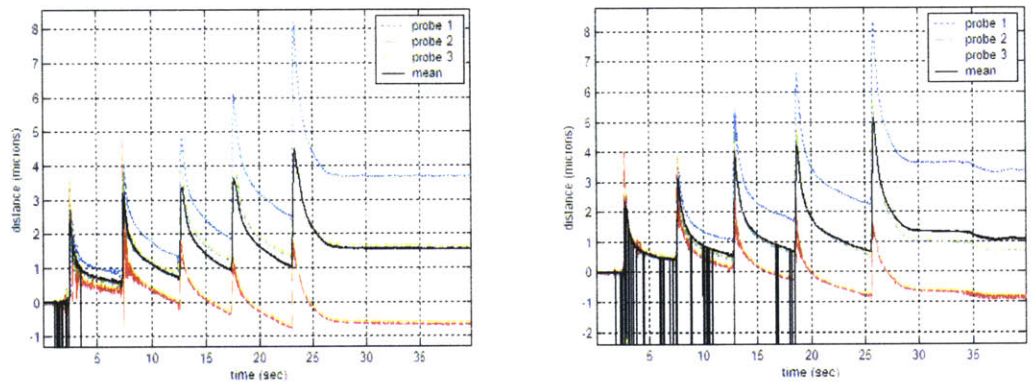

Figure 75: Copper tubing, feed back control on, -45N per step

C. Measuring the Stiffness of the Magnet Coupling

The drive was operated in position control. As shown in the following picture the pump side magnet has been manually turned away from its preferential position. The change in angle as compared to the preferential position of the load (pump head) side magnet has been measured by cutting a segment of a string that had the same length as the circumference in between the corresponding marks on the load side magnet and the drive (DC motor) side magnet. The length of the string could then be measured on a conventional linear scale (such as a ruler or calipers). The angular change can be computed as:

$$\Delta\Phi = \frac{2x}{D} \qquad (40)$$

$x - length\ of\ string$

$D - outer\ diameter\ of\ magnet\ coup\ (\approx outer\ diameter\ of\ drive\ side\ magnet)$

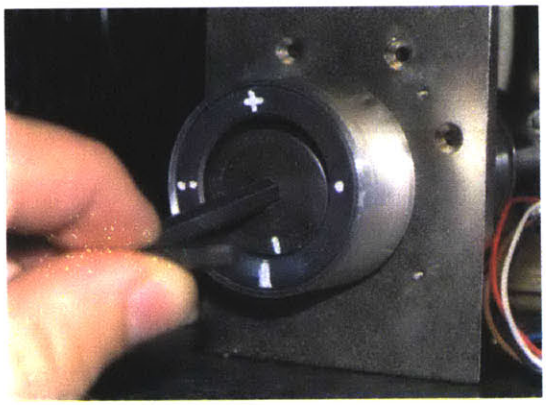

Figure 76: Stiffness measurement of magnet coupling

D. Torque Pressure Relationship of Pump

Based on manufacturer specifications the following torque pressure line has been determined.

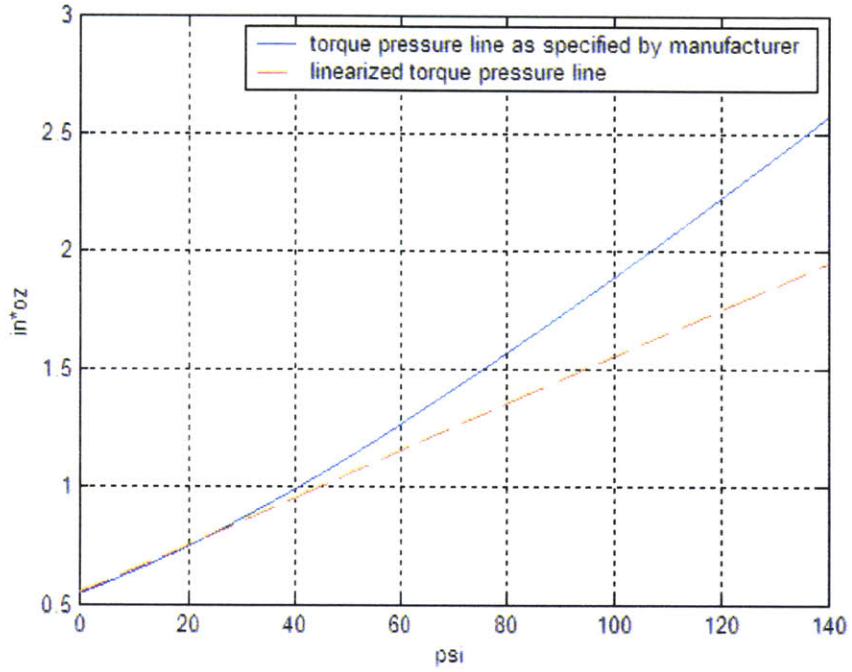

Figure 77: Torque pressure line as specified by manufacturer

For the purpose of the model the torque pressure relationship has been linearized as shown in Figure 77. This is reasonable as the operating pressure of the bearing was not expected to exceed 40psi (276kPa). The exact relation of torque and pressure can be described as:

$k_{Tp}=54.5*(1-exp(-1/30*p);$ *(41)*

$T=k_{Tp}*p$ *(42)*

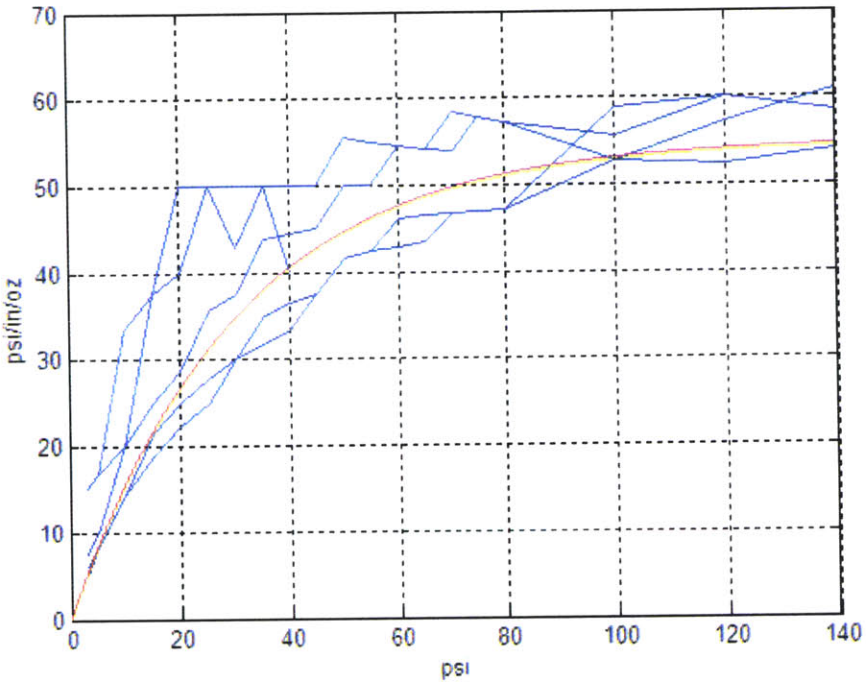

Figure 78: Slope of torque pressure line, manufacturer specification and curve fit

E. DC Motor Model

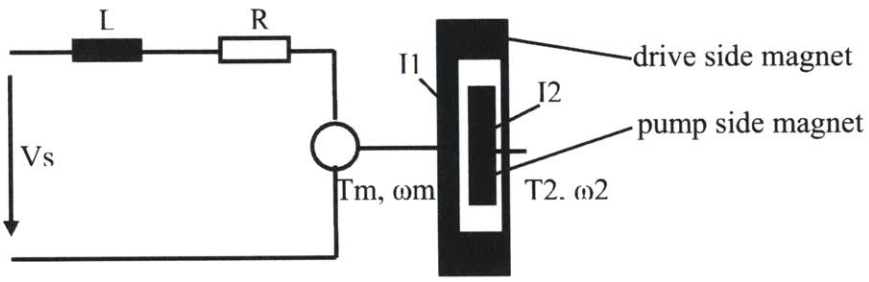

Figure 79: Standard DC motor

if the magnet coupling is not engaged :

$$T_m = k_T * i \tag{43}$$

$$V_{emf} = k_T * \omega_m \tag{44}$$

$$V_s = R * i + L\frac{di}{dt} + V_{emf} = (R + Ls)i + k_T * \omega_m \tag{45}$$

$$\omega_m = -\frac{R + Ls}{k_T{}^2} T_m + \frac{V_s}{k_T} \tag{46}$$

assume motor shaft as infintely stiff:

$$T_m = \frac{k_T}{R+Ls}(V_s - k_T * \omega_m) \tag{47}$$

$$T_m = I_1 \frac{\partial \omega_m}{\partial t} \tag{48}$$

$$\frac{\omega_m}{V_s} = \frac{k_T}{LI_1 s^2 + RI_1 s + k_T} \tag{49}$$

if the magnet coupling is engaged :

$$T_m = T_1 + T_2 \tag{50}$$

where T_i *is the torque that accelerates* I_i

$$\omega_m = \omega_1 = \frac{1}{I_1}\int T_1 dt \tag{51}$$

$$\omega_2 = \frac{1}{I_2}\int T_2 dt \tag{52}$$

$$T_2 = \frac{1}{k_{mc}}(\theta_m - \theta_2) + b_{mc}(\omega_m - \omega_2) \tag{53}$$

$$T_1 = T_m - \frac{1}{k_{mc}}(\theta_1 - \theta_2) + b(\omega_1 - \omega_2) \tag{54}$$

k_{mc} – *stiffness of magnet coupling*

b_{mc} – *damping of magnet coupling*

F. Nulling the Pitch Error of Permanent Magnet Open Face Linear Motion Components

Standardized linear motion components can be used in a motor-preloaded-bearing concept, where an iron core open face linear electric motor's permanent magnets preload aerostatic or hydrostatic bearings. Most open face electric linear motion systems show an inherent pitch moment that limits the accuracy of the movement due to compliance of the bearings. The pitch moment results from sinusoidally varying attractive forces that the carriage is subjected to as it moves along the surface of the magnet track. For a standard open face permanent magnet linear motors the resulting pitch error may only be 1 arc-second and have a repeatability of 0.1 arc-second, but for ultra-precision applications, it is desirable to reduce that value by an order magnitude. By the use of external nulling elements it is possible to create an additional pitch moment to effectively counter the inherent pitch moment of the motor. To minimize the induced pitch error motion, current designs make use of two parallel magnet tracks and forcers, where the pitch error causing moments cancel each other out. But this increases cost and prevents the motors from preloading the bearings. Alternatively the error causing pitch moment can be compensated by pitch nullers. Nullers are blocks of

magnetic material that are attached on both sides of the forcer. The length of those blocks is optimally chosen at less than two magnet pitch.

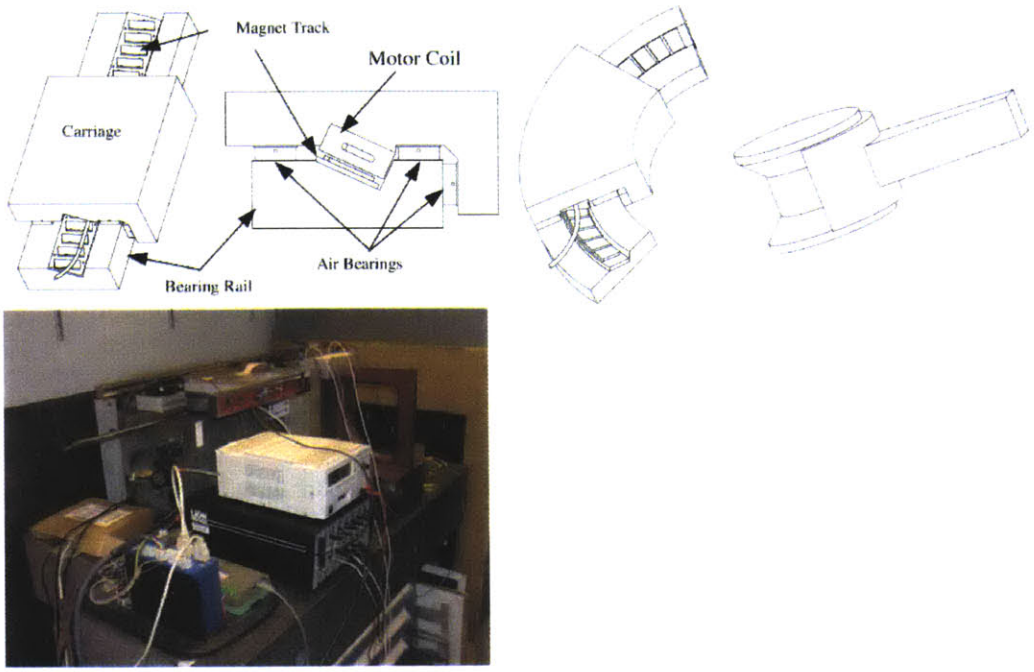

Figure 80: Magnetically preloaded air bearing, patented Axtrusion bearing and machine design

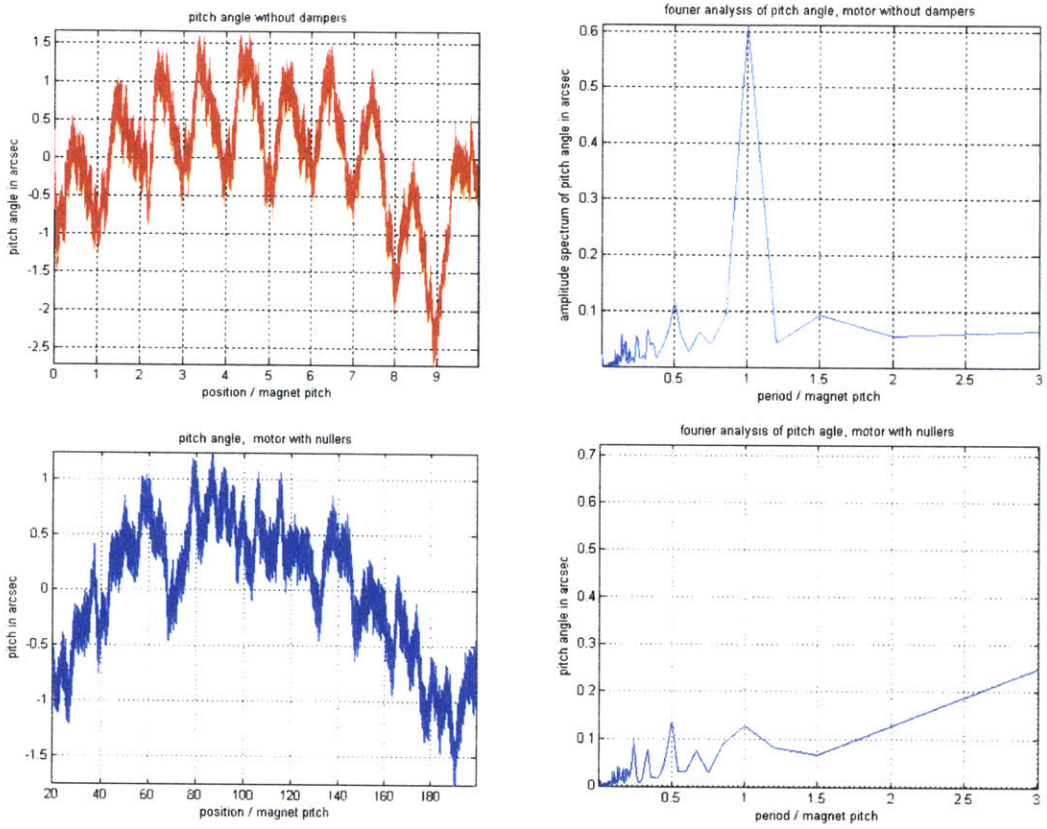

Figure 81: Measured pitch of the carriage without pitch nullers and with pitch nullers

G. Matlab based Design Tool

The user starts the program by entering "bearing_calc" in the Matlab command window. The program will then ask the user to enter the formulas (set of analytic equations) that describe the problem. Once all formulas are entered the program will ask the user to assign values to certain variables. If the user can not assign a value to one of the variables he can simply press return and the program will ask for other variables. Once the program has enough variables to solve the set of equations it will compute a solution.

```
function [result] = bearing_calc

display('If you are asked for a yes or no decision, please enter y for yes. Any
other input will be interpreted as a no.')
if exist('equations.mat', 'file')==0
   [equations]=read_in_eqns;
elseif exist('equations.mat', 'file')==0
   display('No equations have been defined yet.')
   [equations]=read_in_eqns;
elseif strmatch(input('Do you want to import the equations from equations.mat? ',
's'), 'y')
   display('Equations are imported of the files: equations.mat')
   load equations
else
   [equations]=read_in_eqns;
end

equations_out=equations;

%solve system of equations or subsytem of equations if possible
[result, equations_out]=solve_equations(equations_out);

while ~isempty(equations_out) %system is not yet entirely solved
   %ask for input for undefined variable
   n_eqns=length(equations_out);
   vars={};

   for i=1 :n_eqns
      vars_equation=symvar(char(equations_out(i)))';
      vars=unique([vars, vars_equation]);
   end
```

```
   display('please enter values for known variables')

   j=1;
   assign=[];
   while isempty(assign)
      input_value=input([char(vars(j)), ': ']);
      if and(length(input_value)==1, isnumeric(input_value))
         assign_left  = char(vars(j));
         assign_right = mat2str(input_value);
         help_assign  = [assign_left, '=', assign_right];
         help_assign  = {help_assign};
         assign       = help_assign;
      end

      if j<length(vars)
         j=j+1;
      elseif j==length(vars)
         j=1;
      else
         error('j can not be bigger then length(vars)')
      end
   end

%     equations=char(equations);
%     equations=cellstr(equations);
   equations=[equations; assign];
   equations_out=[equations_out; assign];

%    [new_result, equations]=solve_equations(equations);
%    result=merge_structures(result, new_result);
   [result, equations_out]=solve_equations(equations_out);
end

[result, equations]=solve_equations(equations);

display('The result has been saved in result.mat')
save result result
```

```
function[equations_out]=find_equations(equations_in, vars)
equations_out=[];
for i=1 :length(equations_in)
   vars_eqn=symvar(char(equations_in(i)));
   if isempty(setdiff(vars_eqn, vars))
      if isempty(equations_out)
         equations_out=equations_in(i);
      else
         equations_out=[equations_out, equations_in(i)];
      end
   end
end
```

```
function [row_index_array, vars]=find_subset(var_matrix)

% search for a subset of i equations with i variables

n_eqns=size(var_matrix,1);
vars=[];            %nicht sicher ob zulässig an dieser Stelle

if n_eqns>1
   for i=n_eqns-1 :-1 :1
      j=0;
      while j<=n_eqns-i %while j<=maximal number of equations that can have
more than i variables
         %choose one equation
         for k=1 :n_eqns
            %determine how many variables are in the choosen equation
            length_row=row_length(var_matrix, k);
            %make sure that there are no more than i variables in the
            %choosen equation
            if length_row>i
               j=j+1;
               continue
            end

            row_index_array(1)=k;
            n_vars=length_row;
            vars=var_matrix(k, 1 :length_row);

            %find at least i-1 more equations, such that there are no
            %more than i different variables in all i equations

            counter=1;
            m=k+1;

            while m<=n_eqns
               n_vars_test=length(unique([var_matrix(m, 1 :row_length(var_matrix,
m)), vars]));
               if n_vars_test>i
                  j=j+1;
                  if j>n_eqns-i
                     row_index_array=[];
                     break
                  elseif m==n_eqns
                     m=k+counter;
                     counter=counter+1;
                     n_vars=length_row;
                     vars=var_matrix(k, 1 :length_row);
```

```
                row_index_array=[];
                row_index_array(1)=k;
                continue
            else
                m=m+1;
            end
        else
            n_vars=n_vars_test;
            vars=unique([var_matrix(m, 1 :row_length(var_matrix, m)), vars]);
            row_index_array(length(row_index_array)+1)=m;
            m=m+1;
            if length(row_index_array)>=i
                break
            end
        end
    end

    if length(row_index_array)>=i
        break
    else row_index_array=[];
    end
  end %for

  if exist('row_index_array')
    if length(row_index_array)>=i
        break
    end
  else row_index_array=[];
  end
 end

 if exist('row_index_array')
    if length(row_index_array)>=i
        break
    end
 else row_index_array=[];
 end
 end
else
 row_index_array=[];
 vars=[];
end
```

```
function [merged_struct]=merge_structures(struct_one, struct_two)

if isempty(struct_one)
   merged_struct=struct_two;
elseif isempty(struct_two)
   merged_struct=struct_one;
else
   field_names_struct_one=fieldnames(struct_one);
   field_names_struct_two=fieldnames(struct_two);

   field_values_one=struct2cell(struct_one);
   field_values_two=struct2cell(struct_two);

   field_names=[field_names_struct_one', field_names_struct_two'];
   field_values=[field_values_one', field_values_two'];

   % rebuild struct
   merged_struct=cell2struct(field_values,field_names, 2);
end
```

```
function [equations]=read_in_eqns

more_eqns=1;
equations=[];

while more_eqns==1

   while more_eqns==1
      eqn=input('Please enter equation: ', 's');

      if isempty(eqn)==0
         if isempty(equations)
            equations=[{eqn}];
         else
            equations=[equations; {eqn}];
         end
      else
         more_eqns=0;
         break
      end
   end

   display('If you are not yet done with entering equations please press "y"!')

   more_eqns=input('Do you want to enter another equation? ', 's');

   if more_eqns=='y'
      more_eqns=1;
   end
end

if isempty(equations)==1
   display('No equations have been entered yet.')
   read_in_eqns
end

save equations equations
```

```
function [row_length]=row_length(cell_array_of_string_matrix, row_index)

%determine how many variables are in the row row_index of var_matrix

[n_rows, n_columns]=size(cell_array_of_string_matrix);
for l=1 :n_columns
   if iscellstr(cell_array_of_string_matrix(row_index, l))==0
      row_length=l-1;
      break
   else
      row_length=n_columns;
   end
end
```

```
function [result, equations]=solve_equations(equations)

n_eqns=length(equations);
vars={};
for i=1 :n_eqns
   var_matrix_row=symvar(char(equations(i)))';
   vars=unique([vars, var_matrix_row]);
   var_matrix(i, 1 :length(var_matrix_row))=symvar(char(equations(i)));
end
n_vars=length(vars);
if n_vars<=n_eqns
   eqn_string=[char(equations(1))];
   for k=2 :length(equations)
      eqn_string=[eqn_string, ', ', char(equations(k))];
   end
   % solve system for unknowns
   result=solve(eqn_string);
   equations={};
else
   % search for a subset of i equations with i variables
   [eqn_subset, var_subset]=find_subset(var_matrix);
   if ~isempty(eqn_subset)
      %solve subsystem of equations and substitute values for all variables
      %of the subsystem in remaining equations
      eqn_string=[char(equations(eqn_subset(1)))];
      for k=2 :length(eqn_subset)
         eqn_string=[eqn_string, ', ', char(equations(eqn_subset(k)))];
      end
      result=solve(eqn_string);
      equations=setdiff(equations, equations(eqn_subset));
      if ~isstruct(result)
         for k=1 :length(equations)
            %substitute variables that are in the subset of equations by the above
computed
            %solution of the subset of equations
            equations(k)={char(subs(char(equations(k)), var_subset(1), result))};
%              [new_result, equations]=solve_equations(equations);
%              result=merge_structures(result, new_result);
         end
         [new_result, equations]=solve_equations(equations);
         result=merge_structures(result, new_result);
      else
         for j=1 :length(getfield(result, char(var_subset(1))))
%result.(char(var_subset(1))))                          %what if result is empty
            %substitute variables that are in the subset by the above computed
            %solution of the subset of equations
```

```
            for k=1 :length(equations)
               for l=1 :length(var_subset)
                  subs_array=getfield(result, char(var_subset(1)));
                  equations(k)={char(subs(char(equations(k)), var_subset(l),
{subs_array(j)}))}; %{result.(char(var_subset(l)))(j)};
               end
            end
            [result_solve_eqns, eqns_solve_eqns]=solve_equations(equations);
            if ~isempty(result_solve_eqns)
               new_result(j)=result_solve_eqns;
               equations=eqns_solve_eqns;
               new_res(j)=merge_structures(result, new_result(j));
            else
               break
            end
         end
         if exist('new_res')
            for j=1 :length(var_subset)
               %result.(char(var_subset(j)))=new_res(1).(char(var_subset(j)));
               result=setfield(result, char(var_subset(1)), getfield(new_res(1),
char(var_subset(j))));
               for i=2 :length(new_res)
                  %result.(char(var_subset(j)))=[new_res(i).(char(var_subset(j)));
result.(char(var_subset(j)))];
                  result=setfield(result, char(var_subset(j)), [getfield(result,
char(var_subset(j))), getfield(new_res(i), char(var_subset(j)))]);
               end
            end
         end
      end
   else
      result=[];
   end
end
```

8 References

[1] "Hydrostatic Lubrication", Bassani, Piccigallo, Elsevier, 1992
Hydrostatic and hybrid bearing design, W.B. Rowe, Butterworths, 1983

[2] "Linear motion carriage with aerostatic bearings preloaded by inclined iron core linear electric motor", Roger Cortesi, Alexander Slocum, Murat Basaran, Anastasios John Hart, Elsevier 4 March 2003

[3] "An Easy to Manufacture Non-Contact Precision Linear Motion System And Its Applications", Master Thesis of Roger Cortesi, Precision Engineering Research Group, MIT

[4] "Nulling the Pitch Error of Permanent Magnet Open Face Linear Motion Components", Gerald Rothenhöfer, Alexander Slocum, 6th Euspen International Conference, Baden/Wien, May 2006

[5] "Compensation for five DOF motion errors of hydrostatic feed table by utilizing actively controlled capillaries", Precision Engineering, July 2006, C.H. Park, Y.J. Oh, E.Shamoto and D.W. Lee

[6] http://web.mit.edu/~geraldr/www/CV/minimizing%20pitch.pdf

[7] http://web.mit.edu/~geraldr/www/CV/Nulling%20Pitch.pdf)

[8] "Active hydrostatic bearing with magnetorheological fluid", J. Hesselbach and C. Abel-Keilhacka, Institute of Machine Tools and Production Technology, Technical University of Braunschweig, Langer Kamp 19b, D-38106 Braunschweig, Germany

[9] "Accurate Tool Height Control by Bearing Gap Adjustment", A.M. van der Wielen1, P.H.J. Schellekens1 (1), F.T.M. Jaartsveld2, 1Precision Engineering section, Department of Mechanical Engineering, Eindhoven University of Technology, Eindhoven, the Netherlands, 2Philips Research Laboratories Eindhoven, Eindhoven, the Netherlands